Exclusion regions for LTE base stations in heterogeneous cell structures

Bruno Miguel Marques Pires

Thesis to obtain the Master of Science Degree in

Electrical and Computer Engineering

Supervisor: Prof. Luís Manuel de Jesus Sousa Correia

Examination Committee

Chairperson: Prof. José Eduardo Charters Ribeiro da Cunha Sanguino

Supervisor: Prof. Luís Manuel de Jesus Sousa Correia

Members of Committee: Prof. Custódio José de Oliveira Peixeiro

February 2015

To my father

Acknowledgements

In the first place, I would like to thank Professor Luís M. Correia for the opportunity to write this thesis, and for the constant knowledge and support. I am also thankful for all the guidance during our weekly meetings and for all the advices and hints he gave me, which will be useful in my professional life as well.

To Carla Oliveira, Professor Jorge Costa and Eduardo Lima, I would like to thank for all the help regarding the simulator and the antenna models, and to Daniel Sebastião for the availability to help with every problem I had.

To GROW, for the possibility to participate in the meetings, which allowed me to contact with several other areas of wireless and mobile communications, as well as to practice my critical thought and presentations. Also, to all the members with whom I had the opportunity to work.

To Margarida, for the motivation, patience, support and love.

Finally, I would like to thank my family for what I am, especially to my parents and my sister, and for their unconditional and constant support throughout one more journey of my life.

Abstract

The objective of this work was to develop an exclusion region estimation model for base station antennas in heterogeneous cell structures. Two different scenarios were designed, one considering an indoor environment and another for an outdoor one. For the indoor scenario, a microstrip patch antenna was designed in CST, for the 800 MHz, 900 MHz, 1800 MHz, 2100 MHz and 2600 MHz frequency bands. For the outdoor scenario, a dipole array antenna was designed, operating in the same frequency bands as the indoor one. From both simulation results and the far field model, a global indoor model and a global outdoor model were developed, allowing the estimation of the electric field as a function of distance, considering the direction of maximum radiation; the cylindrical exclusion region model is used for other propagation directions. When compared to measurement results, the developed models result in an overestimation 180% for 800 MHz, 335%for 900 MHz, and 676% for 2100 MHz in the region closer to the antennas. It is concluded that the developed model overestimates the real value of an exclusion region, always considering the worst-case perspective of exposure to electromagnetic radiation.

Keywords

Electromagnetic field, Antenna, Exclusion Region, GSM, UMTS, LTE.

Resumo

Este trabalho teve como objetivo desenvolver um modelo de estimação das regiões de exclusão de antenas de estações base em células de estrutura heterogéneas. Dois cenários foram considerados, um para interior e outro para exterior. Para o interior, uma antena *microstrip patch* foi desenvolvida no CST, operando nas bandas de frequências de 800 MHz, 900 MHz, 1800 MHz, 2100 MHz e 2600 MHz, enquanto para o cenário de exterior foi desenvolvido um agregado de dipolos para operar nas mesmas bandas de frequências. Através de simulações e do modelo de zona distante, foi criado um modelo global para ambientes de interior e um outro para ambientes de exterior, permitindo estimar o campo elétrico emitido pelas antenas em função da distância, considerando a direção de máxima radiação; para outras direções de propagação utiliza-se a abordagem do modelo da região de exclusão cilíndrica. Quando comparado com resultados de medições, os modelos desenvolvidos resultam numa sobre-estimação de 180% para 800 MHz, 335% para 900 MHz, e 676% para 2100 MHz. Conclui-se que o modelo desenvolvido sobrestima o real valor da zona de exclusão, considerando sempre a perspetiva de pior caso em termos de exposição à radiação eletromagnética.

Palavras-chave

Campo Eletromagnético, Antena, Região de Exclusão, GSM, UMTS, LTE.

Table of Contents

List of Figures

List of Tables

List of Acronyms

2G	Second-Generation mobile systems
3G	Third-Generation mobile systems
3GPP	Third-Generation Partnership Project
4G	Fourth-Generation mobile systems
ANACOM	*Autoridade Nacional de Comunicações*
ARPANSA	Australian Radiation Protection and Nuclear Safety Agency
BS	Base Station
BSS	Base Station Subsystem
CDMA	Code Division Multiple Access
CEPT	European Conference of Postal and Telecommunications Administrations
CF	Correction Factor
CP	Cycle Prefix
DL	Downlink
DS-CDMA	Direct-Sequence Code Division Multiple Access
ECC	Electronic Communications Committee
EDGE	Enhanced Data Rates for GSM Evolution
EM	Electromagnetic
EMF	Electromagnetic Field
ETSI	European Telecommunications Standards Institute
FDD	Frequency Division Duplex
FDMA	Frequency Division Multiple Access
FDTD	Finite Difference Time Domain
FF	Far Field
FFT	Fast Fourier Transform
FIT	Finite Integration Technique
GPRS	General Packet Radio Service
GSM	Global System for Mobile Communications
HSDPA	High Speed Downlink Packet Access
HSPA	High Speed Packet Access
HSUPA	High Speed Uplink Packet Access
ICNIRP	International Commission on Non-ionising Radiation Protection
IEEE	Institute of Electrical and Electronics Engineers
IR	Ionising Radiation

ISI	Inter-Symbol Interference
LEXNET	Low EMF Exposure Future Networks
LTE	Long Term Evolution
LTE800	Long Term Evolution system in the 800 MHz band
LTE1800	Long Term Evolution system in the 1800 MHz band
LTE2600	Long Term Evolution system in the 2600 MHz band
MIMO	Multiple Input Multiple Output
MSS	Multilevel Subgridding Scheme
MT	Mobile Terminal
NEC	Numerical Electromagnetic Code
NF	Near Field
NIR	Non-ionising Radiation
OFDM	Orthogonal Frequency Division Multiplex
OFDMA	Orthogonal Frequency Division Multiple Access
Omni	Omnidirectional
PAR	Peak-to-Average Ratio
PBA	Perfect Boundary Approximation
PRAT	Rated Output Power
RB	Resource Block
RE	Resource Element
RF	Radio Frequency
RMS	Root mean Square
SAR	Specific Absorption Rate
SC-FDMA	Single Carrier-Frequency Division Multiple Access
SMS	Short Message Service
TDD	Time Division Duplex
TDMA	Time Division Multiple Access
TST	Thin Sheet Technique
Tx	Transmitter
UE	User Equipment
UL	Uplink
UMTS	Universal Mobile Telecommunications System
VoIP	Voice over IP
WCDMA	Wideband Code Division Multiple Access

List of Symbols

Δ_{da}	Spacing between elements of the array antenna normalised to the wavelength
Δ_{sp}	Length between samples (sampling interval)
ε_r	Dielectric constant of the substrate
ε_{ref}	Effective dielectric constant
ε_{r_n}	Error measured at distance n when using the far field model results instead of the simulation ones
θ_{dt}	Downtilt angle
θ_i	Elevation angle of the *i*-th element of the antenna
ψ_i	Associated phase shift of the *i*-th element of the antenna array
ϕ_i	Azimuth angle of the *i*-th element of the antenna
ΔL	Extension of the patch length due to fringing effects
θ	Elevation angle
ρ_i	Power ratio of the *i* mobile system
δ_{max}	Maximum permissible RMSE for the interpolation function
λ	Wavelength of the electromagnetic wave
ϕ	Azimuth angle
B	Magnetic flux density
c	Free space speed of light
D	Largest dimension of the antenna
d	Distance from the antenna to observation point
d_a	Spacing between elements of the antenna array
D_{back}	Back border of an exclusion zone
$d_{c,i}$	Boundary between model from simulations and far field model for indoor scenario
$d_{c,o}$	Boundary between model from simulations and far field model for outdoor scenario
D_{bottom}	Border of the bottom of an exclusion zone
D_{front}	Front border of an exclusion zone
d_i	Distance from the *i*-th antenna element to the observation point
D_{max}	Maximum distance of an exclusion zone
d_{max}	Upper bound for the simulation range
d_{min}	Lower bound for the simulation range
D_{top}	Top border of the exclusion zone

E	Electric field strength
E_θ	Transverse component of the electric field
E_ϕ	Longitudinal component of the electric field
$E(d,\theta,\phi)$	Root-Mean-Square electric field
$E_{fit}(d)$	Interpolation function of the maxima points of $\lvert E(d)\rvert$
E_i	Electric field strength at frequency i
E_r	Radial component of the electric field
$E_{ref,i}$	Electric field reference level from ICNIRP guidelines at frequency i
$E_{upper}(d)$	Upper bound of the electric field
f	Frequency
f_r	Resonant frequency
g	Gap in-between half wavelength dipole
G	Antenna gain
$G(\theta,\emptyset)$	Antenna gain as a function of $\theta,\emptyset$
H	Magnetic field strength
h	Thickness of the substrate
h_{ant}	Height of the antenna
h_c	Height of the back cover
h_{el}	Height of the array element
H_j	Magnetic field strength at frequency j
$H_{ref,j}$	Magnetic field reference level from ICNIRP guidelines at frequency j
I_o	Maximum electric current that crosses the monopole
k	Propagation constant
L	Patch length of the microstrip patch antenna
L_c	Length of back cover
l	Length of the monopole
L_{ef}	Effective length of the patch
$N_{M,i}$	Number of MIMO elements of the BS in the communication system *i*
$N_{c,i}$	Carrier number of the communication system *i*
N_{el}	Number of elements of the collinear array
N_s	Number of communication systems installed in the site
N_{sp}	Number of samples
P_{in}	Input power of the antenna
R	Radius of the diploe wire
$R(d)$	Exposure function
R_{in}	Input resistance of the antenna
S	Power density
$S_{far}(d)$	Power density using the far field model

$S_i(d)$	Power density at frequency *i* as a function of distance
$S_{nupper}(d)$	Upper bound of the $S(d)$ in the near field model
$S_{ref,i}$	Power density reference level from ICNIRP guidelines at frequency *i*
S_{total}	Global model of the radiated field levels
TM_{010}^{x}	Transverse magnetic mode 010
$u(\theta_i, \phi_i)$	Co-polar vector of the *i*-th element of the antenna array
V_0	Voltage across the microstrip slot
W	Patch width of the microstrip antenna
W_c	Width of the back cover
y_0	Physical notch introduced by inset feed
Z_0	Free space characteristic impedance

List of Software

Adobe Photoshop	Graphics editing program
CST MWS	Computer Simulation Tool Microwave Studio
MatLab	Numerical computing environment
Microsoft Excel	Spreadsheet application
Microsoft Visio	Diagramming and vector graphics application
Microsoft Word	Text processor

Chapter 1

Introduction

This chapter provides an overview of the Thesis. Section 1.1 covers the scope and a brief state of the art as well as the motivation and main targets. Section 1.2 concludes the chapter, providing the Thesis structure.

1.1 Overview and Motivation

The mobile cellular era started in the 1980s with the deployment of First Generation System providing basic voice communications. The fact that different countries used different technologies, and the high cost of Mobile Terminals contributed to the end of this analogue system. By then, it was clear that there was the need for a global system that could provide good coverage, capacity and roaming at reasonably low prices.

The digital revolution came with the development of a second generation system carried by the European Conference of Postal and Telecommunications Administrations (CEPT), later becoming a technical committee of European Telecommunications Standards Institute (ETSI). The rapid worldwide penetration of GSM led to its reinterpretation has Global System for Mobile Communications. This system provided good coverage, roaming, voice communication and low rate services, 14.4 kbps, such as the Short Message Service (SMS). Moreover, the growing need for data led to the development of extensions to the standard, such as General Packet Radio Service (GPRS) and Enhanced Data rates for GSM Evolution (EDGE), providing higher data rates. With GSM, the number of mobile phones exceeded the number of landline phones and the mobile phone penetration approached 100% in several markets. Despite these steps forward, the ability of the system to handle higher data rates was still limited.

The Third Generation Partnership Project (3GPP) was born with the purpose of allowing a common system to be developed for Europe, Asia and North America. 3GPP presented the Universal Mobile Telecommunication System (UMTS), designed for multimedia communication, providing high bit-rate services that enable high quality images, video and access to the web with higher data rates. On the first release (release 99), a maximum theoretical peak rate of 2 Mbps was announced, but UMTS provided a data rate of 384 kbps for the Downlink (DL) and Uplink (UL). Release 5 and release 6 provided enhancements to the already deployed UMTS with High Speed Downlink Packet access (HSDPA) and High Speed Uplink Packet Access (HSUPA), allowing theoretical rates of 14.4 Mbps on DL and 5.7Mbps on UL.

Long Term Evolution (LTE) was developed by 3GPP as a fourth generation system (4G). Both core network and air interface were completely redesign in this new standard. This purely IP based system brought several enhancements such as higher modulation, large bandwidth, spectral efficiency (two to four times more than with HSPA Release 6) and the ability to support Multiple Input Multiple Output (MIMO). The LTE solution also enables spectrum flexibility where the transmission bandwidth can be selected between 1.4 MHz and 20 MHz depending on the available spectrum. The maximum bandwidth can provide data rates in DL up to 150 Mbps using a 2x2 MIMO and 300 Mbps with 4x4 MIMO. For the UL, the peak data rate is 75 Mbps. The growth of 4G will help to minimise the gap between mobile and fixed network performance, leading to an even higher adoption of mobile technologies.

Overall mobile data traffic is expected to grow from 1.5 ExaBytes (EB) per month in 2013 to 15.9 EB in 2018, according to [Cisc14]. This massive increase of mobile traffic is directly related to the increasing

number of wireless devices that are accessing mobile networks worldwide. For example, a single smartphone can generate as much traffic as 50 basic-feature phones and a tablet as much traffic as 120 basic-features phones.

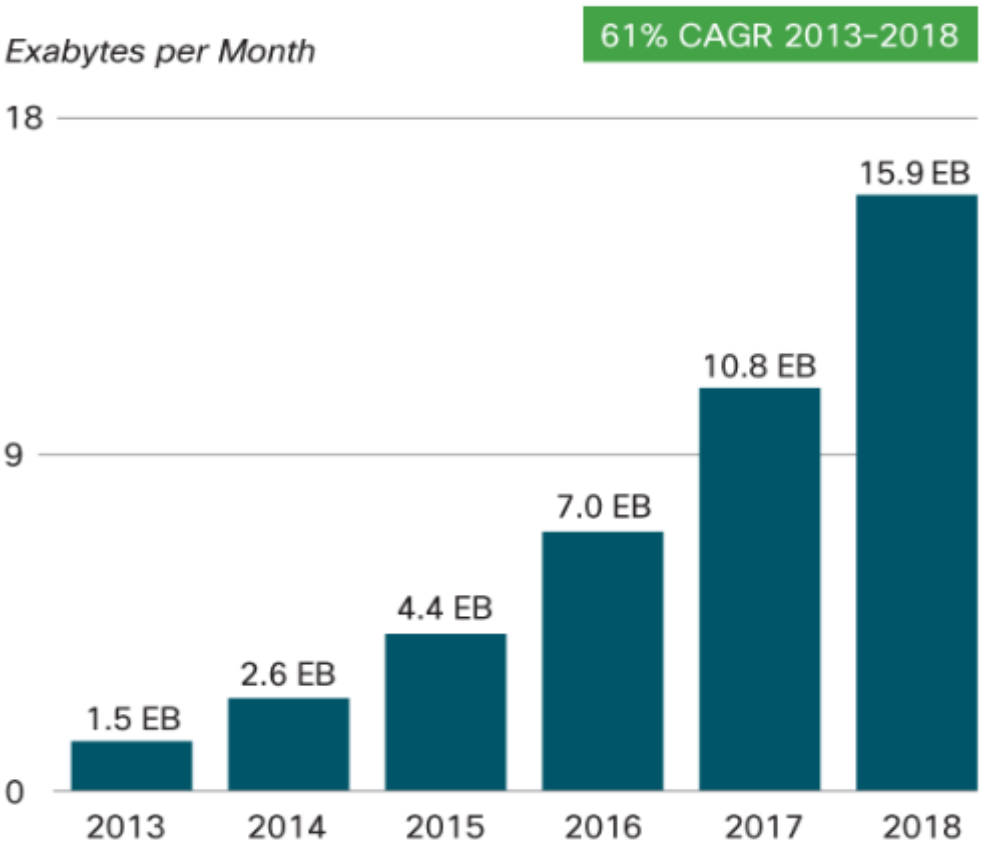

Figure 1.1 - Global mobile data forecast (extracted from [Cisc14]).

This increase of mobile traffic is leading to the deployment of more and more base stations (BSs) in highly populated areas. This is alerting the population to the presence of near BS structures and generating concerns of potential health risk caused by the radiation from the mobile communication systems.

The study of Electromagnetic Fields (EMF) started with the first high-voltage lines and military radar systems in World War II, and since then various international organisations made studies in order to understand the impact of EMF on humans. Based on many of this studies, the International Commission on Non-Ionising Radiation Protection (ICNIRP) established safety thresholds for human exposure to electromagnetic fields to be adopted worldwide, [ICNI98]. Despite these advances in understanding EM radiation, non-thermal effects continue to cause some apprehension, since some contradictory results and deficiencies have been found in some studies, especially concerning real environments application [OICa02], [OFRC05], [COST00].

An exclusion zone is the area around a BS where EMFs exposure guidelines may be exceeded [OFRC05]. This areas are well studied for 2G and 3G [OFRC05], and defined by operators in order to protect the public from potential harmful levels of radiation. In highly populated areas, where the

number of BS is very high and the cell sizes tend to be smaller and heterogeneous, the addition of LTE antennas to the existing infrastructures is most likely to change the EMF behaviour and consequently the exclusion zones may vary from the ones defined for the former technologies. Therefore, there is a need to study and develop accurate models to redefine exclusion zones for the situations where LTE is to be employed.

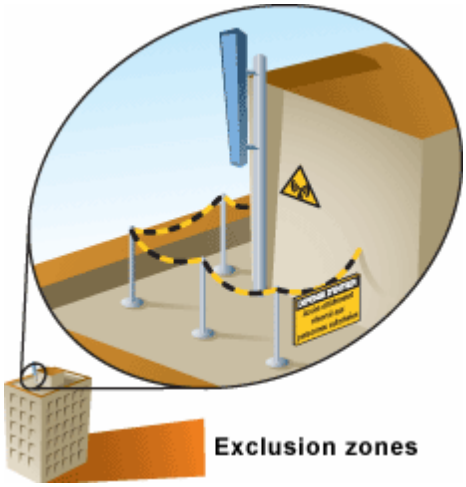

Figure 1.2 - Exclusion zone (extracted from [OFRC05]).

Several models have been developed in order to estimate exclusion zones. The Far Field Model [CENE02a] and the Far Field Approximation [MNMV02] are the most common estimation models that can be found in literature. These are simple models, which most of the times over-predict the real exposure levels and have a limited applicability, since exclusion regions are often smaller than the validity limits of the model. In [MFRL02], a model for exclusion zone of BSs located in free-space areas is presented, taking as assumption that there are no obstacles within the exclusion zone. Synthetic and gain based models are far more accurate and complex than far field models, providing near field estimation for panel antennas [ABDK02].

Hybrid models provide a prediction algorithm to evaluate field strength distributions around BS antennas, making the application in different ranges possible: very near the antenna, near field region, and far field region. Despite being the more complex model, it takes into account the surround environment of the BS, and it is very accurate in the regions near the antenna [BCDF02], [BCFF99]. In [Oliv06] and [BCCP03], the influence in EM of BS installation structures and the presence of penetrable objects are presented.

This work aimed to develop a model to estimate exclusion regions for LTE BSs in heterogeneous cell structures. BS antennas and the radiated EMF needed to be study as well as the impact in the EMF of the heterogeneity of the environment surrounding the BS.

1.2 Contents

This work consists of 5 chapters, including this one, followed by a set of annexes.

In Chapter 2, a description of GSM, UMTS and LTE radio interfaces is given. A characterisation of a BS, focusing on radiation regions, coverage types and classification of BS installations in also presented and EM radiation and exclusion regions are studied. Finally, methods for measurement of electromagnetic radiation are analysed.

Chapter 3 begins with the theoretical models considered in this work in order to estimate EMF, namely the far field model, field models for indoor and outdoor antennas as well as the electric field global model and a distance evaluation model. Then, the development of antenna models is presented, considering a microstrip patch antenna as well as a dipole array. A simulation tool along with simulation methods are described and the developed models of the antennas are assessed for purposes of validation.

In Chapter 4, the scenarios for analysis are defined, according to the environment characteristics of the installations. From simulation results, a global model for each scenario is designed, for the evaluation of the electric field in both the near and far field regions of the BS antennas. The performed measurements are described and a comparison between the developed models, theoretical ones and measurement results is presented. Finally, exclusion zones are obtained, taking into account the different scenarios under consideration.

Chapter 5 finalises the thesis, presenting the main conclusions along with suggestions for future work. A set of annexes with auxiliary information and results is also included. Annex A presents the models of the antennas designed for this work, taking into account the different considered scenarios. In Annex B, complementary results for the developed models, as well as the model comparison and the estimation of exclusion zones are presented. Finally, Annex C presents the measurement data and characteristics of the analysed BS.

Chapter 2

Fundamental Concepts

This chapter provides an overview of radio aspects, such as antennas, basic aspects of coverage and classification of BS installations. The radio interfaces of GSM, UMTS and LTE are also presented. The radiation regions are defined and both the reference levels and guidelines for EMF assessment and measurement established by international bodies are presented. Finally, the EMF estimation models around BS antennas are studied, according to the methodologies of exclusion region estimation proposed by other entities.

2.1 Radio Aspects

This section will cover the basic concepts related to BS antennas [OFRC05] and radio interface of GSM [Moli11], UMTS [HoTo04] and LTE [HoTo09], considering the frequency bands, duplex, multiple access techniques and BS output power.

2.1.1 Base Stations Antennas and Installations

This section provides an overview on BS antennas as well as a classification of BS installations according to their characteristics, based on [OFRC05].

There are two basic types of BS antennas: omnidirectional (Omni) and sectorial ones (Directional), the main difference being the radiation pattern. Sectorial antennas allow the reduction of interference and an increment of the transmitted power in the intended directions, so the common usage of this type of antennas is on high traffic density areas, whereas the omnidirectional antennas are more suitable for lower traffic density areas, such as rural or sometimes in suburban areas, [BFHM02].

The most important parameters of an antenna, such as bandwidth, power density, phase, directivity, radiation intensity, diversity and polarisation can be taken from the antenna technical sheet and from the radiation pattern. The gain of the antenna is an important parameter to measure its performance, as it measures how the antenna can concentrate energy in a given direction in space. In Table 2.1, typical gain values used in mobile communications systems BS antennas are presented.

Table 2.1 - Typical antenna gain values (extracted from [Antu12]).

		Gain [dBi]					
Environment	Antenna type	GSM		UMTS	LTE		
		900 MHz	1800 MHz	2100 MHz	800 MHz	1800 MHz	2600 MHz
Indoor	Omni	[2, 7]					
	Directional	[5, 7]					
Outdoor	Omni	[2, 11]					
	Directional	[5, 22]	[5, 24.2]	[2.9, 24.2]	[2.9, 19.3]	[8, 19.5]	[8, 19.5]

To deploy a cellular network, BS antennas need to be located in places where coverage, capacity and interference conditions are combined in the best possible way. The installation of BS antennas depends heavily on the site surrounding environment, as well as on the conditions for mounting the antenna, such as height. For the purpose of having a better identification of specific conditions of human exposure to EMF, it is useful to define the types of BS installations based on its common characteristics.

A simple and common classification of BS antennas installations is done according to its coverage

range. For example, larger cells usually cover low traffic density areas (rural environments) and small cells cover high density traffic (urban environments). In Table 2.2, this type of classification is described.

Table 2.2 - Classification of cells in mobile communications (extracted from [OFRC05]).

Cell type		Coverage range	Description
Macro	Large	[3, 30] km	Serve either *rural* or *suburban* environments, where the density of BSs is small due to low traffic density; antennas are typically installed on high masts, top of high buildings or other structures, using high-radiated power levels to allow a wide coverage area. Propagation is typically over rooftops.
	Small	[0.5, 3] km	
Micro		[50, 500] m	Provide coverage in *urban* areas, where requirements in terms of capacity are stringent due to high traffic demand; antennas are strategically installed (small towers, top of lower buildings or façades) radiating medium power levels in order to satisfy the capacity demand in a restricted coverage area, and to avoid interference with neighbouring cells. Propagation is typically below rooftops.
Pico		Few tens of meters	Usually used to increase *in-building* coverage, where demand is very high; antennas are typically placed on walls and ceilings inside buildings for the coverage of small areas, thus, requiring lower power levels.

The above classification can give a hint on possible BSs types, but for the purpose of exclusion zones estimation around BS antennas, a more detailed classification is needed. Table 2.3 provides a categorisation based on the cell type, involving environment and the type of infrastructure supporting the antenna.

Table 2.3 - Classification of BS Installations (extracted form [OFRC05] and [Oliv06]).

Denomination	Cell type	Environment	Installation type	Antenna height [m]
Rtower	Macro	Rural, Suburban	Tower, Mast, Water sump, "Tree"	[20, 40]
Uroof	Micro/Macro*	Urban	Roof-top	[2, 5**]
Utower			Tower	[3, 10]
Ufaçade	Micro		Building façade	[3, 10]
Upole			Light pole or other	[3, 5]
Iceil	Pico	In-building	Ceiling	[2, 3]
Iwall			Walls	[2, 3]

: The cell type depends on the coverage area* *: Height from the roof top*

Typically, antennas are installed in places whose height and location is inaccessible to general people. However, there are scenarios where this is not possible, such as the “Ufaçade” and “Upole” installation types, where antennas may be accessed through balconies or windows or the “Iceil” and “Iwall” ones, where antennas are installed closer to people. Therefore, it is important to clearly define exclusion zones to avoid human exposure in high-level radiation areas.

In regions with a relatively small number of users, an Omni BS is typically used, whereas for high traffic density areas, the most common configuration for BS antennas consists of sectorial antennas with three sectors of 120º each. In addition, the sharing of existing sites between different operators for practical and environmental reasons has a cumulative impact on the EMF that has to be considered in exclusion zones calculation.

2.1.2 Radio Interface

In the first version of GSM, the assigned frequency bands were [890, 915] MHz for UL and [935, 960] MHz for DL, this version being called GSM 900. For GSM 1800, the band is [1710, 1785] MHz for UL and [1805, 1880] MHz for DL. A complete list of frequency bands is provided in Table 2.4. The duplex spacing is 45 MHz for GSM 900 and 95 for GSM 1800.

GSM uses Frequency Division Duplex (FDD), and a combination of Time Division Multiple Access (TDMA) and Frequency Division Multiple Access (FDMA). FDMA results in the division in frequency of the DL and UL sub-bands into channels with a bandwidth of 200 kHz. As for the TDMA, the channels are separated in time, each one divided into 8 time-slots, with a duration of 576.92 μs each.

Concerning the maximum output powers from the BS Transmitter, GSM specifies 8 power classes, measured at the input of the BS Subsystem (BSS) Transmitter (Tx) combiner. For micro-BS and pico-BS, the maximum output power per carrier is measured at the antenna connector after all stages of combining, [ETSI100]. The values for BS and Mobile Terminal (MT) maximum output power are presented in Table 2.4.

UMTS uses Wideband Code Division Multiple Access (WCDMA) as air interface technology. The WCDMA air interface uses CDMA to distinguish among different users and between users and control channels. Being a Wideband Direct-Sequence Code Division Multiple Access (DS-CDMA) system, it has two types of codes for spreading and multiple access: Channelisation and Scrambling. Channelisation codes are used within the same sector in order to separate transmissions from the same source in DL and to separate physical data and control information from the same MT in UL. The codes are orthogonal to each other in order to avoid interference among users. Scrambling codes are used to distinguish sectors of the cell in DL and to separate MTs from each other in UL. Scrambling is used on top of spreading in order to preserve the signal bandwidth.

Compared to GSM, UMTS has advantages in terms of improved spectral efficiency, improved handover, enhanced security and offers the possibility of adjacent cells to use the same channel frequency.

UMTS also uses FDD, the frequency band used in Portugal, as well as in the rest of Europe and

Japan, being [1920, 1980] MHz for UL and [2110, 2170] MHz for DL. The regular intercarrier spacing is 5 MHz, but the network provider might select the carrier distance to be any multiple of 200 kHz. Chip rate is 3.84 Mchip/s, which results in a channel bandwidth of 4.4 MHz.

In UMTS, different users can simultaneously transmit at different data rates and data rates can even vary in time, even though each frame has the duration of 10 ms, in which the data rate is kept constant. The values of BS and MT maximum output power for UMTS are presented in Table 2.4.

LTE uses as access schemes Orthogonal Frequency Division Multiple Access (OFDMA) and Single Carrier-Frequency Division Multiple Access (SC-FDMA), for DL and UL respectively. OFDM can be used in both FDD and TDD, resulting in two types of LTE frame structure: Type one uses FDD/TDD, while type two uses TDD only. Since this thesis covers LTE co-existing with GSM and UMTS, only type one is considered.

3GPP specified the frequency bands to be used in LTE, resulting in 17 bands for the FDD mode and 8 for TDD one. In Portugal, the regulatory authority for communications (ANACOM) auctioned frequencies in the bands of 450, 800, 900, 1800, 2100 and 2600 MHz, but only frequencies in the bands of 800, 1800 and 2600 MHz were assigned to the three operators that bid for the auction.

OFDMA has the advantage of being resistant to the damaging effects of multipath delay spread (fading) in the radio channel. Without multipath protection, the symbols in the received signal can overlap in time, leading to inter-symbol interference (ISI). OFDMA avoids ISI by inserting a guard period, Cycle Prefix (CP), between each transmitted symbol. The CP is a copy of the end of the symbol inserted at the beginning and its length must be chosen to be longer than the longest channel impulse response to be supported, in order to completely avoid ISI. The sub-carriers spacing is 15 kHz and the largest time-unit is a 10 ms radio frame. This frame is subdivided into 1 ms sub-frames, each splitting into two 0.5 ms slots. Each slot comprises 7 OFDMA symbols with normal CP or 6 OFDMA symbols with extended CP. The minimum units of allocation distributed among users, called Resource Blocks (RB), are composed of groups of 12 sub-carriers with the duration of one time-slot, while Resource Elements are the smallest units of resource, composed of one sub-carrier for a duration of one OFDMA symbol. An RB contains 84 REs for the normal CP and 72 REs for the extended CP.

OFDMA is based on the Fast Fourier Transform (FFT), which requires a lot of processing power. Whereas in the BS the power is not an issue, the same is not true for the User Equipment (UE). This led to the usage of SC-FDMA in the UL, due to battery limitations on mobile terminals. SC-FDMA is a hybrid access scheme, combining the low peak-to-average ratio (PAR) with multipath resistance and in-channel frequency scheduling flexibility. In SC-FDMA, each data symbol modulates the whole used wideband carrier instead of a narrowband one, and the modulated symbols are transmitted sequentially over the air. The CP for SC-FDMA is the same as for the OFDMA.

In LTE, the maximum rated output power (PRAT) of the BS is defined as the mean power level per carrier that the manufacturer has declared to be available at the antenna connector [ETSI11a]. The values of maximum output power for the BS and UE are presented in the Table 2.4.

Table 2.4 – GSM, UMTS and LTE BS and MT/UE maximum output power (extracted from [ETSI100], [ETSI106], [ETSI11a] and [ETSI11b]).

BS maximum output power [dBm]				
System		GSM 900 MHz, 1800 MHz	UMTS 2100 MHz	LTE 800 MHz, 1800 MHZ, 2600 MHz
Macro-cell		[34,58]	[40,46]	N/A
Micro-cell		[9,32]	[30,33]	38
Pico-cell		[13,23]	N/A	24
Femto-cell	With MIMO	N/A	N/A	17
	Without MIMO			20
MT/UE maximum output power [dBm]		[22,39]	[21,33]	[22,39]

2.2 Radiation Regions

Concerning the EMF in the area surrounding the antenna, one must take the behaviour of EMF into account according to the distance to the antenna. There are three different regions to be considered, according to [Bala05], [OFRC05] and [StTh81]:

- reactive near field region;
- radiative near field region;
- far field region.

The reactive near field region corresponds to the closest region around the transmitting antenna wherein the reactive field predominates. Electric (*E*) and Magnetic (*H*) fields need to be separately estimated to determine the field impedance and power density. This region is delimited by [OFRC05]:

$$d[\mathrm{m}] \leq \frac{\lambda[\mathrm{m}]}{4} \tag{2.1}$$

where:

- d: Distance from the antenna to the point of investigation
- λ: Wavelength of the electromagnetic wave

The radiative near field region, also known as Fresnel zone, is the region of the field of an antenna between the radiative near field and the far field regions, in which the angular field distribution depends on the distance to the antenna. This region may not exist, in the cases where the maximum dimension of the antenna is small, compared to the wavelength. In this region, *E*- and *H*-field measurements are directly interrelated by the free space characteristic impedance and is delimited by [OFRC05]:

$$\frac{\lambda[\mathrm{m}]}{4} \leq d[\mathrm{m}] \leq \frac{2D[\mathrm{m}]^2}{\lambda[\mathrm{m}]} \quad (2.2)$$

where:

- D: Largest dimension of the antenna

In the far field region (Fraunhofer region), the angular field distribution is independent of the distance from the antenna and the *E*- and *H*-field measurements are related by the characteristic impedance of free space (120π). The region is delimited by [OFRC05]:

$$d[\mathrm{m}] > \frac{2D[\mathrm{m}]^2}{\lambda[\mathrm{m}]} \quad (2.3)$$

with the following conditions:

$$d[\mathrm{m}] \gg \mathrm{D} \quad (2.4)$$

$$d\ [\mathrm{m}] \gg\ \lambda \quad (2.5)$$

When these two conditions are not verified, the far field distance may have to be larger than (2.3) so that the conditions can be satisfied.

In Figure 2.1, the boundaries for the different regions are represented.

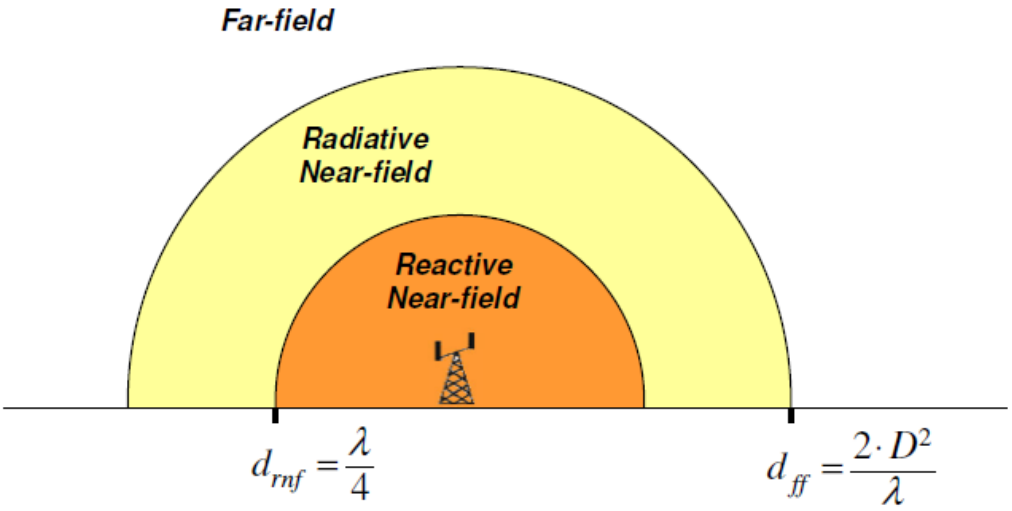

Figure 2.1 - Boundary regions of the different radiation fields existing around an antenna (extracted from [OFRC05]).

In each region, the radiated field does not have the same behaviour, therefore, different models need to be applied to compute the exact field strength at a given distance.

2.3 Electromagnetic Radiation Exposure

The continuous growth of mobile networks and the densification of BS installations in the vicinity of residential and working areas resulted in a higher generalised concern related to possible health risks of human exposure to EMFs by BS antennas. The study of the impact of radiation on humans is as sensitive as an important issue. This section describes the exposure guidelines and measurements that were specified by international entities in order to protect the population from radiation.

2.3.1 Exposure Guidelines

Electromagnetic fields have always been present in the universe, the sun being the most intense source of EMFs one is exposed to. Other sources are power lines, electrical equipment and antennas. There are two types of radiation: Ionising (IR) and Non-ionising (NIR). For the frequencies of interest in this work, the Radio Frequency (RF) band (30 kHz to 300 GHz), the type is NIR. For NIR such as RF, possible biological effects are thermal and non-thermal ones. Thermal effects are well known and can be quantified, since they consist of the heating of the biological tissue. Non-thermal effects are still under study, with the possibility of long term biological effects being still an open issue.

In 1998, the International Commission on Non Ionising Radiation Protection (ICNIRP) issued a publication providing guidelines for limiting exposure to EMFs [ICNI98]. The work followed a thorough review of all published literature and takes into account only established effects, meaning short-term, immediate health effects associated to the exposure to frequency sources up to 300 GHz. It also states that, referring to the literature, potential health effects related to EM exposure, such as tumours and cancer risk, were inconclusive, meaning that no evidence of these effects was provided due to the small number of samples and the inability to reproduce satisfactory laboratory results.

In [ICNI98], two classes of guidelines for limiting EMF exposure are defined: basic restrictions and reference levels. These guidelines were developed for two different population groups, the first group being the occupational exposed population and the second the general public. Occupational exposed population comprises adults who are generally exposed under known conditions and are trained to be aware of potential risk and to take the appropriate precautions. General public consists of individuals of all ages and of varying health status; these individuals may be unaware of their exposure to EMF, which led to the adoption of more stringent exposure restrictions compared to the occupational exposure.

Basic restrictions are based directly on established health effects, presenting thresholds on exposure to time-varying electromagnetic fields. For RF, the physical quantity used to specify these restrictions is the Specific Absorption Rate (SAR), which is the rate at which EM is absorbed by unit of mass, and it depends on various factors, such as incident field parameters, characteristics of the exposed body, ground effects and reflector effects. These restrictions are provided to prevent whole-body heat stress and excessive localised tissue heating, therefore, SAR has to be measured inside the body of the exposed individual, which is not an easy procedure. The basic restrictions for whole body average

SAR and localised SAR are presented in Table 2.5.

Table 2.5 - Basic restrictions for time varying electric and magnetic fields (extracted from [ICNI98]).

Exposure characteristics	Frequency range	Whole-body average SAR [W/kg]	Localised SAR (head and trunk) [W/kg]	Localised SAR (limbs) [W/kg]
Occupational exposure	10 MHz - 10 GHz	0.4	10	20
General public exposure		0.08	2	4

Reference levels are provided for practical exposure evaluation purposes, to determine whether the basic restrictions are likely to be exceeded. The physical quantities used to specify these levels are electric field strength (E), magnetic field strength (H), magnetic flux density (B), power density (S) and current flowing through the limbs. Compliance with the reference levels ensures compliance with the basic restrictions, but if the measured value exceeds the reference value, is does not necessarily follow that the basic restrictions will be exceeded, therefore, this situation requires a more detailed analysis to assess compliance with the basic restrictions. For the frequencies of interest in this work, the E, H, B and S values are evaluated over the entire body and must be measured averaged over any 6-minutes period. The reference levels for RF are presented in Table 2.6.

Table 2.6 - Reference levels for time-varying electric and magnetic fields (unperturbed root mean square) (extracted from [ICNI98]).

Exposure characteristics	Frequency range, f [GHz]	E [V/m]	H [A/m]	B [μT]	S_{eq} [W/m^2]
Occupational exposure	[0.4, 2]	$3f_{[\mathrm{MHz}]}^{1/2}$	$0.008f_{[\mathrm{MHz}]}^{1/2}$	$0.01f_{[\mathrm{MHz}]}^{1/2}$	$\frac{f_{[\mathrm{MHz}]}}{40}$
	[2, 300]	137	0.36	0.45	50
General public exposure	[0.4, 2]	$1.375f_{[\mathrm{MHz}]}^{1/2}$	$0.0037f_{[\mathrm{MHz}]}^{1/2}$	$0.0046f_{[\mathrm{MHz}]}^{1/2}$	$\frac{f_{[\mathrm{MHz}]}}{200}$
	[2, 300]	61	0.16	0.20	10

In order to prevent unintentionally high exposure during the averaging period, ICNIRP guidelines also established peak power limits. For frequencies above 10 MHz, the field strength should not exceed 32 times the reference value and S should not exceed it by 1000 times.

For the situations where the exposure to fields of different frequencies is verified, these exposures are additive on their effects. For the frequencies of interest to this work, two requirements should be applied to the field levels:

$$\sum_{i>400MHz}^{300GHz} \left(\frac{E_i[\mathrm{V/m}]}{E_{ref,i}[\mathrm{V/m}]} \right)^2 \leq 1 \quad (2.6)$$

and

$$\sum_{j>400MHz}^{300GHz} \left(\frac{H_j[\mathrm{A/m}]}{H_{ref,j}[\mathrm{A/m}]} \right)^2 \leq 1 \quad (2.7)$$

where:

- E_i: Electric field strength at frequency i;
- $E_{ref,i}$: Electric field reference level from Table 2.6;
- H_j: Magnetic field strength at frequency *j*;
- $H_{ref,j}$: Magnetic field reference level from Table 2.6;

Portugal, along with most European countries, adopted the exposure thresholds established by the European Union Recommendation for general public [CoEU99] and occupational exposure [CoEU04], based on ICNIRP guidelines [ICNI98].

2.3.2 Measurement Guidelines

Measurement guidelines are important to evaluate EMF in order to verify the compliance with the reference levels. These guidelines have been issued by international entities with the purpose of comparability and acceptance among different measurement values, as well as for results replication.

Reference and alternative methodologies for measuring EMF strength and SAR have been issued by CENELEC, [CENE02a], providing a reference valid in the RF range with the purpose of establishing a compliance boundary applicable to each antenna region; the conclusions are presented in Table 2.7. In [CENE02b] and [CENE02c], CENELEC provides a standard to demonstrate the compliance of radio BSs and fixed terminal stations for wireless telecommunications systems with the basic restrictions or the reference levels related to human exposure to RF EMFs, for occupational and general public exposure respectively.

Table 2.7 - Reference and alternative methodologies established by the EN 50383 standard, (extracted from [CENE02]).

Methodology	Reactive near field region	Radiating near field region	Far field region
Reference	SAR evaluation	SAR evaluation	*E*- or *H*-field Calculation
First alternative	*E*- and *H*-field measurement	*E*- or *H*-field measurement	*E*- or *H*-field measurement
Second alternative	Non applicable	*E*- or *H*-field calculation	Non applicable

In Portugal, ANACOM, [ANAC07], adopted the ECC Recommendation (02)04, [ECCC07], issued by the Electronic Communications Committee (ECC) within the CEPT. The recommendation specifies a measurement method to evaluate non-ionising EMF levels in order to verify compliance with the reference levels. The method follows an approach based on the application of various models, whose accuracy is increased when radiation levels come close to the reference. Table 2.8 provides the measurement method that is recommended according to the field region.

Table 2.8 - Measurement procedure (extracted from [ECCC07]).

	Reactive near field region	Radiating near field region	Far field region
Component to be measured	*E*- and *H*-field	*E*- or *H*-field	*E*- or *H*-field

2.4 Exclusion Zones

The main goal of this section is to present methods found in literature for the assessment of EMF levels and for the estimation of exclusion zones around typical BS installations.

Exclusion zones, inside which exposure thresholds may be exceeded, are typically in the near field region of the radiating antenna. There are different ways for computing these zones, by measurements, by prediction through complex simulations or through the application of simple models, which enable the calculation of the radiation levels in the vicinity of the BS antennas.

Regarding measurements, [CENE02b], [CENE02c] and [ECCC07] provide methods to obtain electromagnetic quantities radiated by an antenna, but the process depends on the type of BS and it consumes too much time. Simulations are an alternative to measurements, since they can be run in order to provide good estimates of the radiated fields. However, in order to obtain precise results, powerful equipment and a lot of time are sometimes required. A simple and more practical way to obtain a good prediction of the radiation levels is by applying adequate models that can be found in literature, some of which are simple and accurate. An overview of these models is presented next.

One of the most common and simple models that can be found in literature is the far field model; this model, [CENE02a], estimates the RMS of the power density S at a distance d from the radiating element to the point of investigation, depending on the values of the wavelength, λ, input power of the antenna, elevation and azimuth angles, (Φ, Θ), antenna gain, G, and the largest dimension of the antenna, D. The applicability of this model is rather limited, as it requires the investigation point to be in the far field, which may correspond to some tens of metres. When used in the near field region, the model over-estimates the field strength and does not take the influence of the environment into account.

The far field approximation model, [MNMV02], provides a good prediction of the EMF at a distance much shorter (1/8) to the BS antenna than the far field model. It presents a comparison between finite-

difference time-domain (FDTD) results and simple expressions based on cylindrical and far field approximations for the estimation of exclusion zones. For distances above $2D^2/\lambda$, the far field approximation model over-estimates the real exposure levels, thus, the far field model should be used instead, as it provides more accurate results.

In order to evaluate compliance with EC recommendation limits on EMF exposure in the vicinity of a BS, a practical assessment procedure is proposed in [MFRL02]. It is considered that for a BS located in free-space areas, where obstacles are not present within the exclusion zone, simple expressions can be used to obtain an accurate prediction of *S*. For a BS located in typical urban environments, where obstacles such as scattered objects exist inside and near the exclusion region and where two or more BSs are located in the same site, additional measurements are required to be able to ensure that EC recommendation thresholds are not exceeded.

The model defines that the power density near the antenna (collinear array of *N* half-wave dipoles) is estimated by computing the power density on the surface of an imaginary cylinder that extends from the bottom of the lowest element to the top of the highest element. The top and bottom of the cylinder, D_{top} and D_{bottom}, as well as the back, D_{back}, are based on the maximum distance of the cylindrical exclusion zone, D_{max}. When a downtilt, Θ_{dt}, is used, a correction of the previous values is needed, using expressions described in the model.

In the situation where several sector antennas are installed in the BS, the total exclusion zone is estimated by the added composition truncated sector cylinders of all the individual exclusion zones. In Figure 2.2, the typical cylinder exclusion zone is represented.

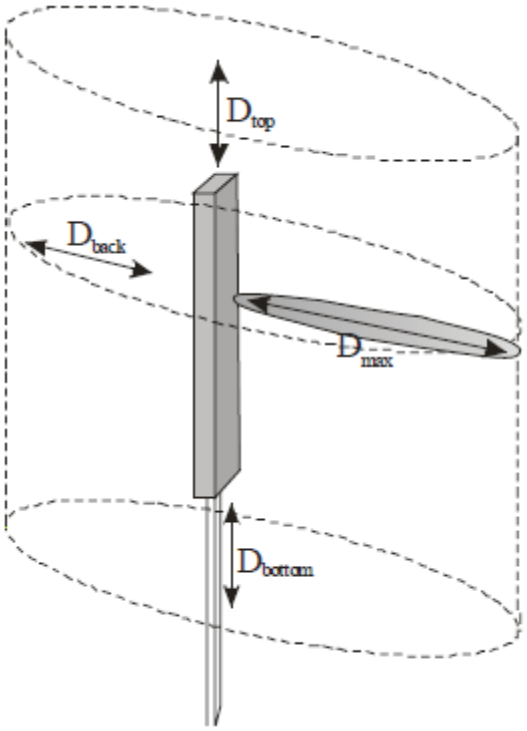

Figure 2.2 - Cylindrical exclusion zone (extracted from [OFRC05]).

In [BiGi99], a model to estimate the EMF radiated around a BS in both the near field and far field

situations is presented. The far field-gain-based model is applicable for distances above 3λ and considers the BS as a uniform array antenna. In order to estimate the radiated near field, the method takes the gain of the antenna as a function of its maximum gain and the radiation pattern in both the vertical and horizontal planes in the far field.

The model provides a two-steps method to determine the radiation pattern of each element of the array. It is fast and efficient, and the obtained values, compared with results of Numerical Electromagnetic Code (NEC) simulations and with measured data, proved to be accurate for the applicable distance. Nevertheless, the model does not take the influence of the environment into account, such as the presence of surrounding buildings, which may have an effect on the field levels.

In [ABDK02], two simple and accurate models for BS panel antennas are presented. Denoted as synthetic and gain-based models, these can be used for human exposure assessment and to verify compliance with the exposure threshold values.

In the synthetic model, the radiated near field of one unit cell of the antenna array is determined in the volume of interest. In order to obtain the radiated near field of the full array, the superposition of contributions of the radiated field of the unit cells of the antenna is considered. For distances to the antenna above one wavelength, the model proved to be accurate, compared with a full-wave analysis of the antenna array.

In the gain-based model, which derives from the synthetic model, the far field radiation pattern is used, instead of the radiated near field of an element. The idea is to compute and store the gain pattern of one single cell for all angles, and by doing so to avoid the full-wave analysis of the entire antenna, resulting that the near field of the antenna is approximated by the sum of the far field contributions in both amplitude and phase. The model approximates reasonably well the near field for a distance of about 2λ away from the antenna, requiring short computation time and lower memory resources.

In [CKLa11], a simple, accurate and very efficient method for the evaluation of the field in the vicinity of GSM BS antennas in urban areas is presented. The method is based on the replacement of the antenna panel by a group of discrete sources in order to provide a simple tool for the estimation of the electric field. The effect of the environment is evaluated by using a geometrical approximation and the calculated results were compared with measurements done with a spectrum analyser, proving that the proposed method can be very accurate in estimating the Electric field in the vicinity of the GSM BS antennas in an urban environment.

In [BCFF99] and [BCDF02], a hybrid prediction algorithm is proposed for the evaluation of field strengths near BS antennas, defining the exclusion zone as a parallelepiped volume around the antenna. This model differs from the previous ones in the way that it combines different propagation models to be used according to the region around the antenna and takes into account the effect of the surrounding environment. The model is applicable in three regions, the near field region of a single antenna element, the area of intersection between the far field-region of each element and the near field region of the whole antenna, and the far field region of the whole antenna.

The chosen model for the near field region of a single antenna element, in which $d << \lambda$, is the

spherical waves triples model [Sche43]. The model allows the evaluation of the exact value of the electrical field radiated by a dipole as the sum of the field radiated from three different sources of spherical non-uniform waves, located in the middle and at the extremes of the dipole. Despite the applicability to the far field region, the model does not take the environment into account, therefore, the analysis is limited to receiving points very close to the antenna, where the results are very rigorous.

For the area corresponding to the intersection between the far field region of each antenna element and the far field of the whole antenna, which corresponds *to* $d >> \lambda$ and $d < 2D^2/\lambda$, a combination of the sub-element radiation pattern antenna model with a ray-tracing propagation tool is used [CGLM99]. The total field at a given point is computed as the sum of all different contributions originated from each sub-element, assuming that these elements are independent non-spherical sources. In this combination, the effects of reflections and diffractions due to obstacles near the antenna are taken into account.

For the far field region, which corresponds to $d > 2D^2/\lambda$, only the ray-tracing propagation tool is used, considering the effect of reflections and diffractions due to the presence of surrounding obstacles near the antenna. Obstacles need to be described according to their Electromagnetic (EM) properties, assuming that these properties are homogeneous within the volume of the obstacle. Considering the BS antenna as a single source, thus, using the overall radiation pattern, the total field is given by the vector sum of all contributions of transmitted, diffracted and reflected rays. If the antenna is located in an open area, where the presence of obstacles, i.e., buildings, can be neglected, one can simply employ the free space propagation expression described in [Gree90] and [Pars92] in order to evaluate the electric field level.

In order to evaluate the reliability of this prediction tool, a comparison with measurements has been conducted, concluding that the environment topology can slightly increase the field strength level in real cases with respect to a free space case. Regarding the relationship between EM exposure and the radius of the cell, it is concluded that in micro-cell scenarios, the reduction of the cell size translates into a better distribution of the field intensity, and consequently, into a reduction of exposure peaks.

In [GCKK09], a study aiming at the quantification of the absorption in the human body exposure in the vicinity of BS antennas by finite-difference time-domain simulations is presented, considering various anatomical characteristics of the exposed subject and typical parameters of BS antennas. The peak spatial average SAR and the whole body average SAR are analysed in three different anatomical models (55-101 kg) relative to the basic restrictions for occupational exposure, at distances between 0.5 m and 4 m from various antenna types operating at frequencies ranging from 450 to 2140 MHz.

Simulations are validated by an analysis of the impact of the mesh resolution on local and whole-body average SAR, as well as by experimental validation of the numerical models. The results demonstrate that the whole-body absorption generally determines the maximum permissible antenna output power for collinear array antennas and that the local exposure depends on various effects that fluctuate strongly among individuals.

In [HIKM08], maximum SAR estimation expressions for RF main beam exposure from mobile communication BS antennas are proposed. The expressions, despite empirical, are based on a set of physical observations, and are supported by results from a large number of studies in the literature. By using exposure limits, the SAR estimation expressions can be easily converted into expressions for distance compliance. The resulting compliance distance estimators produce results that are more accurate compared with results obtained with methods based on reference levels, such as the cylinder and the far field expressions. The behaviour of the SAR estimation expressions in the reactive near field region implies that they can be used to provide guidance on low-power exclusion for antennas that are comprised by the expressions.

Concerning indoor BSs, a method for evaluating the distribution of an electric field in order to assess the RF human exposure is presented in [HiTa11]. Indoor BS have built-in antennas to miniaturise the equipment and the electric field distribution must be measured to determine compliance with the exposure limit. In this study, the volume electric field distribution was evaluated from the two dimensional near field using the near field to far field technique. A measurement system has been developed in order to measure the amplitude and phase of an LTE transmission signal for a 2 GHz band patch antenna. The results proved to be accurate compared to simulation values as the compliance boundary corresponding to the exposure limit was determine from the electric field distribution.

The models previously presented allow the definition of a methodology in order to analyse field exposure levels as well as to identify exclusion regions around BS antennas. In [OFRC05], a simple approach to the estimation of exclusion zones around typical GSM and UMTS BS antennas based on the models found in the literature is presented, which have been adopted by Portuguese mobile phone operators

After the analysis of the different parameters of typical antennas provided by the operators, three installations scenarios were considered, considering similar types of antennas: Rtower/Utower, Uroof and Iceil, which are described in Table 2.3.

The values for the exclusion zones are obtained for the worst case scenario, in the direction of the main lobe of the antenna, whereas for the distance values for the exclusion zones on the sides and on the back of the antennas one needs to apply correction factors, depending on the direction considered. The distance is determined by estimating the distance where the power density or the field strength value is equal to the reference thresholds. The exclusion zone is, then, interpreted as an imaginary surface with a cylindrical shape around the BS antennas, just like the one presented in [MFRL02], Figure 2.2.

In order to evaluate the power density in the worst case, the far field model [CENE02a] is used because of its simplicity. However, the obtained values are around 20 times below the threshold values established in [ICNI98], meaning that the exclusion zone will be smaller than the model validity range ($2D^2/\lambda$). Therefore, the far field approximation model [MNMV02] is applied, since the minimum distance of this model is around 8 times smaller than the previous one, and it allows to get results at a much closer distance from the antennas.

Concerning the Iceil scenario, the obtained values in the minimum value distance are above the threshold values, meaning that the exclusion zone will be larger. For this scenario, the exclusion zone is then determined by estimating the distance from the antennas where the power density equals the threshold values. Since the antennas are omnidirectional, making the exclusion zone circular, there is no need to compute other values than D_{front}. As for the Rtower/Utower and Uroof scenarios, the obtained values are still below the threshold, but the model is still used as a measure of precaution, considering the exclusion zone as being the minimum valid distance of the model.

For the scenarios previously described, a cumulative use of four carriers in each system was also studied, as well as the co-location of networks with the existence of 1 and 4 carriers per system. The values obtained for the D_{front} in the different scenarios are presented in Table 2.9.

Table 2.9 – Exclusion region highest distance (extracted from [OFRC05]).

D_{front} [m]	Rtower/Utower		Uroof		Iceil	
	1 carrier	4 carriers	1 carrier	4 carriers	1 carrier	4 carriers
GSM900	3.00	4.18	2.94	4.17	0.18	0.72
GSM1800	5.87	5.87	5.75	5.75	0.09	0.36
UMTS	3.07	3.07	3.07	3.07	0.08	0.32
GSM900/GSM1800	5.87	5.87	5.75	5.75	0.27	1.09
GSM900/UMTS	3.07	5.59	3.07	5.58	0.26	1.05
GSM900/GSM1800/UMTS	5.87	6.86	5.75	6.87	0.35	1.41

One can conclude that carrier accumulation only presents a small increase in exclusion zones for the Iceil scenario and for GSM900, whereas the co-location of the three systems has an impact on the exclusion zone, making it larger especially in the Iceil scenario. The highest values occur for the situation where there is a co-location of the three systems with 4 carriers each.

The previous models focus mainly on cellular network BSs and access points. Since the exposure is induced by down- and uplinks, these actions do not fully respond to the relevant questions, and they can even induce a rise of exposure. In order to fill in this gap, a group of 17 leading telecommunications operators, vendors, research centres and academic institutions have launched a European project called Low EMF Exposure Future Networks Project (LEXNET) [LEXN13], aiming to develop effective mechanisms to reduce EMF exposure by 50%, without compromising the quality of service.

The strategic goal of LEXNET is to take into account the public concern about possible health effects

of electromagnetic fields and to improve the acceptability of existing and future wireless systems through low exposure systems without compromising the user's perceived quality. The project will:

- define a global index of exposure assessing the averaged exposure of the population over space and time, composed of up- and downlink sources;
- identify future network mechanisms, technologies, architectures and parameters, allowing the reduction of human exposure in the frequency bands from 0.4 to 6 GHz;
- build a "cost function" related to this exposure index, which can be used to optimise network architecture and operation, as well as the related technologies;
- experiment the proposed solutions.

2.5 State of the Art

Regarding the main subject of this work, exposure from BS with multiple systems, there are a few studies found in the literature that are described in this section.

In [OFRC05], as presented in the previous section, exclusion zones where determined in different scenarios considering the co-location of GSM 900, GSM 1800 and UMTS as well as the co-location of networks with the existence of 1 and 4 carriers per system.

In [Antu12], a method for the estimation of exclusion zones for LTE BS co-located with GSM and UMTS is presented and in [Oliv06] a study of the exclusion zones for GSM BS operating at different frequency bands is also presented.

In [CLJJX13], a prediction model for electromagnetic radiation of multi-system BS is presented, considering both 2G and 3G systems. The model takes into account the far field conditions, power density of the various systems and the average transmit power value in order to obtain a prediction of the shared BS electromagnetic radiation. Though antenna characteristic parameters, such as the normalised directivity function, antenna gain, gain of the array element, shaped gain, among others, the distribution of its power density of the multi-radiation source in multi-system BS is calculated with the purpose of establishing a comparison with the surveys and analysis of the actual electromagnetic radiation and environment.

In [AyFa13], a discussion on measurement and method in RF radiation exposure for BS with multiple systems is made, taking into account the type of study area, the need for preliminary study or assessment, study sampling time or period, exposure and distance/height relationship and the option of using a theoretical estimation model. This paper aims at highlighting the important areas of environmental RF exposure assessment, ranging from its dosimetric quantities to methods or procedure used during assessments.

The Australian Radiation Protection and Nuclear Safety Agency, ARPNSA, issued a technical report on Prediction Methodologies for Radio Frequency Electromagnetic Energy Exposure Levels

[ARPN02]. The report aim to provide power density equations as well as methods to determine compliance with relevant exposure limits for shared mobile phone BS sites.

In [AHIS13], a study is conducted in order to predict radio frequency radiation from mobile communication BSs, providing a prediction tool that can be applied to a BS with co-located multiple transmitters. In the proposed tool, one needs only to know the location of the antennas and their frequencies, powers, and gains to provide adequate input to the modelling tool. However, additional data such as the radiation pattern, orientation, height, and loss, can be used in order to improve the accuracy of the estimation.

The Executive Agency for Health and Consumers Framework of the Programme of Community Action in the Field of Health has financed a project with the objective of delivering a report on the level of exposure (frequency, patterns and modulation) in the European Union, the EHFRAN project [EHFRA10]. Along with the EMF exposure assessment in European Countries, the project also presented RF exposure assessments of sources far from the body and sources close to the body, mainly from mobile phones and short range wireless devices, such as Wi-Fi and Bluetooth. It also provides the trends of the RF exposure taking into account the future technologies.

In [KNNP14], a statistical analysis of electromagnetic radiation measurements in the vicinity of GSM/UMTS BSs antenna masts is presented, based on extensive EMF strength measurements carried out for 664 BS locations, classified into three categories: indoor, masts, and locations with installations on buildings. A detailed analysis of this location category was performed, and the measurement results were presented. It was concluded that the total electric field strength in the vicinity of BS antenna masts in no case exceeded $10\,V/m$, which is quite below the ICNIRP's reference levels.

Chapter 3

Model Development

This chapter concerns the EMF theoretical models used in this thesis as well as the developed models for the estimation of exclusion zones. The simulation tool and the implementation of the models is also discussed.

3.1 Theoretical Approximation Model

In order to determine the exclusion zone around an antenna, one needs to define the models to be used in order to evaluate EMF as a function of the distance to verify compliance with the recommendations described in the previous chapter. In this section, the models to be used in the far field and near field regions of an antenna are presented.

3.1.1 Far field Model

As described in Section 2.4, the far field model has been presented in [CENE02a] and can be used to estimate the RMS value of power density, *S*, at a distance *d* from the radiating element to the point of investigation by applying:

$$S(d,\theta,\phi)_{[\mathrm{W/m^2}]} = \frac{P_{in}G(\theta,\phi)}{4\pi d^2} \tag{3.1}$$

for distances:

$$d > \frac{2D^2}{\lambda} \tag{3.2}$$

where:

- *d*: Distance from the evaluation point;
- θ, ϕ: Elevation and azimuth angles;
- P_{in}: Input power of the antenna;
- $G(\theta,\phi)$:Generalised antenna gain;
- D: Largest dimension of the antenna;
- λ: Wavelength of the electromagnetic wave.

As for the RMS electric field, it is given by:

$$E(d,\theta,\phi)_{[\mathrm{V/m}]} = \frac{\sqrt{30P_{in}G(\theta,\phi)}}{d} \tag{3.3}$$

In this region there is no need to compute the magnetic field, as the electric field is enough to obtain all the information about EMF, whereas in the near field region one needs to compute both.

This model is useful for areas in the far field region of an antenna, whereas for distances closer to the antenna, it tends to overestimate the real EMF value and since exclusion regions are typically located in the near field region, there is a need to use an adequate model in this region.

3.1.2 Near field Model for Outdoor Antennas

One should note that the field behaviour in the far field region is well known and presents an inverse linear decrease with the distance. As EMF in the near field region of the antenna does not have the same behaviour, there is a need to apply an adequate model to estimate and take the transition from one region to the other into account. This procedure has been presented in [Antu12], by using the gain-based model [ABDK02] to obtain a linear estimation of EMF, as well as a definition of the field behaviour in between the far field and near field regions.

In the gain-based model, the near field of the entire antenna is approximated by the sum in amplitude and phase of the far field contributions of a shifted unit cell, providing a reasonably approximation at a distance of about two wavelengths away from the antenna, requiring a short computation time:

$$E(d,\theta,\phi) = \sum_{i=1}^{N_{el}} \frac{\sqrt{30 P_{in,i} G_e(\theta_i,\phi_i)}}{d_i} e^{-j(kd_i+\psi_i)} \hat{\mathrm{u}}(\theta_i,\phi_i) \quad (3.4)$$

for distances:

$$d > 2\lambda \quad (3.5)$$

where:

- $E(d,\theta,\phi)$: RMS electric field;
- d_i, θ_i, ϕ_i: Spherical co-ordinates centred at the *i*-th element of the array;
- N_{el}: Number of elements of the array;
- $P_{in,i}$: Input power of the *i*-th unit of the array;
- $G_{el}(\theta_i,\phi_i)$: Generalised gain of the *i*-th element;
- k: Propagation constant equal to $\frac{2\pi}{\lambda}$;
- ψ_i: Associated phase shift of the i-th element;
- $\hat{\mathrm{u}}(\theta_i,\phi_i)$: Co-polar vector of the *i*-th element.

Regarding the phase shift, ψ_i, it is related to the feeding currents of each unit of the array. Without considering the tilt angle and taking into account only the direction of maximum radiation as the perpendicular direction of the axis of the antenna, $\theta = \pi/2$, the phase shift is assumed to be zero so that all antenna elements provide a positive contribution to the antenna radiation [Moli11].

Typically, collinear array antennas have 2, 4 or 8 elements, with uniform spacing in between them equal to λ multiplied by a factor $\Delta_{da} \in [0.45, 1]$, as spacing is not always exactly equal to λ:

$$d_a = \Delta_{da} \ \lambda \quad (3.6)$$

In [Antu12], the author define an interpolation function, $E_{fit}(d)$, which provides the best fit of the maximum points of $|E(d)|$ as well as a function for the upper bound of the electric field, $E_{upper}(d)$. When estimating $E_{fit}(d)$ and $E_{upper}(d)$, the range defined for *d* implies that one should have the lower

bound equal to the limit imposed by the model, $d_{min} = 2\lambda$, and should not have high values for the d_{max} upper limit. Despite this last value is variable in the model, for a value around 6 m it has been proved that it can provide satisfactory results. In Figure 3.1, an example of the application of near field model for an LTE2600 outdoor antenna is presented.

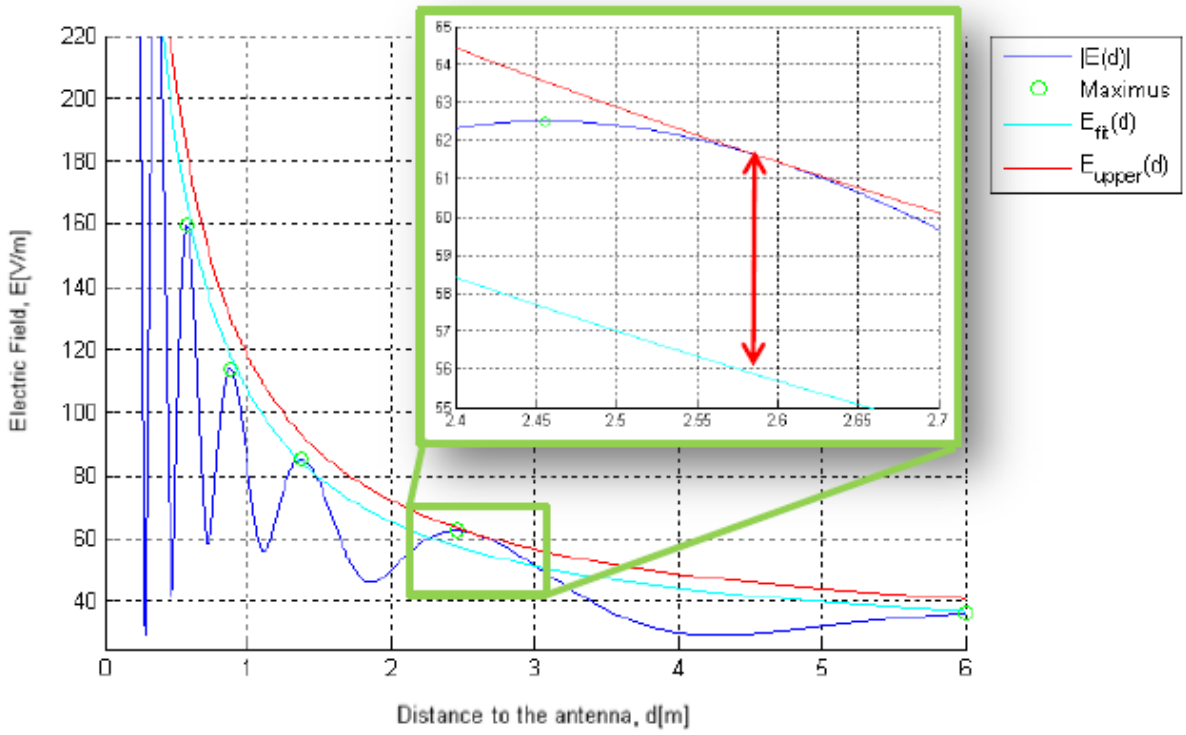

Figure 3.1 – Near field model application example (extracted from [Antu12]).

3.1.3 Field Model for Indoor Antennas

In this section, the field model for indoor antennas developed in [Antu12] is presented, in order to establish a ground for comparison with the model to be developed in this work.

Similarly to outdoors, for indoors one can have two different types of antennas: monopoles used for an omnidirectional radiation pattern, and microstrip antennas for sectorial antennas. For the first type of antennas, the monopole is considered to have a negligible diameter in order to simplify the problem. According to [Bala05], the electric field radiated by a monopole is given by:

$$E(d) = j\frac{Z_0 I_0 e^{-jkd}}{2\pi d}\frac{\cos(kl)\cos(\theta) - \cos(kl)}{\sin(\theta)}, \qquad 0 \leq \theta \leq \frac{\pi}{2} \tag{3.7}$$

where:

- Z_0:Free space characteristic impedance;
- I_0: Maximum electric current crossing the monopole;
- l: Length of the monopole.

The results from (3.7), when used in the near field region, may lead to a maximum phase error greater

than $\pi/8$ rad. For these antennas, it is also important to determine the field in the direction of the maximum radiation, using $\pi/2$ rad. Taking into account that the most common monopole length used in the systems considered in this work is $\lambda/4$, this value have been adopted, I_0 being given by:

$$I_0 = \sqrt{\frac{P_{in}}{R_{in}}} \tag{3.8}$$

As for the microstrip antennas, manufacturers do not usually provide all the important parameters that are required to perform the simulations, therefore, there is the need to define and determine these parameters. According to [Bala05] and [KaTH12], the length of the patch, *L*, has typically a value on the order of $\lambda/2$ and for the value of the width, *W*, one can apply:

$$W = \frac{\lambda}{2}\sqrt{\frac{2}{\varepsilon_r + 1}} \tag{3.9}$$

where ε_r is the relative dielectric constant of the substrate, with values between 2.2 and 12. One should note that the antenna performs better when ε_r is smaller, being more efficient, having a larger bandwidth and reducing the loss of radiated fields in space. On the other hand, the smaller ε_r gets, the thicker the dielectric substrate becomes. According to [PaPH12], [Tuan10], [ABOM09] and [LeSu09], for multiband antennas in wireless systems, typical values for $\varepsilon_r$and thickness, *h*, are 4.4 and 1.6 mm, respectively. According to [Bala05], the thickness of the patch can be neglected. In Figure 3.2, a scheme of a typical microstrip antenna is presented.

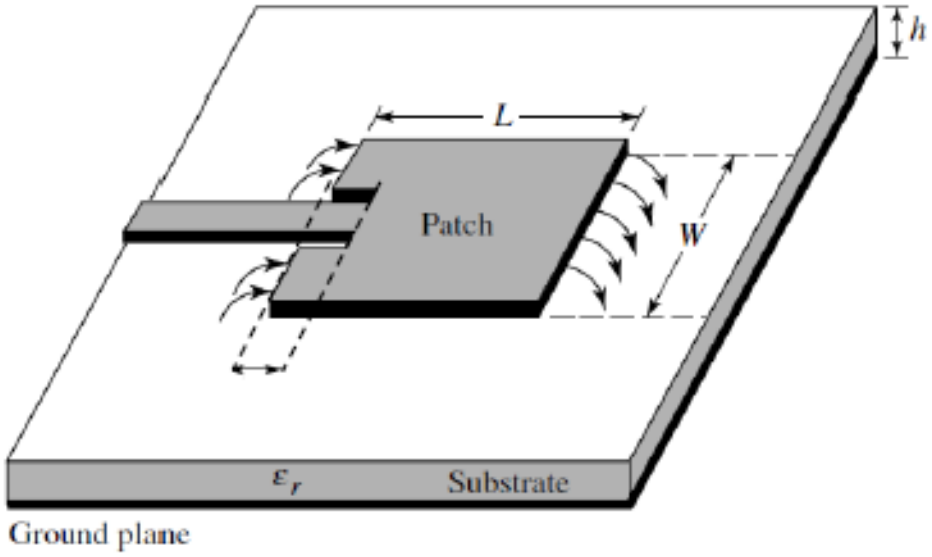

Figure 3.2 – Microstrip antenna (extracted from [Bala05]).

The values of *W* and *L* vary according with the working frequency, as the resonant frequencies affect different areas of the patch, being higher for lower frequencies.

The coordinate system for a microstrip antenna is presented in Figure 3.3. For the case where the

field configuration is the Transverse Magnetic mode TM_{010}^{x}, the radiated far field according to the cavity model, in the plane ($\theta = \pi/2$), is given by:

$$E_r \approx E_\theta \approx 0 \tag{3.10}$$

$$E_\phi(d) = j\frac{kWV_0 e^{-jkd}}{\pi d}\frac{\sin(\frac{kh}{2}\cos\phi)}{\frac{kh}{2}\cos\phi}\cos(\frac{kL_{ef}}{2}\sin\phi) \tag{3.11}$$

where:

- V_0: Voltage across the slot;
- L_{ef}: Effective length of the patch.

For the case when $L = \lambda/2$ and $L > W > h$, TM_{010}^{x} is the dominant mode.

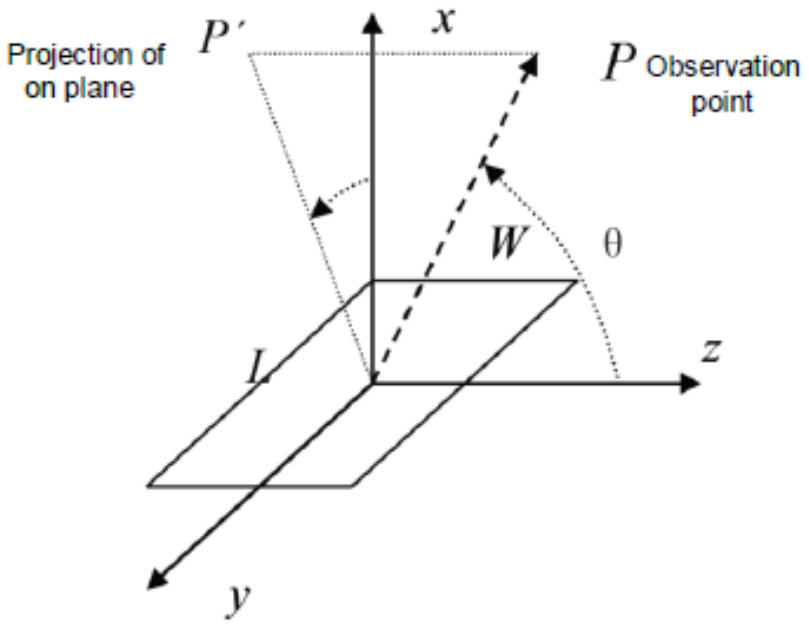

Figure 3.3 – Coordinate system for a microstrip antenna (extracted form [More12]).

3.1.4 Electric Field Global Model

Taking into account the methods defined in the previous sections for the estimation of EMF in the far field and near field regions of an antenna in [Antu12], a method for linking the two models has also been defined, in order to obtain an estimator of EMF continuously throughout distance.

The continuity is achieved by an interpolation between the two models, with the interpolation points being carefully chosen for this purpose. One of the chosen points limits the validity of the far field model, $S_{far}(d = 2\frac{D^2}{\lambda})$, resulting in an interpolation point equal to $P_b = (2\frac{D^2}{\lambda}, S_{far}\{d = 2\frac{D^2}{\lambda}\})$. As for the interpolation point relative to the near field model, it has been chosen as the intersection point between the electric field estimated by the gain based model $|S_{near}(d)|$ and its upper

bound, $S_{nupper}(d)$, resulting in the interpolation point $P_a = (d_{Pa}, S_{nupper}\{d = d_{Pa}\})$.

The defined strategy for point P_a consists on the determination of all intersection points, giving preference to the most distant points of the antenna. To do so, an auxiliary variable has been defined, indicating which value of *d* is used by the model to find a point of intersection. This value is supposed to be less than the far field distance and, for the purpose of this work, a value of 4 m has been considered acceptable. For the case where the program does not find an intersection point within this range of values, the farthest point of intersection from the antenna is used.

The new interpolation function is obtained in the radiating near field region and, therefore, the interpolation polynomial function is also given by (3.12) with the same algorithm being used to determine new values for the coefficients *A'*, *B'* and *C'*. The expression of S_{total} of the global model is given by:

$$S_{total} = \begin{cases} S_{nupper}(d), & 2\lambda \leq d < d_{Pa} \\ A'd^{-2} + B'd^{-1} + C', & d_{Pa} \leq d < \dfrac{2D^2}{\lambda} \\ \dfrac{P_{in}G}{4\pi d^2}, & d \geq \dfrac{2D^2}{\lambda} \end{cases} \tag{3.12}$$

with $S_{nupper}(d) = {Z_0}^{-1} \; E^2_{upper}(d)$.

The most important auxiliary variables are the simulation range and the number of samples (N_{sp}) contained within this range. The lower bound (d_{min}) takes values of λ and 2λ for indoor and outdoor antennas, respectively, and for the outdoor antennas, the upper bound (d_{max}) should always be greater than the far field distance. The accuracy of the model is directly related to the number of samples, and therefore a value above 60,000 samples is considered acceptable in order to obtain accurate results. The sampling interval is obtained by:

$$\Delta_{sp} = \frac{d_{max} - d_{min}}{N_{sp}} \tag{3.13}$$

The values for the electric field of the global model coincides with the estimated ones for the near field region at a distance up to d_{Pa}. The global model is given by the interpolation method described above when the distance has values between d_{Pa} and far field distance. From the validity limit of the far-field, the electric field of the global model coincides with the far field one. In Figure 3.4, an example of the global model for an LTE 2600 outdoor antenna is presented.

The main input parameters of the model are the antenna dimensions, input power, gain, mobile communication system, input resistance and environment, but other parameters such as N_{sp}, d_{max}, d_{min} or N_{el} can be managed as well. The performed approaches had in mind the worst-case perspective of EM radiation exposure, meaning the BS resources are fully used at the lowest frequency of the used band. The environment around the antenna has not been considered.

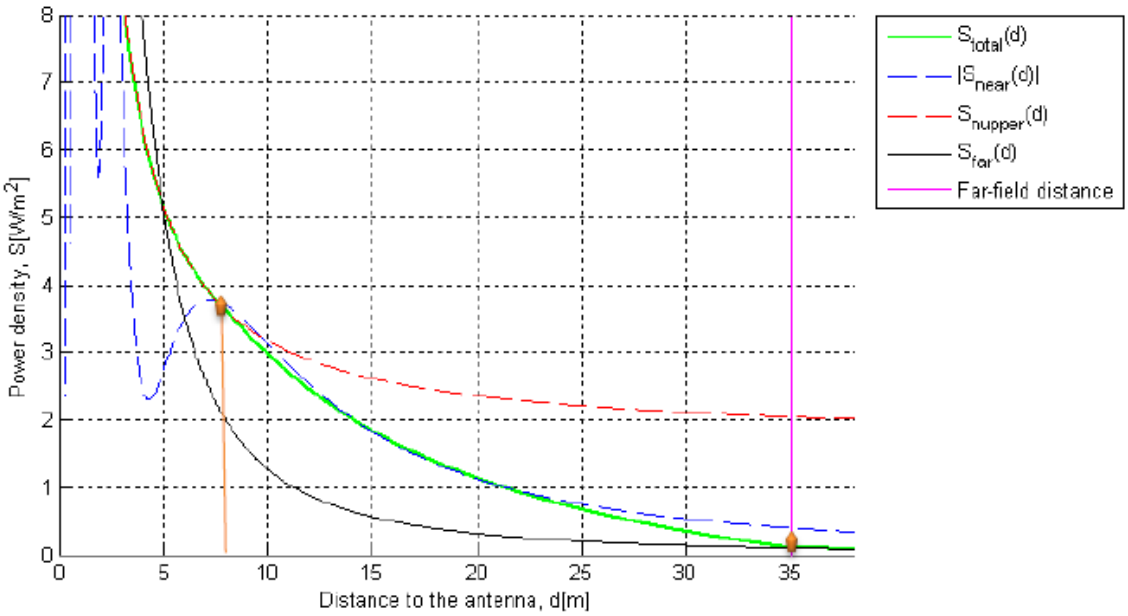

Figure 3.4 – Global model example for an LTE 2600 antenna (extracted from [Antu12]).

3.1.5 Distance Evaluation Model

The global model developed in [Antu12] and presented in the previous sections allows the estimation in the direction of maximum radiation so that the value of the front border of the exclusion zone, D_{front}, can be determined. Regarding the other directions, a model considering correction factors has been described in [MFRL02] and [Antu12] for a cylindrical exclusion zone, being presented in this section.

Using the expression that relates the reference levels with the electric field, as a function of *d*, one can obtain the D_{front} value:

$$\sum_{i>400MHz}^{300\,GHz} \frac{S_i(d)}{S_{ref,i}} \leq 1 \leftrightarrow (\dots) \leftrightarrow d \geq D_{front} \tag{3.14}$$

where:

- $S_i(d)$: Power density at frequency i as a function of the *distance;*
- $S_{ref,i}$: Power density reference level from ICNIRP guidelines at frequency i.

Taking into consideration the conditions of the problem, (2.1) can be rewritten according to the number of carriers, number of MIMO antennas as well as the number of communication systems installed in the same site:

$$R(d) \leq 1 \tag{3.15}$$

with:

$$R(d) = \sum_{i=1}^{N_s} N_{c,i} \quad N_{M,i} \quad \frac{S_{total,i}(d)}{S_{ref,i}} \tag{3.16}$$

where:

- N_s: Number of communication systems installed in the site;
- $N_{c,i}$: Carrier number of the communication system i;
- $N_{M,i}$: Number of MIMO elements of the BS in the communication system i;
- $S_{total,i}(d)$: Power density of the system i obtained with the global model;
- $R(d)$: Exposure function.

In [Antu12], a method of iteration of the value *d* that verifies the condition $R(d) \leq 1$ has been presented in order to reduce the complexity of (3.29), since it requires the computation of a system with three equations. Therefore, the value of D_{front} is given by the value of *d* that verifies $R(d) = 1$. As for the simulation range, d_{min} takes the value 2λ, with λ being the maximum wavelength of all the systems involved in the simulation, for the outdoor scenario and equal to λ for the indoor scenario. As for the upper bound, d_{max} should ensure $d_{max} > D_{max}$ for both outdoor and indoor scenarios.

For the situation when $d_{max} < D_{max}$, no conclusions can be taken regarding the exact value of the exclusion region, because of the limitations of the model. Nevertheless, one can apply a model from those presented in Chapter 2, which are valid for distances closer to the antenna, but are considerably more complex compared to the model presented in this work.

As for the implementation in a MatLab program, the main input parameters are $N_{c,i}$, $N_{M,i}$ in addition to the input parameters of the electric field global model. When considering a system or an antenna without the MIMO technology, $N_{M,i}$ is equal to one.

For the purpose of analysing the power contribution that GSM, UMTS or LTE BS antennas have on the exclusion zone, a power ratio (ρ_i) has been defined, with the values ranging from zero to one:

$$\rho_i = N_{c,i} \quad N_{M,i} \quad \frac{S_{total.i}(d = D_{front})}{S_{ref,i}} \tag{3.17}$$

Since the model was developed mainly for the direction of maximum radiation, perpendicular to the array alignment and with the axis in the mass centre of the antenna, the values to be obtained for the other directions, are overestimated.

The determination of the values for the back (D_{back}), bottom (D_{bottom}), top (D_{top}) and side (D_{side}) borders of the exclusion zone is made by applying the method of cylindrical exclusion zone [MFRL02] presented in Chapter 2. The normalised gains are determined as a function of the propagation direction from the analysis of the antenna radiation patterns, then being applied as correction factors (CF) to the values obtained in the direction of maximum radiation. In multiband BSs, the normalised gain used corresponds to the smallest value found in bands/antennas (value that provides more gain).

Also from [MFRL02], the expressions for the top and bottom borders of the exclusion zone, taking the tilt used to maximise the coverage of a given antenna into account, are the following:

$$D'_{top} = D_{top} \cos\theta_{dt} \quad (3.18)$$

$$D_{bottom}{}' = D_{bottom}(1 + \sin\theta_{dt}) \quad (3.19)$$

where:

- $D_{top}{}'$: Top border of the exclusion zone when downtilt is used;
- $D_{bottom}{}'$: Bottom border of the exclusion zone when downtilt is used.

For the case where the BS radiates omnidirectionally, the horizontal plane has a circular exclusion zone, which means:

$$D_{side} = D_{back} = D_{front} \quad (3.20)$$

3.2 Antenna Modelling

In order to obtain results that allow the improvement of the theoretical models described in the previous sections, one has chosen to use the CST Studio Suite [CSTe14] to develop models for the antennas.

3.2.1 CST Antenna Design

In CST, there are several Design Environments, but one has used the CST Microwave Studio since it is the more adequate to simulate 3D electromagnetic high frequency problems.

For the purpose of antenna modelling, there are a number of parameters that need to be defined, such as the dimensions of the antenna, the frequency band and the materials that constitute each part of the antenna. In CST, there is the possibility of defining several parameters in a parameter list and then associate the parameters with objects is the design environment, e.g., defining the physical dimensions of the antenna in the list and then create a rectangle with the dimensions defined in order to create the back of a panel antenna. After creating the physical structure of the antenna, CST allows one to define the material that constitutes each part of the antenna, using for example copper or nickel.

The frequency range chosen must be as wide as possible, because the solver used in the simulations is the Transient Solver [CSTe14]. This solver calculates fields' developments in time, so, with a wide frequency band, the excitation signal will be small in time, decreasing the time of each simulation, comparing with a simulation with a narrower band. The selection of the best meshing for the simulations is also a very important matter, because, similar to the frequency band, much time and processing power may be spared, as it is explained in the next section.

Bandwidth and simulation time have an inverse relation, but the upper frequency must not be defined

randomly, because the higher it is the higher the number of mesh cells will be. This results in a higher simulation time and more memory requirements for each simulation, meaning that a balance, between bandwidth and the maximum frequency, must be found.

In this work, one uses two different models, one for an indoor scenario using a microstrip patch antenna, and another for an outdoor scenario using a dipole array in a panel antenna, which are detailed in the following sections.

3.2.2 Indoor Model

For an indoor environment, one has considered a typical microstrip patch antenna [Bala05], which can be used for GSM, UMTS and LTE in the frequency bands of interest for this work.

A microstrip antenna generally consists of a dielectric substrate sandwiched between a radiating patch on the top and a ground plane on the other side, the patch being generally made of conducting material, such as copper, which is used in the model for this scenario.

For a simplicity of analysis, the patch is generally square, rectangular, circular, triangular, and elliptical or some other common shape. In this scenario, one considers a rectangular patch, where the length L of the patch is usually in the range 0.33 $\lambda_0 < L < 0.5\ \lambda_0$, λ_0 being the free space wavelength. The patch is selected to be very thin, such that $M_t << \lambda_0$, where M_t is the patch thickness. The height h of the substrate is usually $0.003\ \lambda_0 \leq h \leq 0.05\ \lambda_0$. The relative dielectric constant of the substrate ε_r is typically in the range $2.2 \leq \varepsilon_r \leq 12$.

Microstrip patch antennas can be fed by a variety of methods. These methods can be classified into two categories; contacting and non-contacting. In the contacting method, the RF power is fed directly to the radiating patch using a connecting element such as a microstrip line. In the non-contacting scheme, electromagnetic field coupling is done to transfer power between the microstrip line and the radiating patch. In the model for this work, the antenna is fed using a microstrip line, which consist of a conducting strip connected directly to the edge of the microstrip patch. The conducting strip is smaller in width compared to the patch. This kind of feed arrangement has the advantage that the feed can be etched on the same substrate to provide a planar structure.

The representation of the dimensions of a microstrip patch antenna is presented in Figure 3.2. According to [Bala05], the design procedure starts by defining the values of the relative dielectric constant of the substrate,ε_r, the intended resonant frequency, f_r, and h. The next step is the determination of the width, *W* of the patch, for which there is the following equation:

$$W = \frac{c}{2f_r}\sqrt{\frac{2}{\varepsilon_r + 1}} \tag{3.21}$$

where c is the free space speed of light.

From the electrical point of view, the antenna looks greater than its physical dimensions, due to fringing effects, defining the effective length as well as the effective dielectric constant, ε_{reff}, due to

the waves that travel in the substrate and air. The value of ε_{reff} is given by:

$$\varepsilon_{reff} = \frac{\varepsilon_r + 1}{2} + \frac{\varepsilon_r - 1}{2}\left[1 + 12\frac{h}{W}\right]^{-1/2} \tag{3.22}$$

with $\frac{W}{h} > 1$.

In order to determine the effective length of the patch, one needs to compute the extension of the length, ΔL, as a function of ε_{reff} and the width-to-height ratio, $\frac{W}{h}$ using the following equation:

$$\frac{\Delta L}{h} = 0.412\frac{\left(\varepsilon_{reff} + 0.3\right)\left(\frac{W}{h} + 0.264\right)}{\left(\varepsilon_{reff} - 0.258\right)\left(\frac{W}{h} + 0.8\right)} \tag{3.23}$$

This length extension is shown in Figure 3.5.

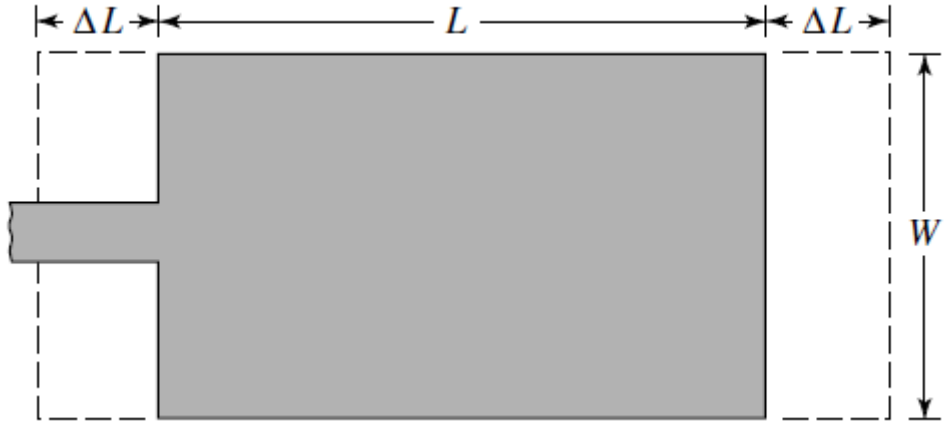

Figure 3.5 – Effective lengths of a rectangular microstrip patch (extracted from [Bala05]).

The actual length of the patch can now be determined by solving:

$$L = \frac{c}{2f_r\sqrt{\varepsilon_{reff}}} - 2\Delta L \tag{3.24}$$

Finally, the effective length is computed using:

$$L_{eff} = L + 2\Delta L \tag{3.25}$$

Once having determined the dimensions of the patch, one needs to design the microstrip line feed, as shown in Figure 3.6. According to [Bala05], the typical impedance at the edge of a resonant rectangular patch ranges from 100 to 400 Ω. The radiation impedance of a patch at the edge, Z_a can be approximated as:

$$Z_a \approx 90\frac{\varepsilon_r^2}{\varepsilon_r - 1}\left(\frac{L}{W}\right)^2 \tag{3.26}$$

For the cases when the value of Z_a does not match well with a 50 Ω standard microstrip, a transition

section should be used, with a characteristic impedance, Z_T given by:

$$Z_T = \sqrt{50 \ Z_a} \tag{3.27}$$

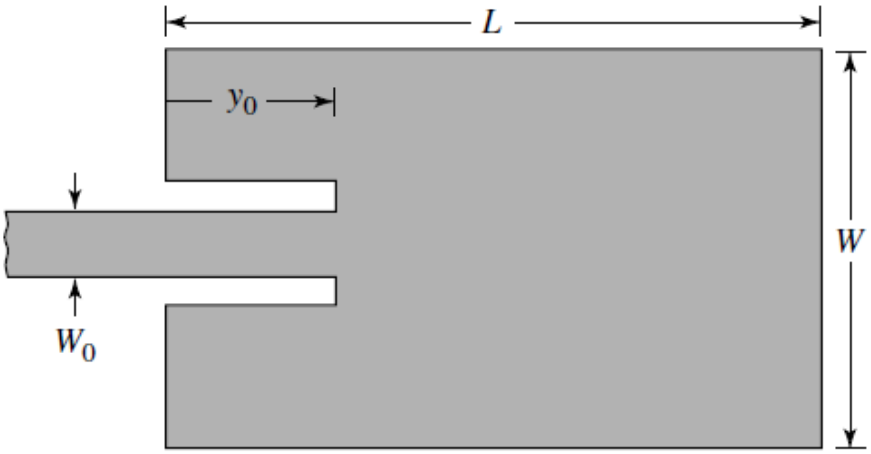

Figure 3.6 - Microstrip line feed (extracted from [Bala05]).

The design of the inside feed can be done using the following equation:

$$R_{in}(y = y_0) = R_{in}(y = 0) \ \cos\left(\frac{\pi \ y_0}{L}\right)^2 \tag{3.28}$$

Where the recessed distance (the length cutting into the patch), y_0 can be obtained by:

$$y_0 = \frac{L}{\pi}\cos^{-1}\left(\sqrt{\frac{50}{Z_T}}\right) \tag{3.29}$$

The width of the inset feed, W_0 can be obtained from the characteristic impedance of the line, Z_0 which for this work is considered to be the standard 50 Ω, using the following equation:

$$Z_0 = \frac{120\pi}{\sqrt{\varepsilon_r}\left(\frac{W_0}{h} + 1.393 + 0.667 \ \ln\left(\frac{W_0}{h} + 1.44\right)\right)} \tag{3.30}$$

with $\frac{W}{h} > 1$ and $Z_0 < \frac{126}{\sqrt{\varepsilon_r}}$.

With this, all the main parameters of a microstrip patch antenna using an inset feed are obtained, allowing for the development of the antenna, either in a real fabrication or using a simulation tool, which is the case for this work, allowing one to develop various models for the various scenarios of interest.

One should note that the main parameters of the antenna should be chosen in order to obtain the worst case scenario in terms of EM radiation, providing a ground for comparison with the recommended values.

3.2.3 Outdoor Model

For an outdoor environment, a dipole array for a panel antenna has been considered. In Figure 3.7, the structure of the antenna is presented, outlining the main physical dimensions.

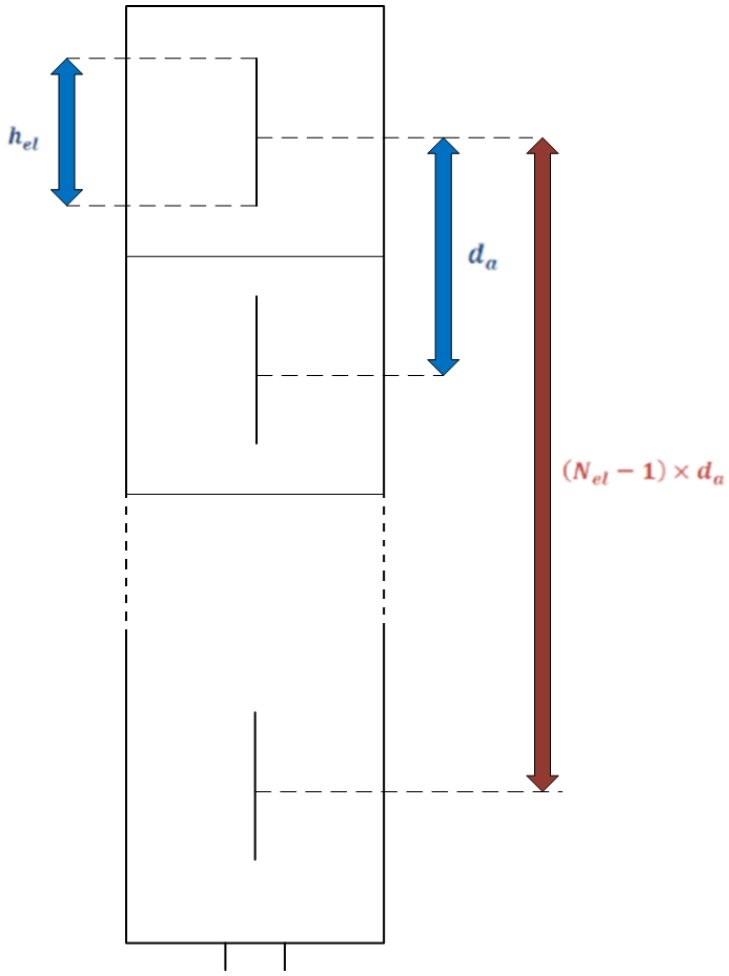

Figure 3.7 – Dimension analysis of an antenna array.

The length (L) and radius (R) of the dipole as well as the gap (g) in-between the dipole can be computed from [Bala05], by using the following expressions:

$$L = 0.45\lambda \tag{3.31}$$

$$R = 0.005\lambda \tag{3.32}$$

$$g = 0.0224\lambda \tag{3.33}$$

As discussed in Section 3.1.2, the spacing between dipoles, d_a is given by:

$$d_a = \Delta_{da}\ \lambda \tag{3.34}$$

where $\Delta_{da} = [0.45, 1]$. Usually, the value of d_a is not provided by manufacturers in antennas datasheets, and it cannot be much larger than a wavelength. When it takes values equal to one, it can

lead to values without any physical meaning, especially if the total length of all the spacing elements is larger than the real height of the antenna.

The height of the antenna array is given by:

$$h_{ant} = (N_{el} - 1) \;\; d_a + h_{el} \tag{3.35}$$

with:

$$h_{el} = L + g \tag{3.36}$$

where h_{el} is the height of an antenna element.

In order to design the back cover of the antenna, one has to define its dimensions and characteristics. In Figure 3.8, the height (h_c), width (W_c) and thickness of the panel as well as the length (L_c) of the top and bottom of the cover are presented.

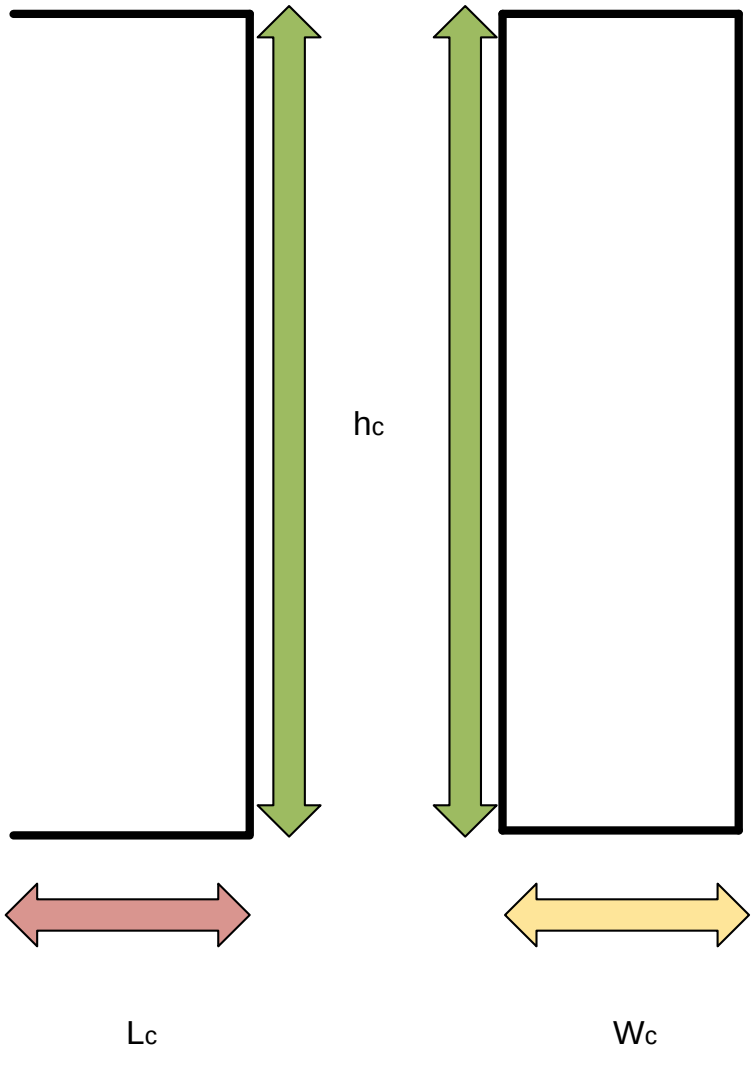

a) Side View b) Back View

Figure 3.8 – Dimensions analysis of the metal cover of the antenna.

From the analysis of a real antenna, one has defined equations to determine all the dimensions of the cover. Thus, the width and height of the back panel are obtained from:

$$W_c = 2L \tag{3.37}$$

$$h_c = N_{el}\ d_a \tag{3.38}$$

For the top and bottom of the cover, the length can be obtained from:

$$L_c = \frac{2\lambda}{3} \tag{3.39}$$

The dipoles are considered to be at a distance of $\frac{\lambda}{3}$ from the back panel and the cover is made of aluminium with a thickness of 3 mm.

3.3 CST Simulator

The main parameters that need to be defined within CST are the units, frequency band and meshing. The antennas previously developed can be used and the surrounding environment such as walls and materials can be drawn within CST as well. For the purpose of analysing the field radiated by the antenna, one can use one of the models provided in CST, such as the far field model, or use probes to determine a certain field component in a certain position.

CST uses FIT (Finite Integration Technique), which consists of a numerical method that performs a spatial discretisation in the time or frequency domains of the integral form of Maxwell's equations, instead of the usual differential one. In order to solve Maxwell's equations numerically, a finite calculation domain needs to be defined, which is to be divided into small cell grids. Equations are established for each side of the cells, as shown in Figure 3.9. Using the example in Figure 3.10, the closed integral on the equation's left side can be rewritten as the sum of all four grid components in each face of the cell. The right-hand side of the equation corresponds to the time derivative of the magnetic flux defined on the enclosed primary cell facet.

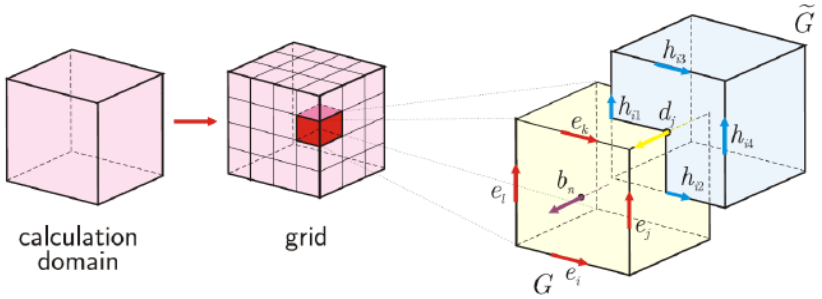

Figure 3.9 – FIT spatial discretisation scheme (extracted from [CSTe14]).

The repetition of this procedure for all cell sides introduces the topological matrix **C**, as the discrete

equivalent of the analytical curl operator, as shown in Figure 3.10.

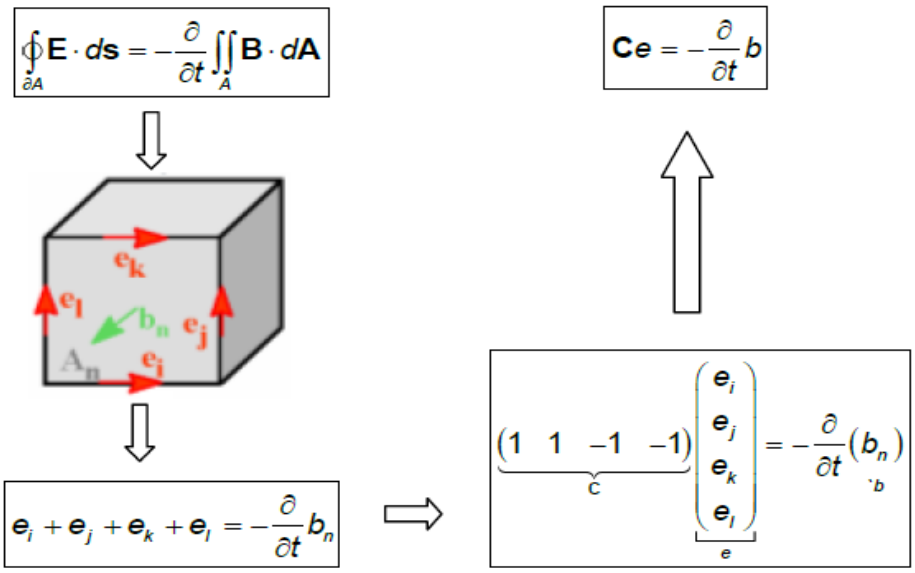

Figure 3.10 - Graphic representation of the discretisation of Maxwell's integral equations (extracted from [CSTe14]).

When applying the method to all four Maxwell's equations, one can obtain the complete discrete Maxwell's Grid Equations (MGEs):

$$\boldsymbol{C}e = -\frac{d}{dt} b \tag{3.40}$$

$$\tilde{\boldsymbol{C}}h = -\frac{d}{dt} d + j \tag{3.41}$$

$$\boldsymbol{S}b = 0 \tag{3.42}$$

$$\tilde{\boldsymbol{S}}d = q \tag{3.43}$$

where:

- b: Magnetic flux;
- d: Electric flux;
- j: Electric flux density;
- h: Magnetic voltage;
- e: Electric voltage;
- q: Electric charge;
- $\boldsymbol{C}$: Discrete curl operator;
- $\tilde{\boldsymbol{C}}$: Dual discrete curl operator;
- $\boldsymbol{S}$: Discrete divergence operator;
- $\tilde{\boldsymbol{S}}$: Dual discrete divergence operator;

At this point, no errors have been introduced with the discretisation of Maxwell's equations. Also, with FIT, the important properties of the continuous gradient, curl and divergence operator, are still maintained in the grid space. The missing material relations introduce numerical inaccuracy due to spatial discretisation, however, since the set of MGEs maintain energy and charge conservation, the FIT approach is not affected by this problem.

When defining the basic relations concerning voltages and fluxes, their integral values have to be approximated over grid edges and cell areas, respectively. Therefore, the resulting coefficients depend on the averaged material parameters as well as on the spatial resolution of the grid, being represented in corresponding matrices, [Oliv13].

FIT supports a number of unique advanced meshing features that differentiate it from other numerical techniques. Such features include the so called Perfect Boundary Approximation (PBA), Thin Sheet Technique (TST) and Multilevel Subgridding Scheme (MSS), [CSTe14].

PBA is a proprietary technology that allows to accurately represent curved geometrical features in the model without resorting to any geometrical simplifications. In particular, it helps to avoid the geometrical simplifications typically incurred by the staircase approximation, Figure 3.11. The staircase approximation results because in most time domain techniques, such as the FDTD, a given mesh cell can only represent the material properties (permittivity, permeability, etc.) of one type of material. Thus, when a mesh cell is partially filled with two different materials, the ambiguity can only be resolved by filling the cell with the material properties of one or the other material; at best, with an average value based on the filling ratio between the two materials.

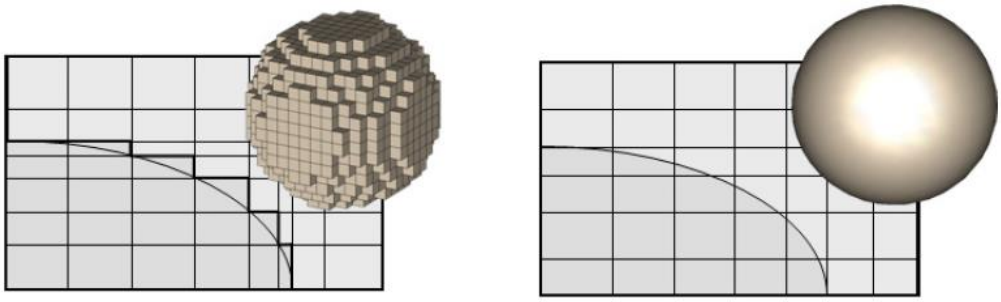

a) Staircase approximation. b) PBA.

Figure 3.11 – Different types of meshing a sphere (extracted from [CSTe14]).

PBA is based on the fact that the path for integration (needed for the numerical solution of Maxwell's equations within each mesh cell), can be chosen to conform to the geometry of the object inside the cell, rather than to the edges/faces of the cell itself. In this way, the simulated structure and the electromagnetic fields can be mapped to the hexahedral mesh. This allows a very good approximation of even curved surfaces within the cuboid mesh cells.

As PBA can be used to conform the geometry of a given object within a mesh cell, TST allows to conform to the geometry of a thin metallic sheet inside a mesh cell, Figure 3.12. The major advantage of this technique is that it allows to properly represent thin metallic sheets without having to explicitly mesh them using a fine mesh, which has a huge impact on the simulation time.

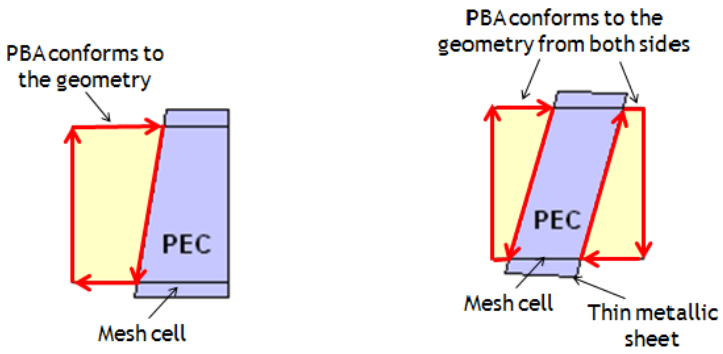

a) PBA b) TST

Figure 3.12 – Meshing techniques (extracted from [CSTe14]).

MSS is also a proprietary technology that guarantees that a very dense mesh is only created within critical regions of the model. However, the computation overhead that results from the complex interfaces caused by MSS is only justified if the number of mesh cells is decreased by a factor of 3 to 5, which limits the number of models where the use of this technology is justified. A typical application where the use of MSS is fully recommended is the simulation of small antennas inside large computational volumes, as shown in Figure 3.13.

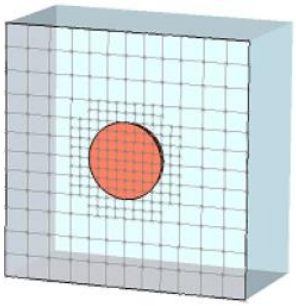

Figure 3.13 – Mesh using MSS (extracted from [CSTe14]).

3.4 Model Assessment

In order to validate the developed models, CST has been used to perform simulations in order to obtain the electric field values for the scenarios of interest in this work. The simulations were made for both indoor and outdoor scenarios, considering GSM, UMTS and LTE in their respective bands.

The values of the electric field were obtained in the direction of maximum radiation as a function of the distance from the antenna. This was achieved by placing near and far field probes at various distance points from the antennas. Each probe has the capability of computing a field component value, the far field probes performing the calculations by using the far field approximation.

These results allow the possibility to study the field behaviour both in near and far field regions as well as the near field to far field transition. With these results, a comparison between simulation results and

the values obtained with from theoretical models previously presented can be made, in order to improve the theoretical models, especially concerning the transition between near and far fields.

The scenarios are detailed in the next chapter, along with the simulation conditions for each scenario. The obtained results and the analysis of the results for the context of this work are also presented in Chapter 4.

In order to validate the developed models, one has to analyse the radiation pattern of the antennas as well as some obtained results from simulations. As described in Section 3.2.2, for an indoor model one has considered a microstrip patch antenna. In Figure 3.14 and Figure 3.15, the horizontal and vertical radiation patterns of a patch operating at 800 MHz are presented.

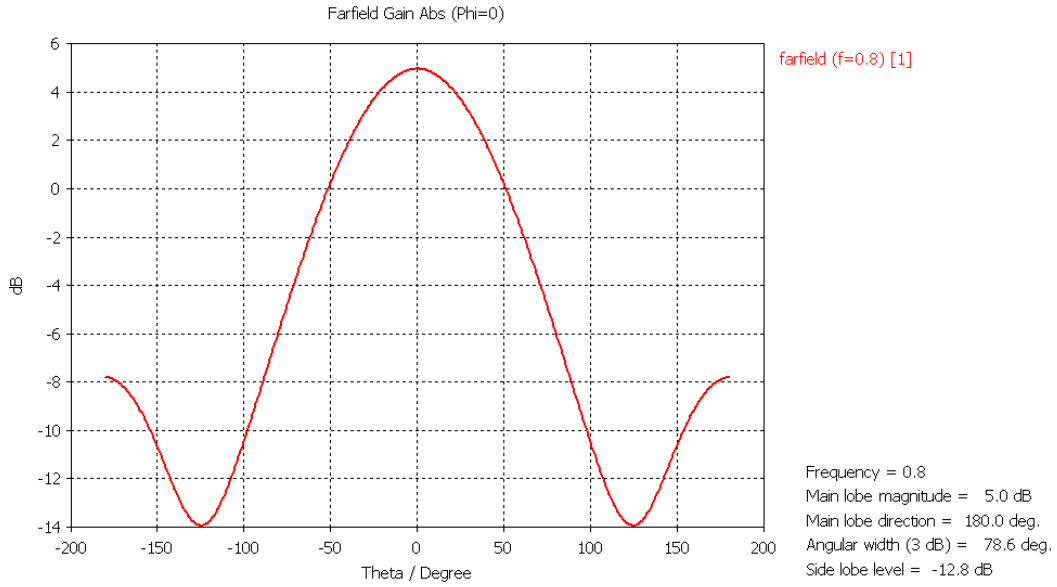

Figure 3.14 - Horizontal radiation pattern of an 800 MHz microstrip patch antenna.

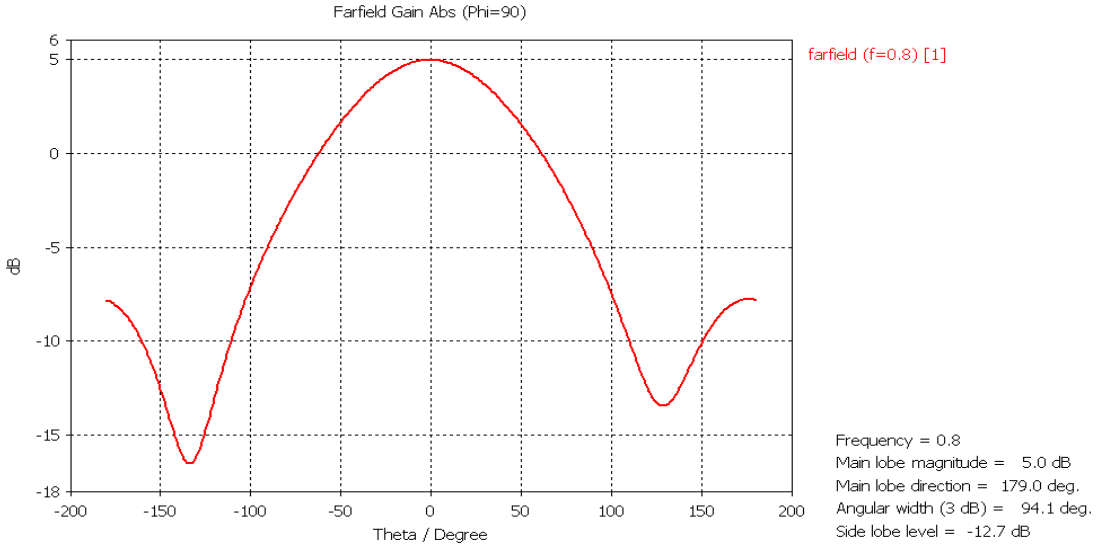

Figure 3.15 – Vertical radiation pattern of an 800 MHz microstrip patch antenna.

In Figure 3.16, an example of the comparison between electric field results obtained with simulations and the ones computed with the far field model for the 800 MHz microstrip patch antenna is presented, considering a distance range of 50 cm in the direction of maximum radiation and an input power of 1W. The results are consistent with the assumptions made when using the far field model, in which the obtained values for the electric field are overestimated in the region closer to the antenna, the near field region. With the increase of distance, especially in the far field region, results have proven to be accurate compared to the ones obtained by simulations, and one can conclude that the model is well designed.

For an outdoor model, one has considered a dipole array, as described in Section 3.2.3. Similarly to the previous model, one is going to analyse an outdoor antenna operating at 800 MHz. In Figure 3.17 and Figure 3.18, the horizontal and vertical radiation patterns of the array are presented, considering the antenna with the back cover.

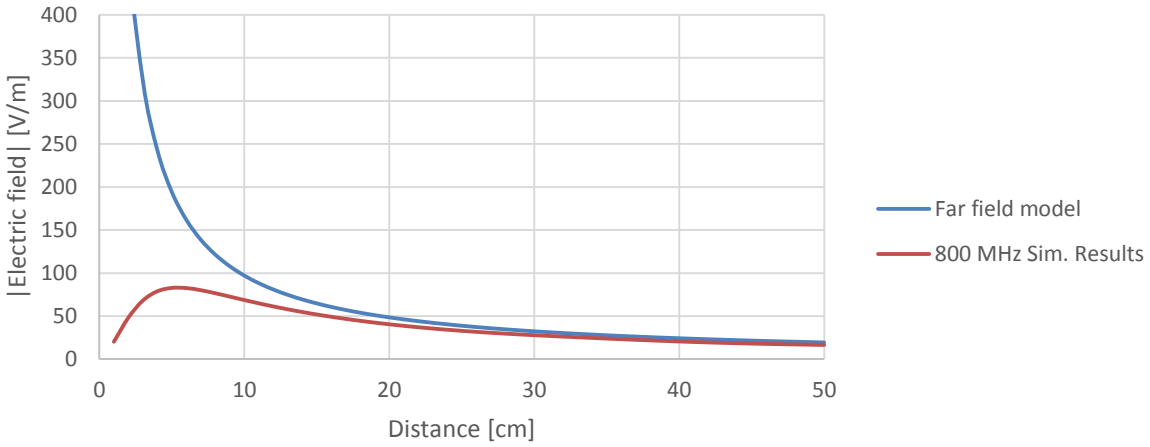

Figure 3.16 – Comparison between electric field results obtained from simulations and the ones from applying the far field model for an indoor model.

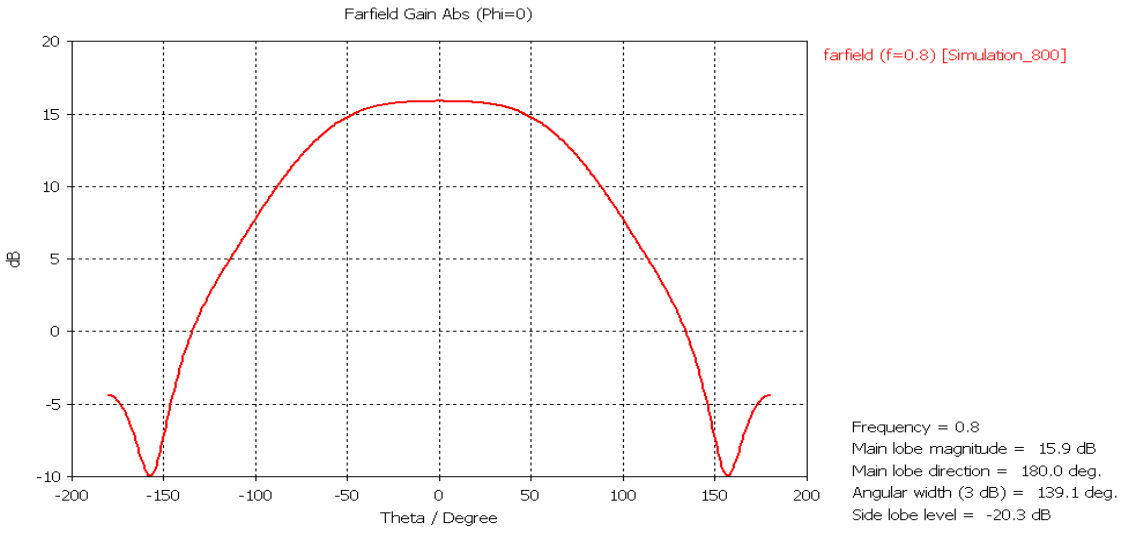

Figure 3.17 – Horizontal radiation pattern of an 800 MHz dipole array antenna.

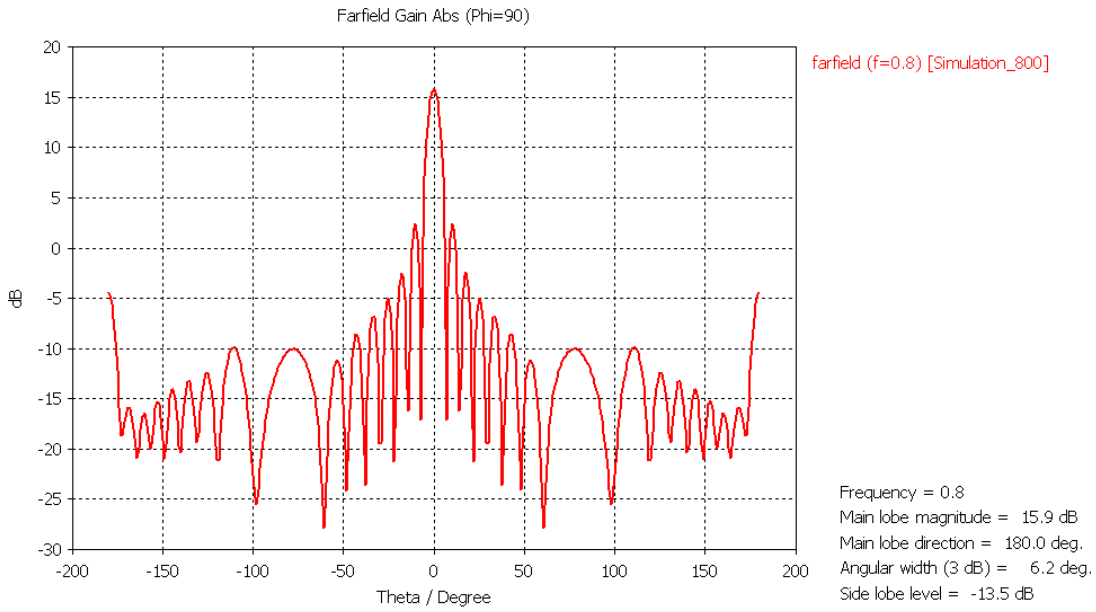

Figure 3.18 – Vertical radiation pattern of an 800 MHz dipole array antenna.

Similarly to the previous model, in Figure 3.19 an example of the comparison between electric field results obtained with simulations and the ones computed with the far field model for the 800 MHz dipole array antenna is presented, considering a distance range of 30 m in the direction of maximum radiation and an input power of 1 W.

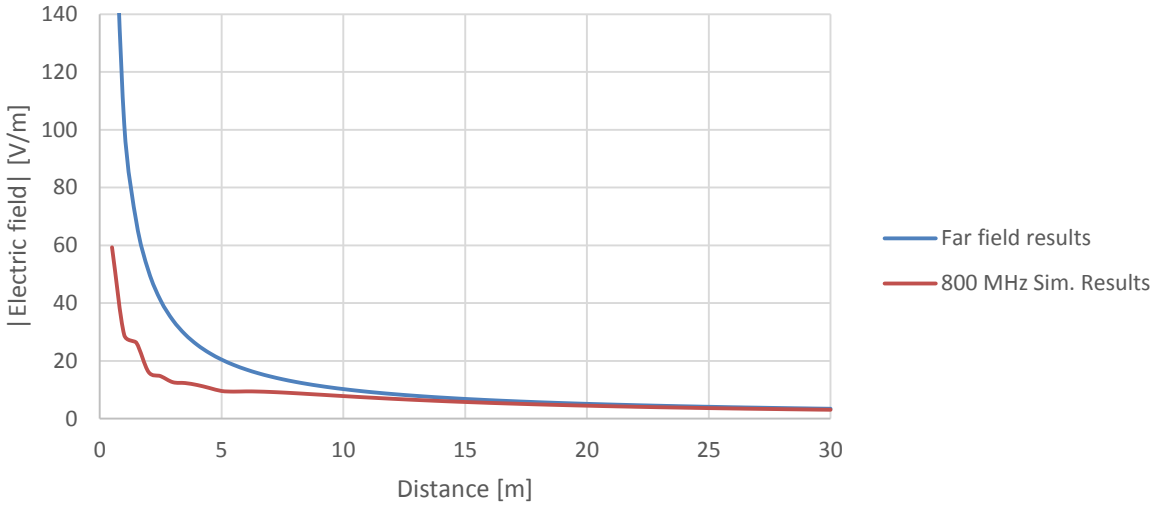

Figure 3.19 - Comparison between electric field results obtained from simulations and the ones from applying the far field model for an outdoor model.

Again, the results are consistent with the assumptions made when using the far field model, in which the obtained values for the electric field are overestimated in the region closer to the antenna, the near field region. With the increase of distance, results have proven to be accurate compared to the ones obtained by simulations, and one can conclude that the model is well designed.

From this analysis, the models are validated in order to be applied under the different scenarios that are described in the following chapter.

Chapter 4

Result Analysis

In this chapter, the scenarios analysed in this work are presented. Both simulation and theoretical results are analysed and the resulting models are defined. The models are compared with data from measurements, and the values of the obtained exclusion zones are presented.

4.1 Scenarios Definition

In this section, the scenarios under analysis are presented: first, an indoor scenario where the model of a microstrip patch antenna is used, and then an outdoor scenario with the model of a dipole array. For both scenarios, the surrounding environment of the antennas as well as the simulation conditions, such as the meshing, are defined.

4.1.1 Indoor Scenario

In an indoor scenario, the typical installations of BS antennas are on the ceiling and on walls. The antennas are usually at a height of at least 50 cm people [OFRC05], as shown in Figure 4.1.

a) Indoor antenna in ceiling b) Indoor antenna in the wall

Figure 4.1 – Typical indoor BS installations (extracted from [OFRC05]).

For the purpose of this work, and taking the characteristics of indoor BS installations into account, one has considered to model a microstrip patch antenna in CST. As the physical dimensions of the antenna depend on the intended resonant frequency, different antennas were developed in this scenario, one for each frequency of interest, the antenna parameters for each frequency being computed according to the indoor model described in Section 3.2.2 and the results presented in Table 4.1.

Table 4.1 - Parameters of the indoor model correspondent to each considered frequency.

f [MHz]	800	900	1800	2100	2600
ε_r	4.30				
h [mm]	4.50				
W [mm]	115.18	102.38	51.20	43.88	35.33
ε_{reff}	4.01	3.98	3.80	3.75	3.67
ΔL [mm]	2.09	2.08	2.05	2.04	2.02
L [mm]	89.44	79.32	38.64	32.78	25.99
L_{ef}[mm]	93.62	83.49	42.74	36.86	30.00
y_0 [mm]	31.00	27.50	13.46	11.44	9.10
W_0 [mm]	8.5				

Regarding the environment surrounding the antenna, as the typical cover of a microstrip antenna is made of plastic and the antenna is usually located on the ceiling or walls, it is neglected, as it poses no substantial effect into the exclusion region from the antenna in the direction of interest. Consequently, the scenario consists only of the microstrip patch antenna. In Figure 4.2, an example of the model of the microstrip patch antenna for the 1800 MHz band developed in CST is presented. The complete set of models developed is presented in Annex A.1.

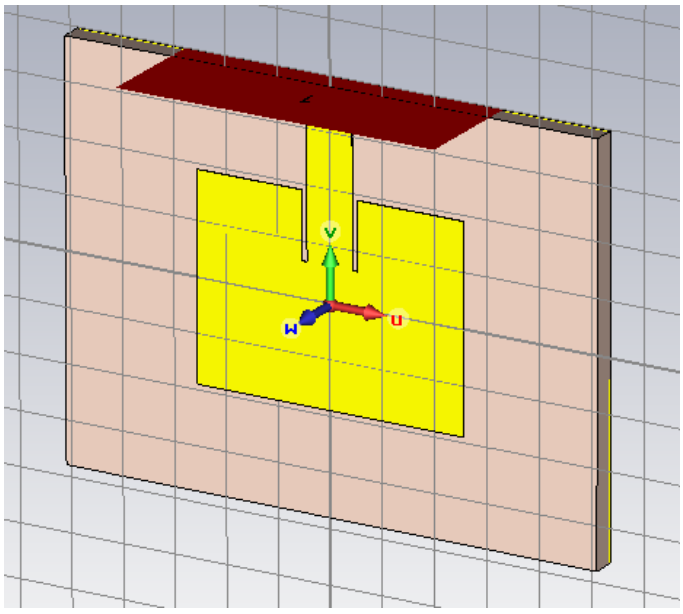

Figure 4.2 – 1800 MHz microstrip patch antenna model from CST.

Due to the planar geometry of the antenna, a hexahedral mesh is used. As described in Section 3.3, both TST and PBA are used, in order to minimise the simulation time while optimising simulation results. In Table 4.2, the mesh parameters for all the considered scenarios are defined.

Table 4.2 – Mesh parameters for the different frequencies considered in the indoor scenario.

f [MHz]	800	900	1800	2100	2600
Lines per wavelength	30				
Lower mesh limit	20				
Mesh line ratio limit	20				
Number of mesh cells	696 696	746 460	1 338 444	1 505 520	1 852 740

Despite the fact that the models for the lower frequencies have larger dimensions, the number of mesh cells is also related to the frequency range of the simulation. A narrowband analysis (e.g., [2.4, 2.6] GHz) has the disadvantage of reaching unfeasible computation times, while a wideband one performs faster due to the shorter excitation signal. However, the upper frequency should be chosen carefully, not being too large, as the number of mesh cells rapidly increases with it. In Table 4.3, the frequency range for each model is specified.

Table 4.3 – Frequency range defined in CST for each indoor antenna model.

f [MHz]	800	900	1800	2100	2600
Frequency range	[0.3, 1]	[0.3, 1]	[0.3, 2]	[0.3, 2.3]	[0.3, 2.8]

4.1.2 Outdoor Scenario

The most common outdoor BS installations are on rooftops and façades for urban sites and in masts for rural sites, as the ones presented in Figure 4.3. For this scenario, one has decided to model a dipole array on a panel antenna, as described in Section 3.2.3.

For the panel antenna, one has considered a dipole array with $N_{el} = 8$. The value of Δ_{da} was defined from [Bala05], as being equal to λ. The values of all the physical dimensions of the antenna, needed for the design and taking into account the value of N_{el} and the frequency in consideration, are presented in Table 4.4.

a) Rooftop BS installation. b) Mast BS installation.

Figure 4.3 – Typical outdoor BS installations (extracted from [OFRC05]).

Table 4.4 – Parameters of the outdoor model correspondent to each considered frequency.

f [MHz]	800	900	1800	2100	2600
λ [m]	0.375	0.33	0.167	0.143	0.115
Δ_{da}	1				
h_{el} [mm]	177.15	157.31	78.89	67.55	54.32
d_a [mm]	0.375	0.33	0.167	0.143	0.115
h_{ant} [m]	2.63	2.33	1.17	1.00	0.81
L [mm]	168.75	149.85	75.15	64.35	51.75
g [mm]	8.40	7.46	3.74	03.20	2.57
R [mm]	1.875	1.665	0.835	0.715	0.575

The back cover of the antenna has also been modelled according to the analysis presented in Section 3.2.3, the dimensions for all the considered frequencies being presented in Table 4.5.

Table 4.5 – Dimensions of the back cover for each considered frequency.

f [MHz]	800	900	1800	2100	2600
Thickness [mm]	3				
h_c [m]	3.00	2.67	1.34	1.14	0.92
W_c [cm]	33.75	29.97	15.03	12.87	10.35
L_c [cm]	25.00	22.20	11.13	9.50	7.60

In Figure 4.4, an example of the model of the dipole array antenna operating at the 800 MHz band developed in CST is presented. The complete set of models developed is presented in Figure A.6 to Figure A.10. In Table 4.6, the mesh parameters for the models designed in this scenario are presented. The frequency range considered for the simulations are the same as in the indoor model. Similarly to the indoor model, a hexahedral mesh is used along with TST and PBA to reduce the simulation time while providing the most accurate results possible.

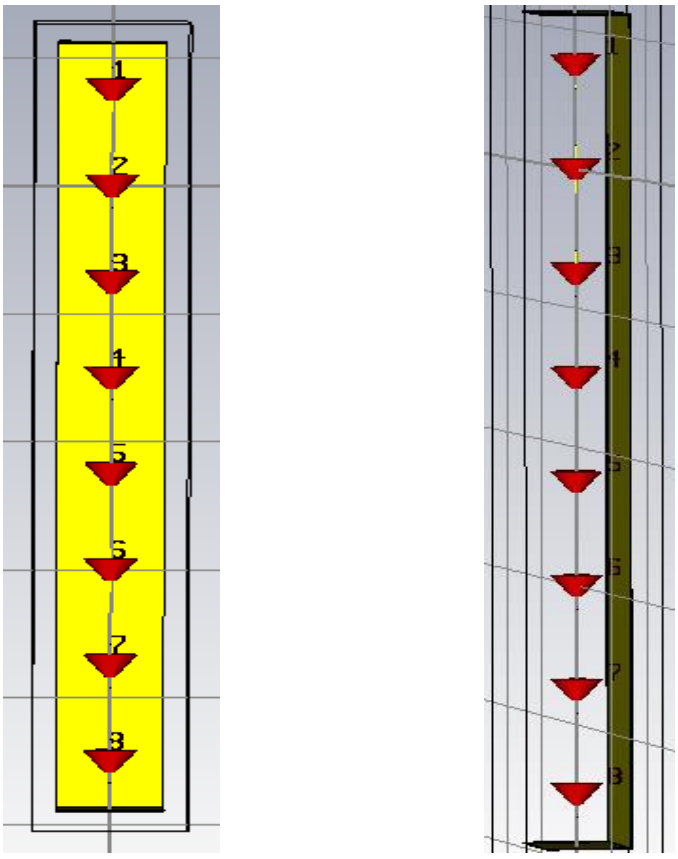

a) Front view. b) Side view.

Figure 4.4 – Example of an 800 MHz outdoor dipole array from CST.

Table 4.6 – Mesh parameters for the different frequencies considered in the outdoor scenario.

f [MHz]	800	900	1800	2100	2600
Lines per wavelength	20				
Lower mesh limit	15				
Mesh line ratio limit	20				
Number of mesh cells	48 698 640	62 114 304	128 208 624	134 249 574	157 394 812

4.2 Model from Simulations

In order to design a model for the evaluation of the electric field in both indoor and outdoor scenarios, one has performed simulations to provide a ground for comparison with theoretical results obtained with the far field model described in Section 3.1.1.

4.2.1 Global Indoor Model

First, the indoor scenario is analysed. The far field distance values for the different frequencies considered in this scenario, computed from (2.3), are presented in Table 4.7. One should note that the largest dimension of the antenna is obtained through the diagonal between 2*L* and 2*W*, which are the dimensions of the substrate.

Table 4.7 - Far field distance for the antenna models in the indoor scenario.

f [MHz]	800	900	1800	2100	2600
d_{ff} [cm]	45.4	40.3	19.8	16.8	13.4

In Figure 4.5, an example of the comparison between simulation results and the values obtained with the far field model is presented. The electric field values were obtained for the 800 MHz scenario, considering the direction of maximum radiation and an input reference power of 1 W.

In order to design an equation to model the behaviour of the electric field, the following border condition is required:

$$\overline{\varepsilon_r} = \frac{1}{n} \sum_{n=1}^{10} \varepsilon_{r_n} \quad (4.1)$$

with:

$$\overline{\varepsilon_r} \leq 10\% \quad (4.2)$$

were:

- ε_{r_n}: Error measured at distance n [cm] when using the far field results instead of the simulation ones.

This equation is useful to determine the distance $d_{c,i}$ below which one should use the model resulting from the simulations instead of the far field one. This condition implies that the maximum acceptable error within a distance range of 10 cm is 10%. In Table 4.8, the values of $d_{c,i}$ obtained for the considered frequencies are presented.

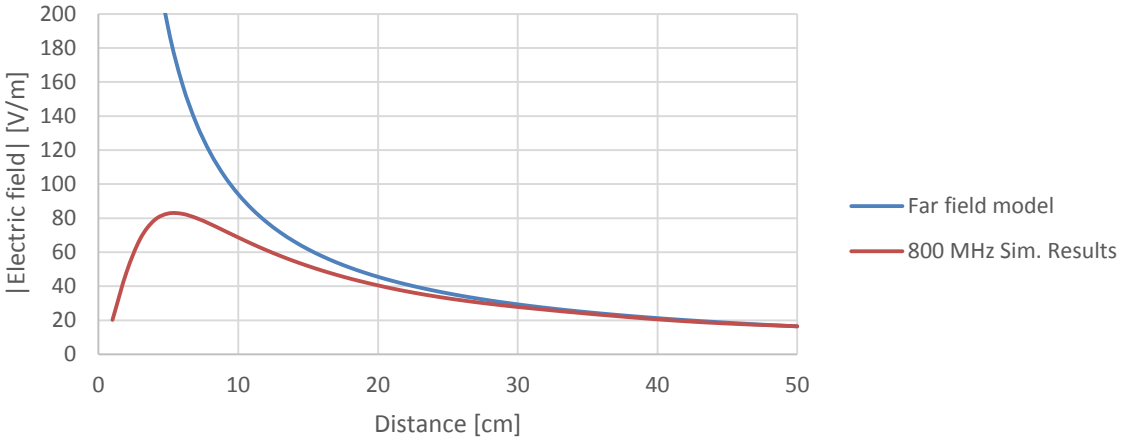

Figure 4.5 - Comparison between far field model results and simulation results for the 800 MHz indoor scenario.

Table 4.8 – Boundary condition ($d_{c,i}$) between the model from the simulations and the far field model for the indoor scenario.

f [MHz]	800	900	1800	2100	2600
$d_{c,i}$ [cm]	25	24	15	14	13
$d_{c,o}$ [m]	26	25	13	12	11

Taking these values into account, one has to determine equations to model the behaviour of the field for distances below $d_{c,i}$. In order to simplify the expression of the model, in Figure 4.6, an example of the comparison between simulation results and the values obtained with the far field model is presented, considering the same values in dB, and in Figure 4.7, a comparison between the results for all the considered frequencies is presented. The results for the other frequencies are presented in Annex B.1.

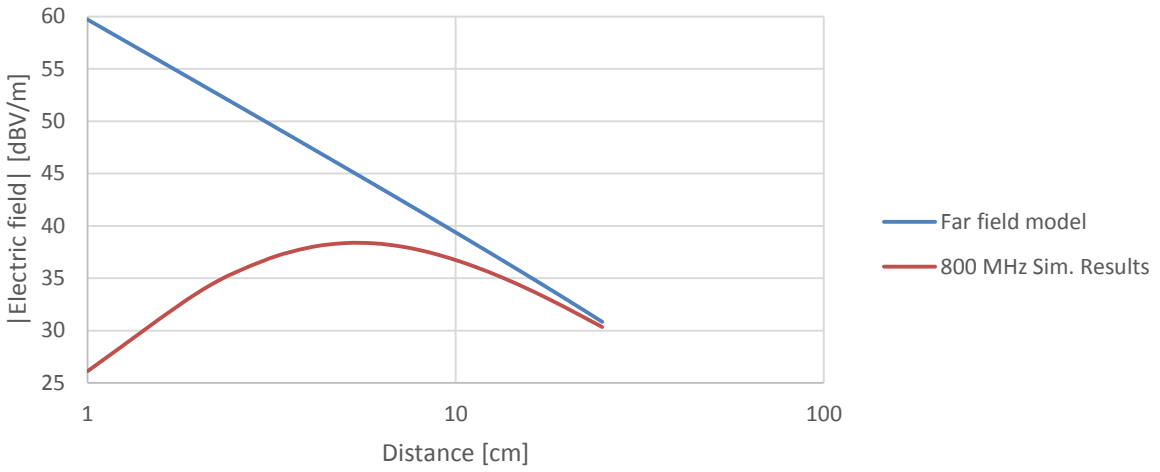

Figure 4.6 - Comparison between far field model results and simulation results in dBV/m for the 800 MHz indoor scenario.

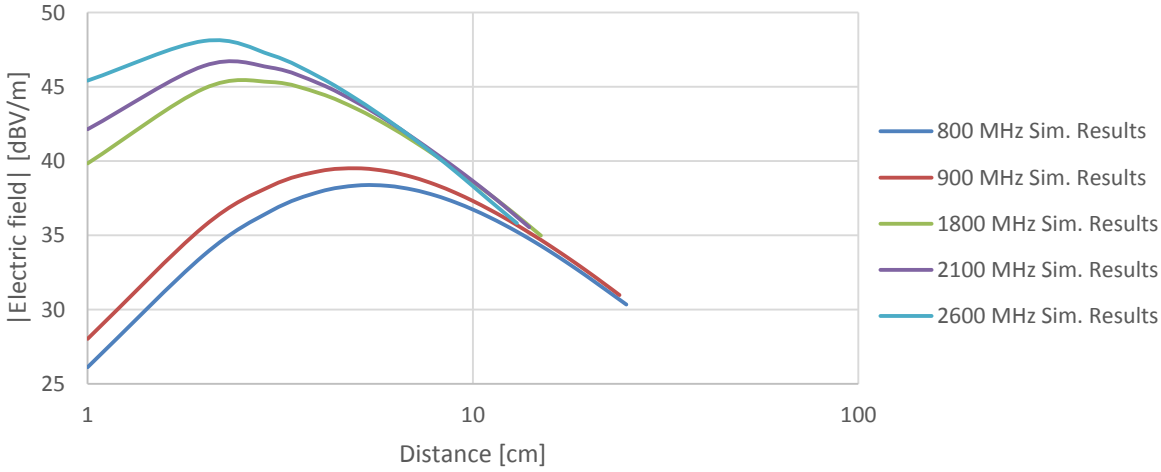

Figure 4.7 – Comparison between electric field results in dBV/m from simulations for all the frequencies considered in the indoor scenario.

Using these curves, one is able to design an equation to model the behaviour of the field radiated from microstrip patch antennas operating in different frequencies. The goal is to obtain an expression in the form:

$$E(d)_{[\mathrm{dBV/m}]} = \sum_{n=0}^{2} \{C_n(f) \ \ (20\log(d_{[\mathrm{cm}]}))^n\} \tag{4.3}$$

where:

- $C_n(f)$: Coefficient dependent on the working frequency;
- d: Distance point of analysis;

The expressions of the curves corresponding to the simulation results, along with the coefficients for each frequency considered in this scenario, were obtained by using the trend line option for polynomial functions of Excel, allowing one to design the resulting model from the simulations given by:

$$E(d)_{[\mathrm{dBV/m}]} = \left\{C_2(f)\ \ \left(20\log\left(d_{[\mathrm{cm}]}\right)\right)^2 + C_1(f)\ \ 20\log\left(d_{[\mathrm{cm}]}\right) + C_0(f)\right\}, \qquad d < d_{c,i} \tag{4.4}$$

with the coefficients for the frequencies under analysis presented in Table 4.9.

Table 4.9 – Indoor simulation model coefficients.

f [MHz]	C_2	C_1	C_0
800	-0.049	1.537	26.363
900	-0.049	1.468	28.482
1800	-0.049	0.933	40.385
2100	-0.049	0.785	42.671
2600	-0.049	0.509	45.867

From both mathematical analysis and the trend line option for linear and polynomial functions of Excel, expressions for the determination of the coefficients were determined:

$$C_2(f) = 0.000003\ f_{[\mathrm{MHz}]} - 0.0537 \tag{4.5}$$

$$C_1(f) = -0.0006\ \ f_{[\mathrm{MHz}]} + 1.9833 \tag{4.6}$$

$$C_0(f) = -0.000004\ f_{[\mathrm{MHz}]}^2 + 0.0235\ \ f_{[\mathrm{MHz}]} + 10.205 \tag{4.7}$$

From Figure B.6 to Figure B.8, a comparison between the coefficient values from Table 4.9 and the ones obtained from (4.5) to (4.7) is presented. The average error resulting from the application of the functions in the determination of the coefficients for the considered frequencies is 4% for $C_2(f)$, 7% for $C_1(f)$ and 2% for $C_0(f)$, which are considered to be acceptable error values.

The comparison between simulation results and the ones obtained by using the indoor model from simulations for the considered frequencies is presented from Figure B.9 to Figure B.13, resulting in an average error of 1% for all frequencies, which again is considered to be an acceptable error.

With these results, a global indoor model can be designed, considering the model from equations for distances below $d_{c,i}$ and the far field one for distances higher than $d_{c,i}$. This model is valid for microstrip patch antennas with an input power of 1 W, allowing one to determine the electric field in the direction of maximum radiation without overestimating the field values in the region closer to the antenna. The global indoor model is then, given by:

$$\begin{cases} E(d)_{[\mathrm{dBV/m}]} = \sum_{n=0}^{2} \left\{C_n(f)\ \ \left(20\log\left(d_{[\mathrm{cm}]}\right)\right)^2\right\}, & d < d_{c,i} \\ E(d)_{[\mathrm{dBV/m}]} = 20\log\left(\dfrac{\sqrt{30G_T}}{d_{[\mathrm{m}]}}\right), & d \geq d_{c,i} \end{cases} \tag{4.8}$$

4.2.2 Global Outdoor Model

Similarly to the indoor scenario, the far field distance for the different frequencies considered in the outdoor scenario, computed from (2.3), are presented in Table 4.10.

Table 4.10 - Far field distance for the antenna models in the outdoor scenario.

f [MHz]	800	900	1800	2100	2600
d_{ff} [m]	48.00	42.62	21.38	18.30	14.72

In Figure 4.8, an example of the comparison between the variation of the electric field with distance obtained from simulations and the one obtained with the far field model is presented. The electric field values were obtained for the 800 MHz scenario, considering the direction of maximum radiation and an input reference power of 1 W. The results for the other frequencies are presented in Annex B.1.

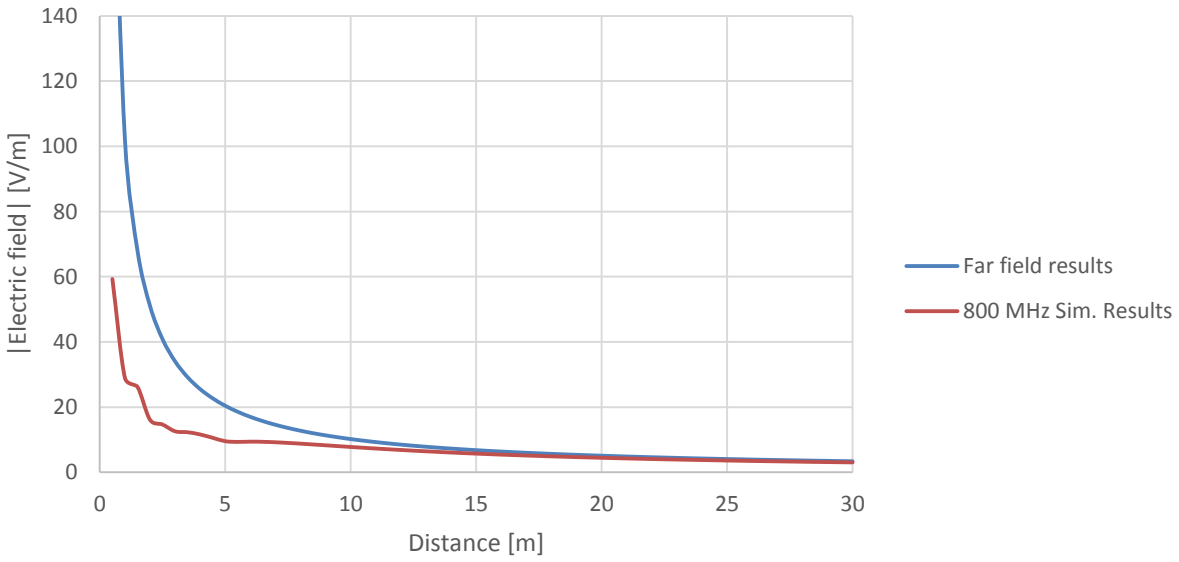

Figure 4.8 - Comparison between far field model results and simulation results for the 800 MHz outdoor scenario.

For the outdoor scenario, the boundary condition, $d_{c,o}$ is determined throughout an analysis similar to the one that was done on the indoor one:

$$\bar{\varepsilon_r} = \frac{1}{n} \sum_{n=1}^{i} \varepsilon_{r_n} \tag{4.9}$$

with:

$$\bar{\varepsilon_r} \leq 10\% \tag{4.10}$$

were:

- ε_{r_n}: Error measured at the distance n [m] when using the far field results instead of the simulation ones.

For this scenario, one has considered a maximum acceptable error of 10% within a distance range of 1 m. The obtained results for $d_{c,o}$ are presented in Table 4.11.

Table 4.11 – Boundary condition ($d_{c,o}$) between the outdoor model from simulations and the far field model for the outdoor scenario.

f [MHz]	800	900	1800	2100	2600
$d_{c,o}$ [m]	26	25	13	12	11

Again, following the approach made for the indoor scenario, one has to determine equations to model the behaviour of the field for distances below $d_{c,o}$. In order to simplify the expression, in Figure 4.9, an example of the comparison between simulation results and the values obtained with the far field model is presented, considering the same values in dB, and in Figure 4.10, a comparison between the results for all the considered frequencies is presented. The results for the other frequencies are presented individually in Annex B.1.

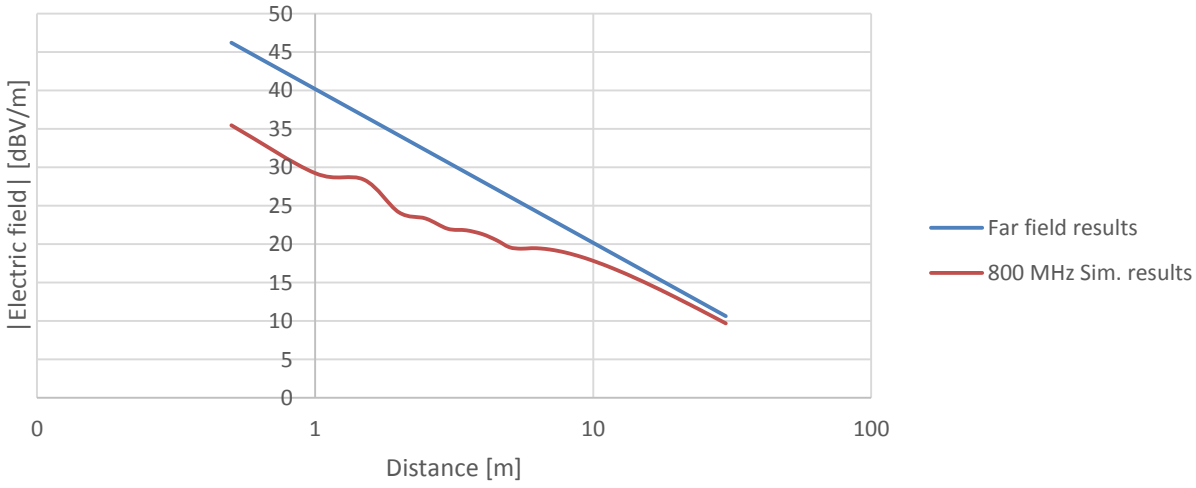

Figure 4.9 - Comparison between far field model results and simulation results in dBV/m for the 800 MHz outdoor scenario.

Using this curves, one is able to design an equation to model the behaviour of the field radiated from the dipole array antennas operating in different frequencies. The goal is, then, to obtain an expression in the form:

$$E(d)_{[\mathrm{dBV/m}]} = \sum_{n=0}^{1} \left\{ C_n(f) \quad \left(\log\left(d_{[\mathrm{cm}]} \right) \right)^n \right\} \tag{4.11}$$

where:

- $C_n(f)$: Coefficient dependent on the working frequency;

- d: Distance point of analysis;

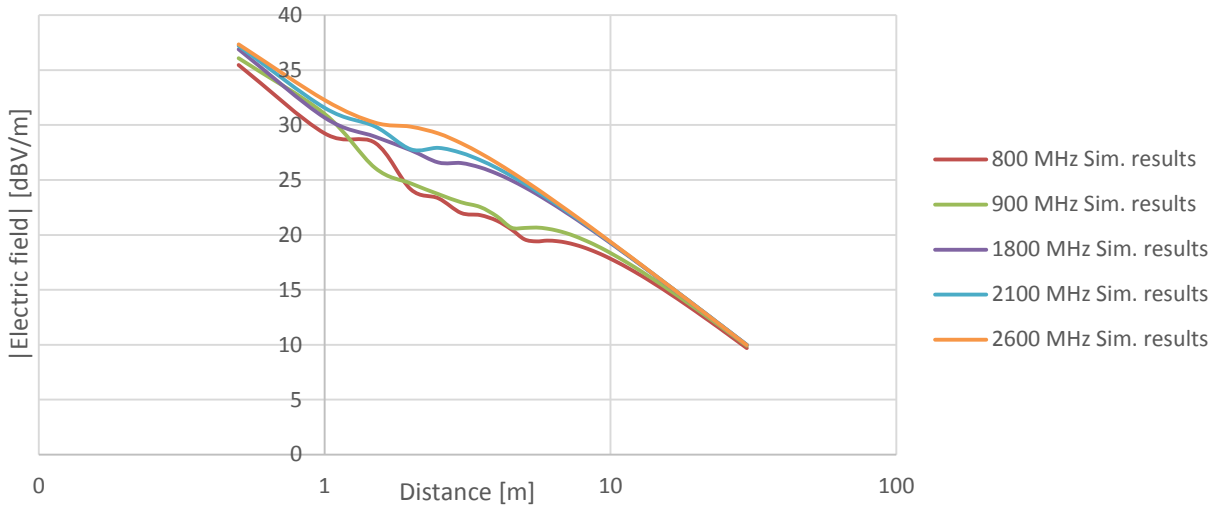

Figure 4.10 - Comparison between electric field results in dBV/m from simulations for all the frequencies considered in the outdoor scenario.

The expressions of the curves corresponding to the simulation results, along with the coefficients for each frequency considered in this scenario were obtained by using the trend line option for polynomial functions of Excel, allowing one to design the resulting model from the simulations given by:

$$E(d)_{[\mathrm{dBV/m}]} = \{C_1(f)\ \log(d_{[\mathrm{m}]}) + C_0(f)\}, \qquad d < d_{c,o} \tag{4.12}$$

with the coefficients for the frequencies in analysis presented in Table 4.12.

Table 4.12 - Outdoor simulation model coefficients.

f [MHz]	C_1	C_0
800	-13.081	29.934
900	-13.351	30.615
1800	-15.402	33.742
2100	-15.941	34.452
2600	-16.537	35.223

From both mathematical analysis and the trend line option for linear and polynomial functions of Excel, expressions for the determination of the coefficients were determined:

$$C_1(f) = -0.002\ f_{[\mathrm{MHz}]} - 11.595 \tag{4.13}$$

$$C_0(f) = -0.000001\ f_{[\mathrm{MHz}]}^2 + 0.0065\ f_{[MHz]} + 25.527 \tag{4.14}$$

In Figure B.19 and Figure B.20, a comparison between the coefficient values from Table 4.12 and the

ones obtained from (4.13) and (4.14) is presented. The average error resulting from the application of the functions in the determination of the coefficients for the considered frequencies is 1% for both $C_1(f)$ and $C_0(f)$. The comparison between simulation results and the ones obtained by using the indoor model from simulations for the considered frequencies is presented from Figure B.21 to Figure B.25, resulting in an average error of 4% for 800 MHz and 900 MHz and 5% for the other frequencies.

With these results, a global outdoor model can be designed, considering the model from equations for distances below $d_{c,o}$ and the far field model for distances higher than $d_{c,o}$. The global outdoor model is then, given by:

$$\begin{cases} E(d)_{[\mathrm{dBV/m}]} = \sum_{n=0}^{1} \left\{ C_n(f) \ \left(20\log\left(d_{[\mathrm{cm}]}\right)\right)^n \right\}, & d < d_{c,o} \\ E(d)_{[\mathrm{dBV/m}]} = 20\log\left(\frac{\sqrt{30G_T}}{d_{[\mathrm{m}]}}\right), & d \geq d_{c,o} \end{cases} \tag{4.15}$$

This model is valid for dipole array antennas with an input power of 1 W and $N_{el} = 8$, allowing one to determine the electric field in the direction of maximum radiation without overestimating the field values in the region closer to the antenna.

4.3 Measurements

By performing measurements, one is able to analyse the behaviour of the electric field radiated by a real antenna and its impact on EM exposure, in order to compare with the results of the model described in the previous section. The conducted measurements were focused on public access areas in zones close to BSs. A spectrum analyser with an omnidirectional antenna was used as measuring equipment, working in a safety evaluation mode, which allows one to determine the electric field radiated from an antenna, as well as the contribution of each frequency band on the total field value measured [Nard07]. The equipment keeps a digital record of the collected data, which can be exported to Excel or Matlab software for analysis purposes.

Before starting the measuring process, the BS should be characterised by the factors influencing its radiation as well as the environment surrounding it, and the measuring equipment should be calibrated, defining the frequency range, resolution bandwidth and the method of evaluation. The procedure followed for the measurements in this work consists of the definition of measurement points coinciding with imaginary radials around the BS antennas separated by 45º. The number of points on each radial should be enough to describe the field behaviour as a function of distance, where the measured average values are recorded for 1 minute for each mobile communication system, in order to obtain a good resolution in each band for distances from 0.5 m from the BS and an interval of 0.5 m between each measurement point.

For this work, one has conducted measurements in four different BS sites, characterised in Table 4.13.

Table 4.13 – General characteristics of the BS's that were targeted measures.

BS	Environment	Scenario	Installed systems	Measurement sites
BS1	Outdoor	Urban	LTE 800, GSM 900, UMTS 2100	Back side of the BS on the building terrace
BS2			LTE 800, GSM 900, UMTS 2100	
BS3			GSM 900, UMTS 2100	
BS4			GSM 900, UMTS 2100	

In Figure 4.11, a sketch of the BS1 measurement site is presented, while a photograph of the site is shown in Figure 4.12. The sketch and photographs of the other sites are presented in AnnexC.1.

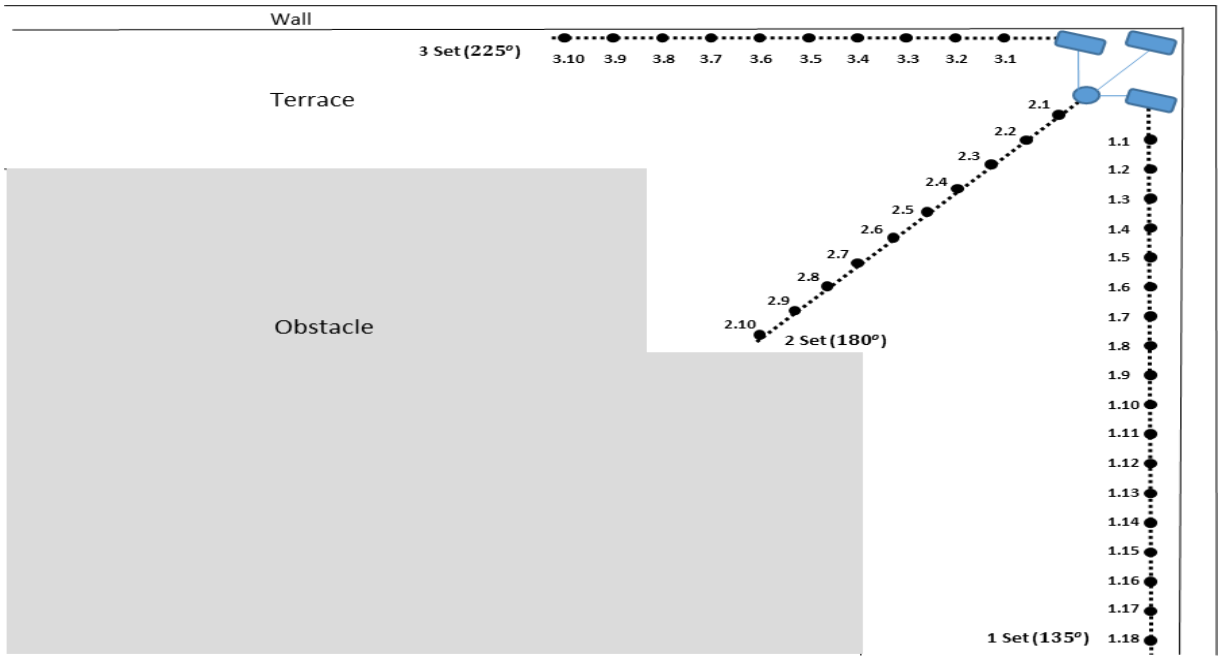

Figure 4.11 – Sketch of the BS1 measurement site.

Figure 4.12 – Point of view from the terrace access of the BS1.

In the following graphs, the measured values of the electric field for the first, second and third set of data are presented. The sets correspond to the measurements performed for 135º, 180º and 225º direction, respectively, as presented in Figure 4.11.

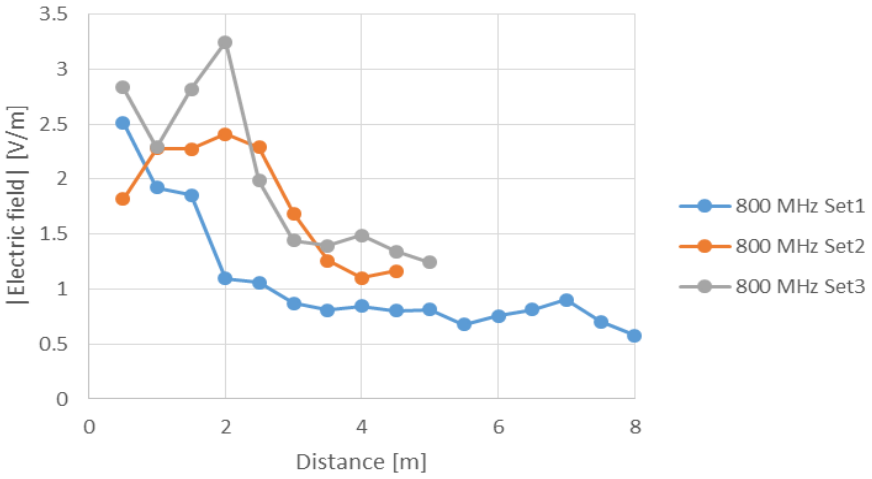

Figure 4.13 – Measured values of the electric field for 800 MHz on BS1.

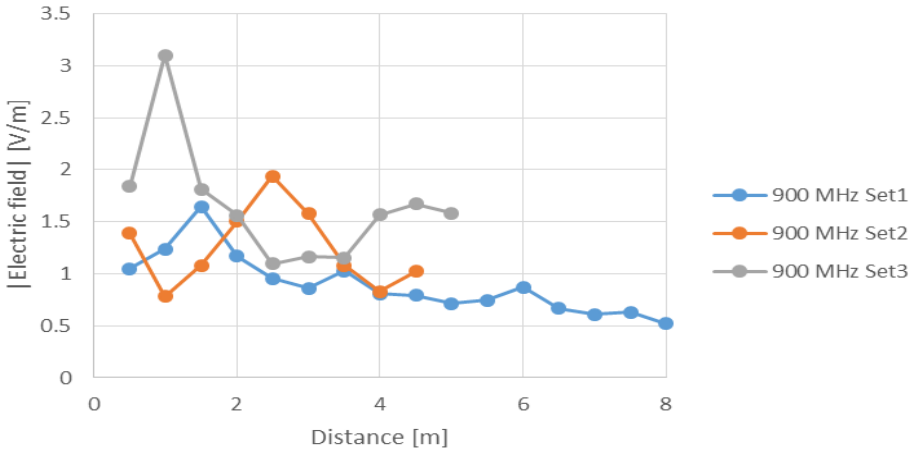

Figure 4.14 - Measured values of the electric field for 900 MHz on BS1.

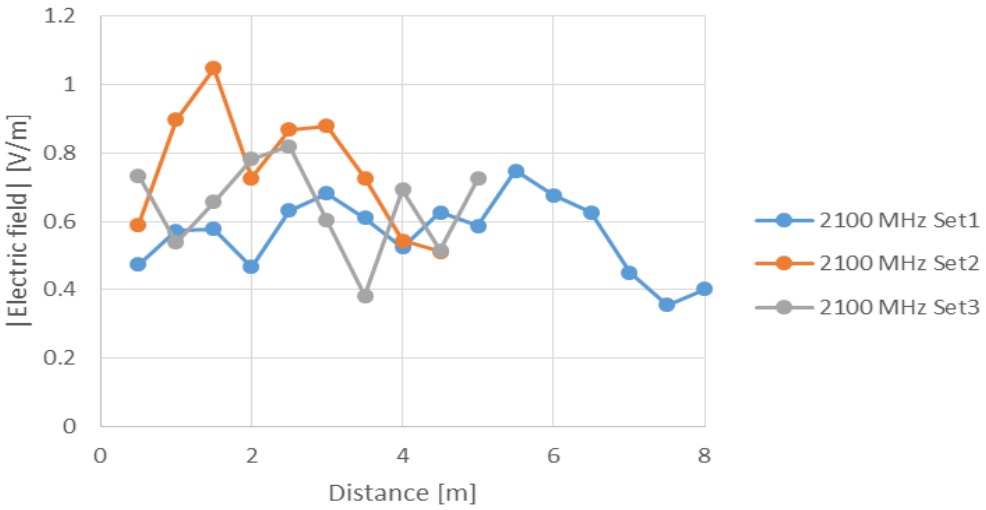

Figure 4.15 - Measured values of the electric field for 2100 MHz on BS1.

From these values, and taking the typical radiation pattern of the antennas into account, one can apply correction factors so that an approximation of the electric field values for the front direction of the BS (0º) can be determined. From the results obtained for the back side of the BS, and applying a correction factor (CF) of 20 dB [Antu12], the electric field in the front direction of the BS is determined and presented in Figure 4.16.

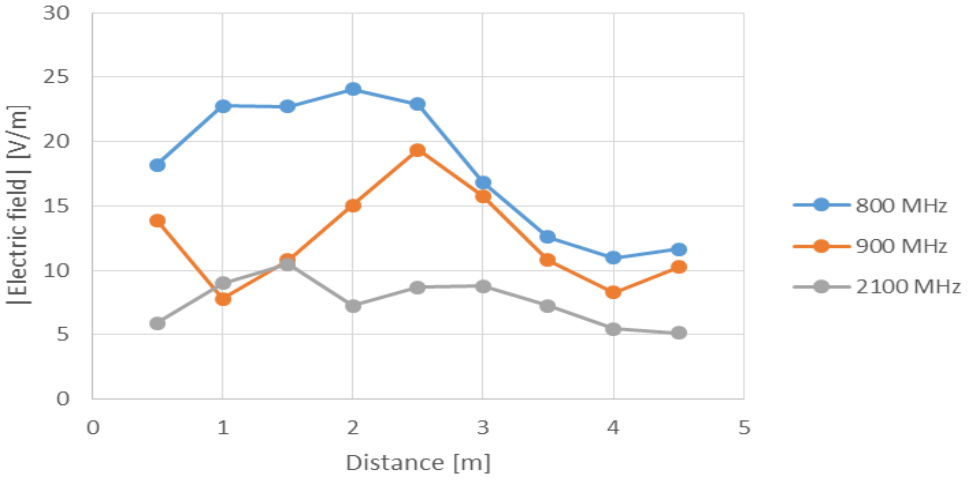

Figure 4.16 – Electric field obtained for the front side of the BS1.

The measurement results for the other BS, as well as the values of the electric field for the front side of the BS are presented in AnnexC.2.

These results allow one to establish a ground for comparison with the ones obtained through the application of the developed models as well as from the theoretical models presented in Chapter3.

4.4 Model Comparison

In this section, the models developed in Section 4.2 are compared with the theoretical ones presented in Chapter 3, as well as with the measurement results presented in the previous section.

Considering the indoor scenario, in Figure 4.17, an example of the comparison between the electric field computed from the global indoor simulation model with the values obtained by applying the field model for indoor antennas described in Section 3.1.3 for 800 MHz is presented. The results for all frequencies are presented in Annex B.2.

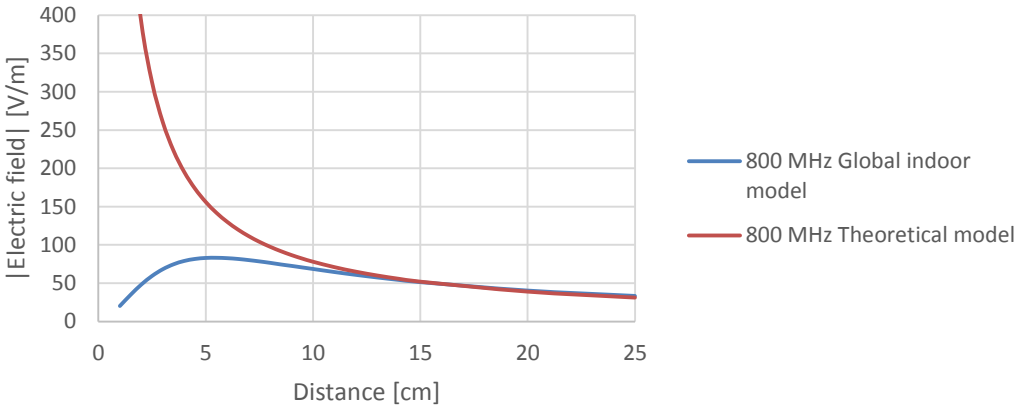

Figure 4.17 – Comparison between electric field values obtained from the global indoor model from simulations and the field model for 800 MHz indoor antennas.

Following the approach done in Section 4.2, the $d_{c,i}{}'$ values were determined for the comparison between the global indoor model from simulations and the one from Section 3.1.3, being presented in Table 4.14.

Table 4.14 - Boundary condition ($d_{c,i}{}'$) between the model from the simulations and the field model for indoor antennas considering the indoor scenario.

f [MHz]	800	900	1800	2100	2600
$d_{c,i}{}'$ [cm]	16	15	8	8	7

The obtained results are lower than the ones obtained from the comparison with the far field model, meaning that the model for indoor antennas is valid for distances lower than the far field one. However, for distances below $d_{c,i}{}'$, the global indoor model from simulations should be used in order to avoid overestimating the values of the electric field.

For the outdoor scenario, the electric field global model described in Section 3.1.4 was used in order to compare with the global outdoor model from simulations. In Figure 4.18, a comparison between the two models and measurements obtained for the 800 MHz frequency band in BS1 is presented. For the other frequency bands measured in BS1 and other BSs, results are presented in Annex B.2

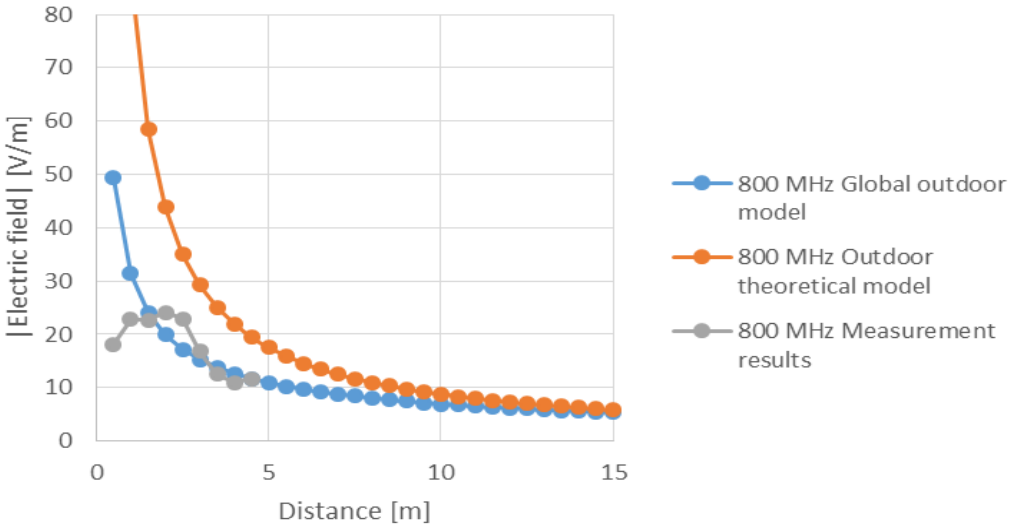

Figure 4.18 – Comparison between results obtained from global outdoor model, theoretical model and measurement results for 800 MHz in BS1.

When comparing the results obtained from the outdoor global model with the measurement data, the highest error value, ε_{max} as well as the average error, $\bar{\varepsilon}$ obtained for all the frequency bands in each BS are presented in Table 4.15.

Table 4.15 – Maximum error value from using the global outdoor model compared to measurement data for each BS.

BS	Frequency band [MHz]	ε_{max} [%]	$\bar{\varepsilon}$ [%]
1	800	171	32
1	900	335	104
1	2100	488	252
2	800	180	74
2	900	192	72
2	2100	392	83
3	900	162	40
3	2100	676	327
4	900	133	49
4	2100	532	431

The comparison allows one to conclude that, despite the fact the developed models being more accurate that the theoretical ones, it still overestimates the values of the electric field, with high maximum and average error values.

4.5 Estimation of Exclusion Zones

In this section, one applies the models developed in Section 4.2 in order to estimate exclusion zones around BS antennas.

In Table 4.16, the electric field reference levels issued by ICNIRP for the general public are presented, providing the condition that must be guaranteed when defining the exclusion zones. The values were computed from the equations presented in Table 2.6 for all the frequencies considered in this work, both for indoor and outdoor scenarios.

Table 4.16 – Electric field reference levels for the general public.

f [MHz]	Reference *E* Levels for General Public [V/m]
800	38.90
900	41.25
1800	58.34
2100	61.00
2600	61.00

The exclusion region values in the direction of maximum radiation (D_{front}) were obtained for both indoor and outdoor scenarios, for all the frequencies considered in this work.

Considering the indoor scenario, in Figure 4.19, the D_{front} values obtained by applying the global indoor model for the different analysed frequencies are presented, considering an input power of 1 W.

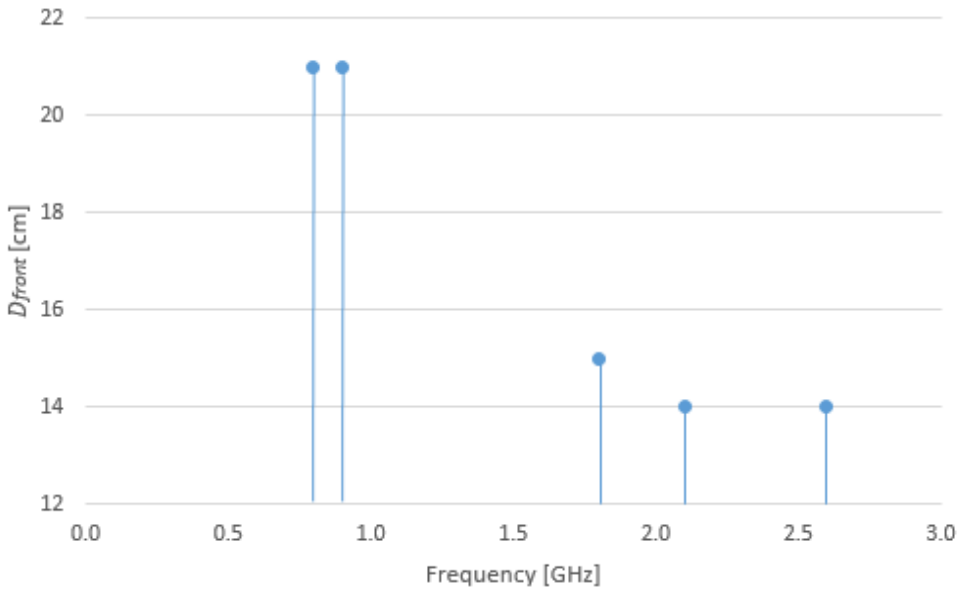

Figure 4.19 – D_{front} values obtained with the global indoor model for the indoor scenario.

One should note that the estimated exclusion zone is lower than one wavelength for all the frequencies analysed with the exception of 2600 MHz, which is not possible to verify with accuracy by using the far field model, as it is only valid for distances above $\frac{2D^2}{\lambda}$. In Figure 4.20, a comparison between these results and the ones obtained by using the far field model is presented.

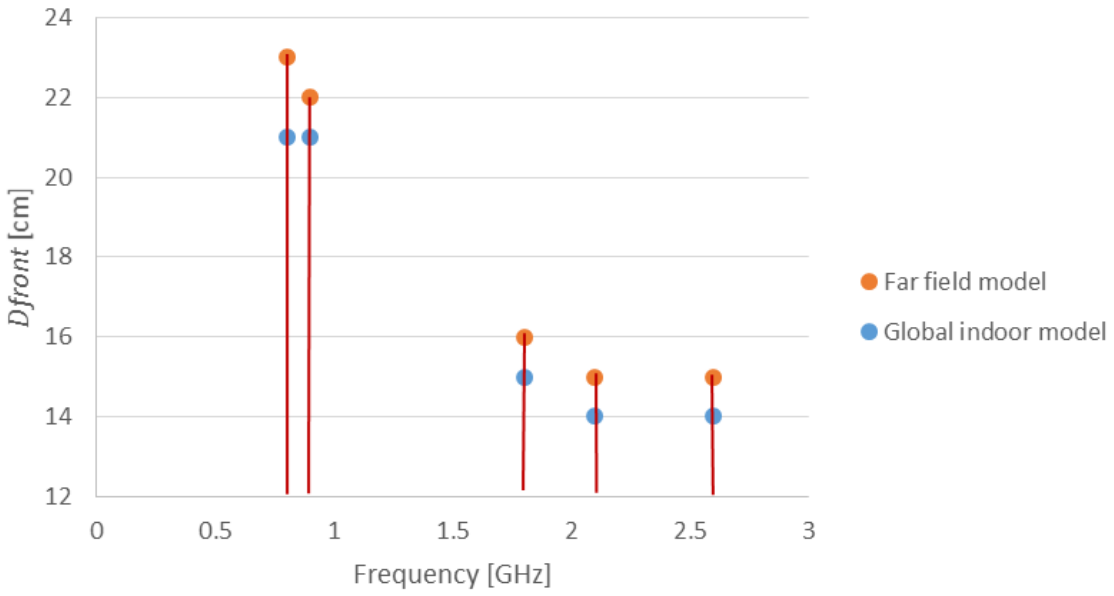

Figure 4.20 – Comparison between the D_{front} values obtained with the global indoor model and the ones obtained with the far field model for the indoor scenario.

When using the far field model, the resulting values for D_{front} are higher than the ones obtained from the global indoor model. The highest error occurs for the 800 MHz case, being 10%, which is an acceptable error.

Regarding the other directions, the bottom (D_{bottom}), top (D_{top}) and side (D_{side}) borders of the exclusion zone are determined by the method of cylindrical exclusion zone model [MFRL02]. The back border of the exclusion zone is not considered, due to the fact that the indoor antennas are usually located on walls or on the ceiling, as shown in Figure 4.1. From the analysis of the antenna radiation pattern, the normalised gains are determined as a function of the propagation direction, being applied as CFs to the D_{front} values. For this scenario, the directions considered are presented in Table 4.17.

Table 4.17 – Directions analysed for the bottom, top and side border of the exclusion zone for the indoor scenario.

Bottom	Top	Side
-90º (V plane)	90º (V plane)	-90º, 90º (H plane)

The obtained CFs that allow to obtain the values of the exclusion zone borders are presented in Table 4.18, and the obtained border values in Table 4.19. One should note that when the values of the

electric field are above the reference levels for a given direction, there is no need to define a border for the exclusion zone in that direction.

Table 4.18 – Correction factors obtained for the microstrip patch antenna.

Border	D_{side}	D_{top}	D_{bottom}
CF [dB]	-10	-15	-15

Table 4.19 – Exclusion zone borders for the frequencies considered in the indoor scenario and an input power of 1 W.

f [MHz]	800	900	1800	2100	2600
D_{front} [cm]	21	21	15	14	14
D_{side} [cm]	< 1	< 1	< 1	4	4
D_{top} [cm]	< 1	< 1	< 1	< 1	< 1
D_{bottom} [cm]	< 1	< 1	< 1	< 1	< 1

For the purpose of analysing the impact of these results on the need to define physical barriers, taking into account that the typical distance from an indoor antenna to the people is around 50 cm, and that the values of the exclusion zone borders are always below that value, there is no need to define this type of barriers.

The previously presented results were obtained by considering an input power of 1 W. Following a different analysis, one has defined the condition $D_{front} \geq 20\ cm$ and $D_{side} \geq 10\ cm$ in order to determine the input power needed to fulfil this condition for each considered frequency. The obtained input power values are presented in Table 4.20.

Table 4.20 – Input power values needed in order to verify $D_{front} \geq 20\ cm$ and $D_{side} \geq 10\ cm$.

f [MHz]	800	900	1800	2100	2600
Input power [W]	3	3	4	4	5

For each input power presented in Table 4.20, the borders of the exclusion zone for each considered frequency are presented from Table B.1 to Table B.3.

From these results, and taking the typical distance from indoor antennas to the public as 50 cm, one can conclude that for all the frequencies considered in this work, and for an input power in the range

between 1 W and 5 W, there is no need to define physical barriers for this type of antennas. Input power in indoor environments varies between 34 dBm and 38 dBm, which leads to $D_{front} \geq 20\ cm$ values always lower than 50 cm.

For the outdoor scenario, in Figure 4.21, the D_{front} values obtained by applying the outdoor global model for the different analysed frequencies are presented, considering an input power of 1 W.

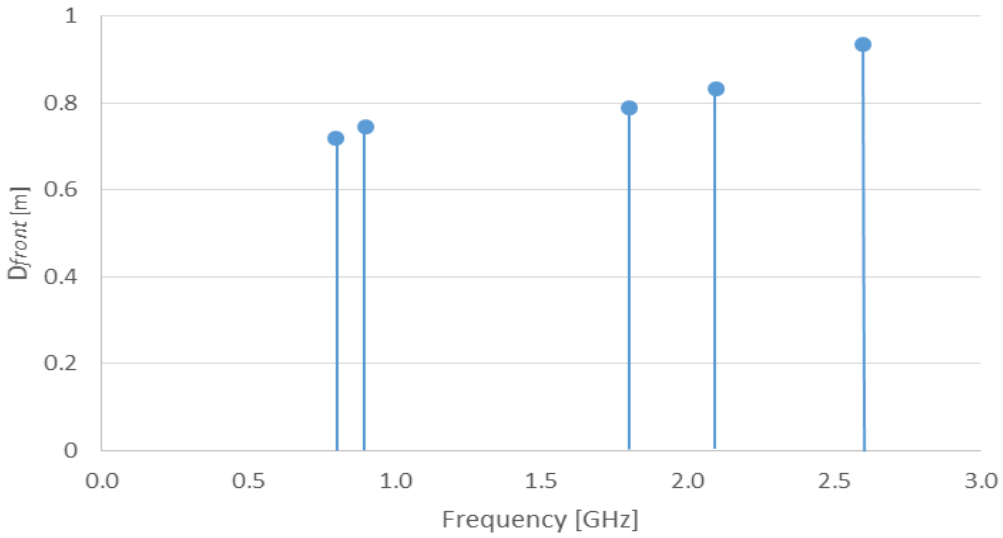

Figure 4.21 - D_{front} values obtained with the global outdoor model for the outdoor scenario.

Again, one should note that the estimated exclusion zone is at distances lower than the validity distance of the far field model, which means that is not possible to verify with accuracy by using the model, as it is only valid for distances above $\frac{2D^2}{\lambda}$. In order to determine the error resulting from using the far field model, in Figure 4.22, a comparison between the D_{front} values obtained from both models is presented.

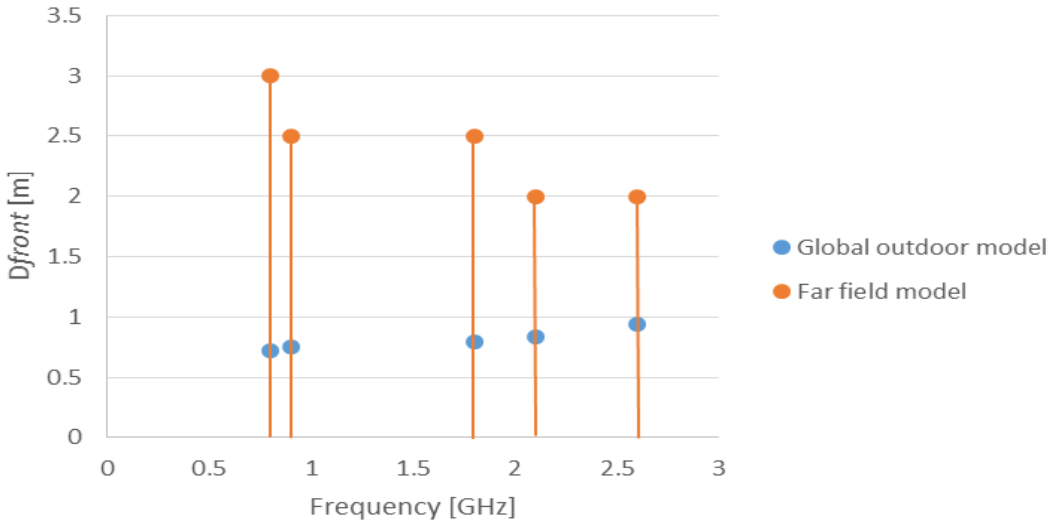

Figure 4.22 - Comparison between the D_{front} values obtained with the global outdoor model and the ones obtained with the far field model for the outdoor scenario.

As stated before, the application of the far field model in regions close to the antennas lead to overestimated results. For the outdoor scenario, the error resulting from using the far field model varies from 317% for 800 MHz and 114% for 2600 MHz, making the global outdoor model more suitable for defining exclusion zones.

The back (D_{back}), bottom (D_{bottom}), top (D_{top}) and side (D_{side}) borders of the exclusion zone are determined by the method of cylindrical exclusion zone model, such as for the indoor scenario. For the outdoor scenario, the considered directions are presented in Table 4.21.

Table 4.21 - Directions analysed for the back, bottom, top and side border of the exclusion zone for the outdoor scenario.

Bottom	Top	Back	Side
-90º (V plane)	90º (V plane)	180º (H plane)	-45º, -90º, -135º, 135º, 90º, 45º (H plane)

From the analysis of the antenna radiation pattern, one has determined normalised gains as a function of the propagation direction, being applied as CFs to the D_{front} values and presented in Table 4.22.

Table 4.22 - Correction factors obtained for the outdoor dipole array antenna.

Border	D_{side}	D_{back}	D_{top}	D_{bottom}
CF [dB]	-6.3	-20.6	-30	-30

From the application of the correction factors, one has obtained the dimensions of the exclusion zones around the antennas defined in the outdoor scenario, considering an input power of 1 W. The obtained results for the D_{front} border are above 1 m for all the frequencies considered and the D_{bottom}, D_{top} and D_{side} borders of the exclusion zone are above 0.5 m for all frequencies.

However, as the input power in outdoor environments is typically in the range between 37 dBm and 47 dBm, a study to determine the exclusion zone borders for different input powers is needed. In order to determine the lowest values of the exclusion zones for typical outdoor BS antennas, in Table 4.23 the exclusion zone borders are presented, considering an input power of 5 W.

For a worst case scenario perspective, the exclusion zone borders for an input power of 50 W were determined, being presented in Table 4.24.

The D_{front} border of the exclusion zone take values between 2.3 m and 2.5 m with an input power equal to 5 W, and between 9.7 m and 14.3 m with 50 W. These results show that operators need to perform safety evaluations when installing new antennas on outdoor BS installations, in order to ensure the safety of the public from electromagnetic radiation.

Table 4.23 - Exclusion zone borders for the frequencies considered in the outdoor scenario and an input power of 5 W.

f [MHz]	800	900	1800	2100	2600
D_{front} [m]	2.5	2.5	2.3	2.3	2.5
D_{side} [m]	0.9	0.9	0.9	1.0	1.1
D_{back} [m]	< 0.1	< 0.1	0.1	0.1	0.2
D_{top} [m]	< 0.1	< 0.1	< 0.1	< 0.1	< 0.1
D_{bottom} [m]	< 0.1	< 0.1	< 0.1	< 0.1	< 0.1

Table 4.24 - Exclusion zone borders for the frequencies considered in the outdoor scenario and an input power of 50 W.

f [MHz]	800	900	1800	2100	2600
D_{front} [m]	14.3	14	10.1	9.7	9.9
D_{side} [m]	4.8	4.8	3.9	3.9	4.2
D_{back} [m]	0.4	0.4	0.5	0.5	0.6
D_{top} [m]	< 0.1	< 0.1	0.2	0.2	0.2
D_{bottom} [m]	< 0.1	< 0.1	0.2	0.2	0.2

The proposed models are a practical tool to estimate exclusion zones for microstrip patch and dipole array antennas, in order to determine if any public access areas are inside the exclusion region. In this case, measurements can be performed to verify that the limit levels are exceeded, and if there is need to define/redefine physical barriers in these zones.

Chapter 5

Conclusions

This chapter finalises the thesis, highlighting the main conclusions as well as some suggestions for future work.

The objective of this work was to estimate exclusion regions from BSs in heterogeneous cell structures, and to establish design rules that simplify the estimation process. Exclusion regions are zones around the antennas where the reference levels are exceeded, which is why it is important to define physical barriers to protect the public from possible harmful effects due to radiation, namely in public areas. As exclusion regions are usually defined in the near field regions, one needs to develop models to access the EMF behaviour in areas very close to the antennas.

To be able to achieve the proposed goals, the most common BS antennas and the different types of installations were analysed. The radiation regions and radio interfaces of GSM, UMTS and LTE were studied, the main parameters that can influence the estimation of exclusion regions being identified. Another area of study was EM radiation exposure, mainly by examining exposure and measurement guidelines established by international entities. Finally, the existing models for the determination of exclusion zones around BSs were studied, by analysing the validity and methodologies of each model.

For the purpose of model development, a theoretical approach was studied. For an indoor model, the EMF of a microstrip patch antenna is obtained from the field model for indoor antennas described in Section 3.1.3, being valid from one wavelength from the antenna. Considering an outdoor antenna, the EMF is described by two models: the far field model, being valid in the far field region, and the near field model for outdoor antennas, described in Section 3.1.2, which is valid for distances greater than two wavelengths. The continuity of the EMF as a function of the distance is ensured by an interpolation process. This models provide a ground for comparison with models resulting from simulations.

The modelling of antennas using the CST MWS simulator was evaluated, two types of antennas being identified to be designed in this work: a microstrip patch antenna for an indoor scenario and a half wavelength dipole array as a panel antenna for an outdoor scenario. The methodologies for the design of the two types of antennas were studied, considering their main parameters and characteristics, in order to create the antennas on a simulation environment. The simulator was also studied, by analysing its main characteristics and functionalities, focusing on the computation of the electric field radiated from the antennas as well as its meshing properties. Finally, the models were accessed by analysing some of the obtained results, namely radiation patterns and electric field behaviour compared to the one obtained from theoretical models.

Two scenarios were defined: an indoor scenario considering a microstrip patch antenna, and an outdoor one where an 8 element dipole array was used. For the outdoor scenario, the dimensions of the antenna, as well as the back aluminium cover, were determined by analysing a real antenna. In both scenarios, the antennas were designed in CST MWS for each frequency of interest for this work: 800 MHz, 900 MHz, 1800 MHz, 2100 MHz and 2600 MHz, resulting in 5 antenna models for each scenario.

In order to design a model for the electric field in the region near the antennas, one has performed simulations for both indoor and outdoor scenarios. Values of the electric field in the direction of maximum radiation, and considering an input power of 1 W, were obtained and compared with the ones from applying the far field model for distances larger than d_{ff}.

For the indoor scenario, the results obtained from simulations were compared with the ones from the far field model, a distance $d_{c,i}$ above which the far field results present an error less than 10% when compared with the simulation results being defined. From this analysis, one has designed an indoor model from simulations for distances above $d_{c,i}$. A global indoor model was then developed, by using the indoor model from simulations for distances below $d_{c,i}$ and the far field model for distances above $d_{c,i}$. For the outdoor scenario a similar analysis was performed.

For the outdoor scenario, a similar approach has been made, by comparing the electric field values obtained from simulations with the ones obtained with the far field model. A distance, $d_{c,o}$ above which the error resulting from the application of the far field model is less than 10% was determined for all the frequencies considered, being the field behaviour for distances below $d_{c,o}$ modelled in order to develop a global outdoor model. This model is then defined by the electric field obtained from simulations for distances below $d_{c,o}$ and the far field model for distances above $d_{c,o}$.

Measurements were performed on four different BSs in outdoor urban scenarios, in order to verify the electric field behaviour of real BS installations that provide a ground for comparison with the developed model.

The results obtained from the global indoor model were then compared with the ones obtained with the field model for indoor antennas from [Antu12], being verified that in the regions closer to the antenna, the resulting error from the application of the theoretical model is higher than 100%. For the outdoor scenario, the electric field values obtained from the global outdoor model were compared with the ones from the theoretical model from [Antu12] and with measurement results. The developed models have proven to be more accurate than the theoretical ones. Nevertheless, by comparing the global outdoor model results with the measurement results, one is able to conclude that the developed model still overestimates the field values. The maximum error resulting from using the developed model for 800 MHz is 180%, while for 900 MHz is 335% and 676% for 2100 MHz. For all the measured BSs, the average error from using the develop model is 32% to 74% for 800 MHz, 49% to 104% for 900 MHz and 83% to 431% for 2100 MHz.

The global indoor and outdoor models were used to estimate the exclusion zone in the direction of maximum radiation D_{front}. For the D_{side}, D_{back}, $D_{bottom}$and D_{top}directions of the exclusion zone, the approach adopted is the cylindrical exclusion zone model, in which the normalised gains taken from the antenna radiation patterns are applied as correction factors on the exclusion region obtained in the direction of maximum radiation.

The obtained D_{front} values for the indoor scenario, considering 800 MHz, 900 MHz, 1800 MHz, 2100 MHz and 2600 MHz and an input power of 1 W, are between 21 cm for the lower frequency and 14 cm for the higher frequency, and the values of D_{side}, D_{top} and D_{bottom} are between 10 dB and 15 dB lower. As the typical installation of indoor antennas is on wall or the ceiling, the D_{back} distance has not been considered. A study to determine the minimum input power that leads to D_{front} equal to 20 cm and D_{side} equal to 10 cm was made, resulting in an input power of 3 W for 800 MHz and 900 MHz, 4 W for 1800 MHz and 2100 MHz and 5 W for 2600 MHz. From this analysis, the highest value of

D_{front} was obtained for 800 MHz with an input power of 5 W, being 48 cm. From these results, and taking the typical distance from indoor antennas to the public as 50 cm, one can conclude that for all the frequencies considered in this work, and for an input power from 1W to 5W, there is no need to define physical barriers for this type of antennas.

Considering the outdoor scenario, the obtained D_{front} values for all the considered frequencies and an input power of 1 W, range between 0.8 m for 800 MHz and 1 m for 2600 MHz, whereas for 5 W the obtained values are between 2.3 m for 2100 MHz and 2.5 m for 800 MHz, and for 50 W between 9.7 m for 2100 MHz and 14.3 m for 800 MHz. When analysing the other directions, the D_{side}, D_{back}, D_{top} and D_{bottom} results are between 6.3 dB and 30 dB lower. The highest obtained value of D_{side} was 4.8 m, for 800 MHz with an input power of 50 W, for D_{back}, 0.6 m was obtained for 2600 MHz also with an input power of 50 W and for D_{top} and D_{bottom} a value of 0.2 m, again for 2600 MHz with an input power of 50 W. These results show that operators need to perform safety evaluations when installing new antennas on outdoor BS installations, in order to ensure public safety from electromagnetic radiation.

The proposed models are a practical tool to estimate exclusion zones for microstrip patch and dipole array antennas, in order to determine if any public access areas are inside the exclusion region. In this case, measurements can be performed to verify that the limit levels are exceeded, and if there is need to define/redefine physical barriers in these zones.

For future research, one suggests the simulation of other types of antennas, such as outdoor arrays of patch antennas or arrays in indoor environments. Also, it would be interesting to run simulations for scenarios considering co-location of systems in indoor and outdoor environments as well as the co-location of mobile systems and Wi-Fi in indoor ones. It would also be relevant to study the impact of the surrounding environment of the antennas, such as the infrastructure that supports the antenna or the wall and ceiling in indoor cases.

Annex A

Antenna Models

In this annex, the models of the antenna developed in CST are presented, for both indoor and outdoor scenarios.

A.1 Indoor Scenario

The antennas designed in CST for the indoor scenario and described in Section 4.1.1 are presented in the following figures.

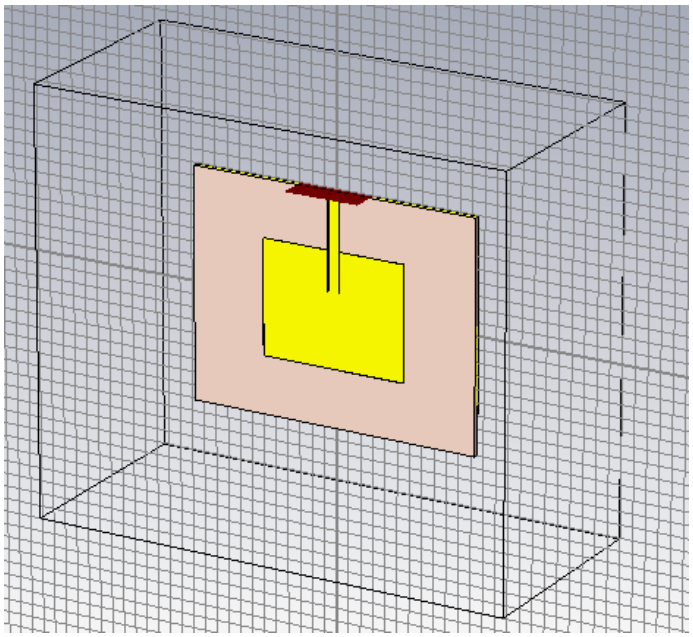

Figure A.1 - 800 MHz microstrip patch antenna model from CST.

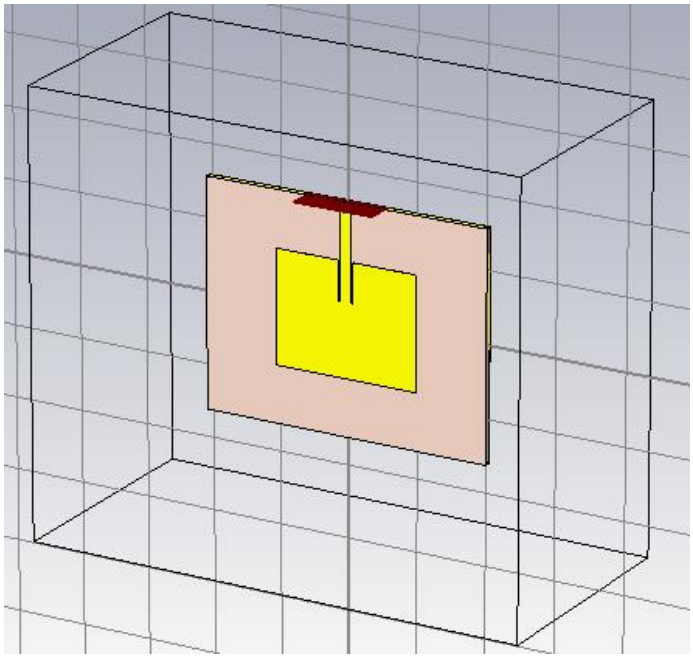

Figure A.2 - 900 MHz microstrip patch antenna model from CST.

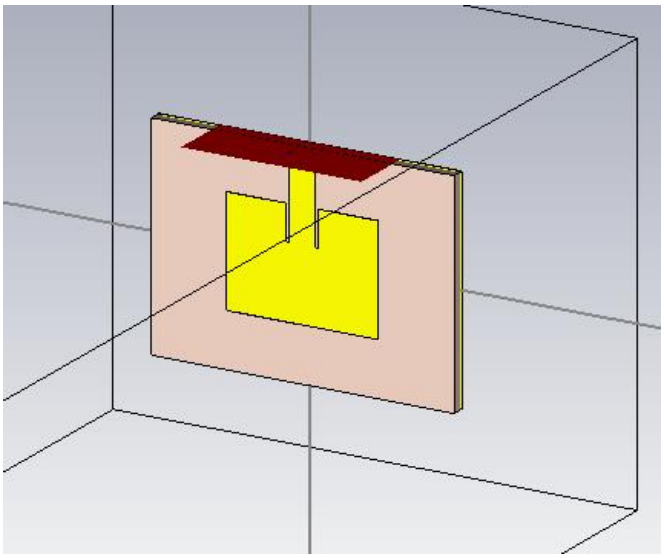

Figure A.3 - 1800 MHz microstrip patch antenna model from CST.

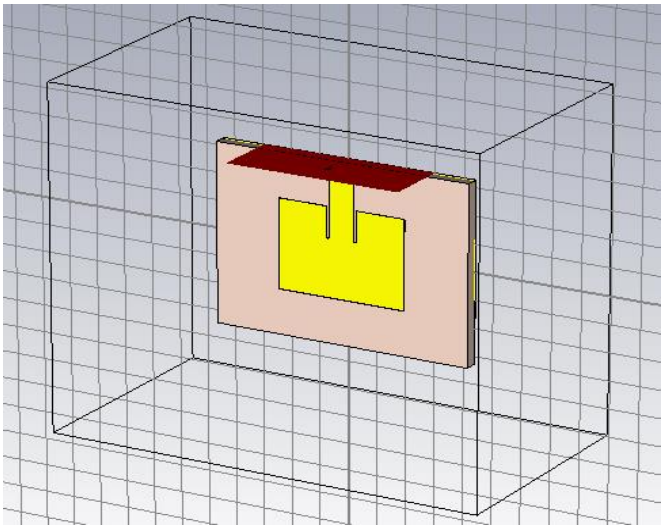

Figure A.4 - 2100 MHz microstrip patch antenna model from CST.

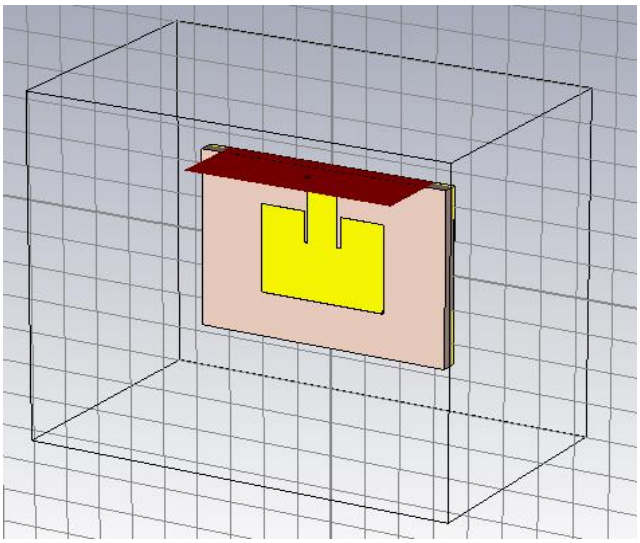

Figure A.5 - 2600 MHz microstrip patch antenna model from CST.

A.2 Outdoor Scenario

The antennas designed in CST for the outdoor scenario and described in Section 4.1.2 are presented in the following figures.

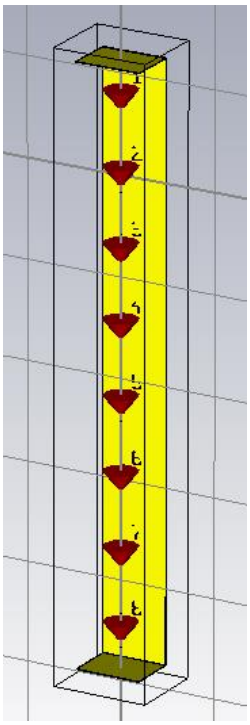

Figure A.6 – 800 MHz dipole array antenna model from CST.

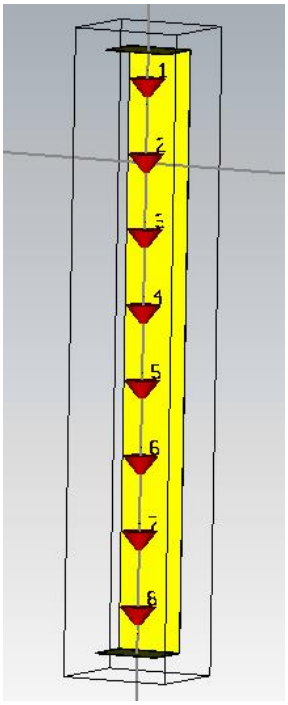

Figure A.7 - 900 MHz dipole array antenna model from CST.

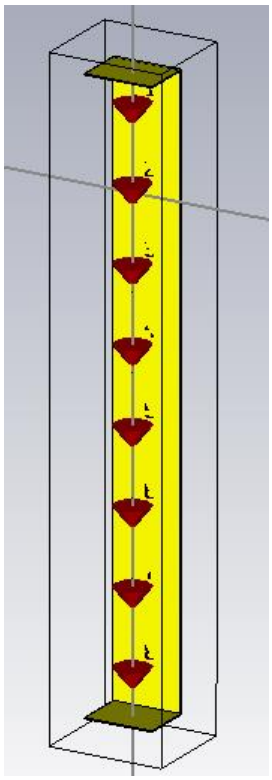

Figure A.8 – 1800 MHz dipole array antenna model from CST.

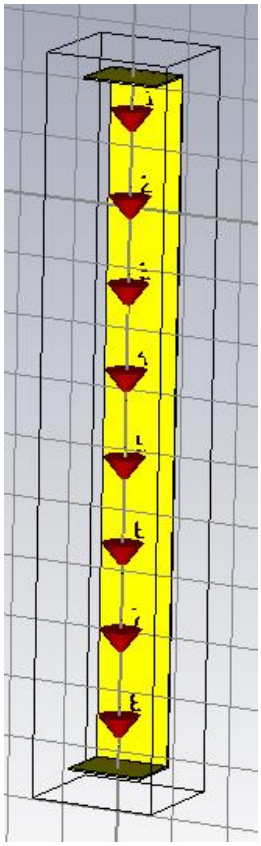

Figure A.9 - 2100 MHz dipole array antenna model from CST.

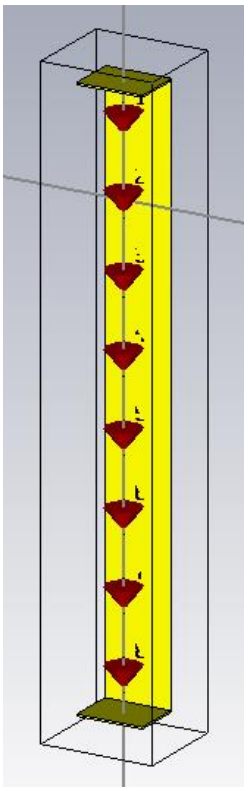

Figure A.10 - 2600 MHz dipole array antenna model from CST.

Annex B

Simulation and Theoretical Results

In this annex, all simulation and theoretical results obtained and analysed in Chapter 4 are presented.

B.1 Model from Simulations

The comparison between simulation results and the ones obtained from the far field model for the indoor scenario for the considered frequencies are presented in the figures below.

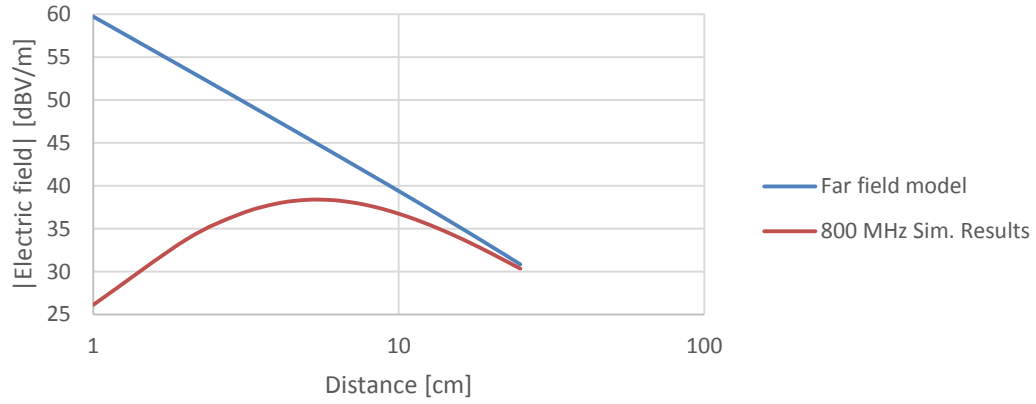

Figure B.1 – Comparison between simulation and far field model results for indoor 800 MHz.

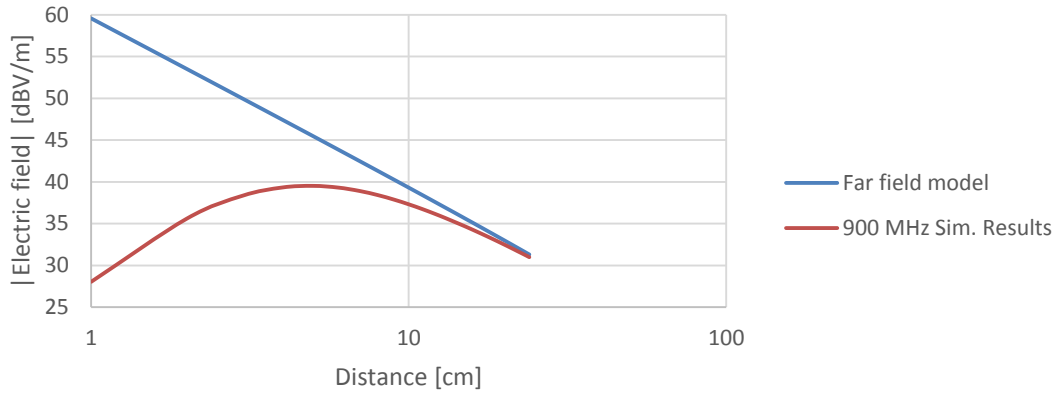

Figure B.2 - Comparison between simulation and far field model results for indoor 900 MHz.

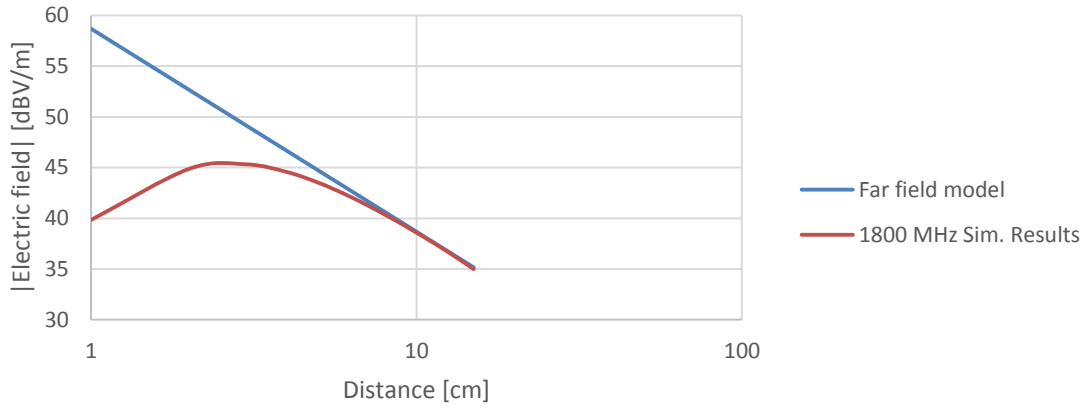

Figure B.3 - Comparison between simulation and far field model results for indoor 1800 MHz.

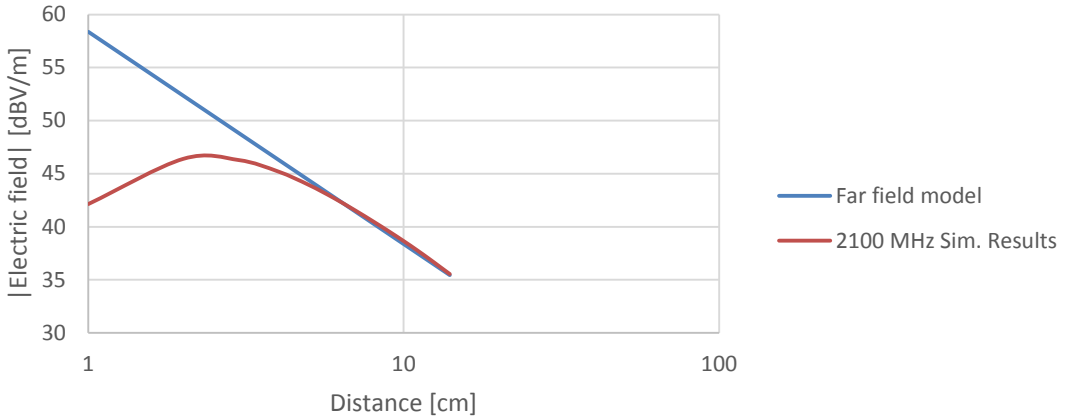

Figure B.4 - Comparison between simulation and far field model results for indoor 2100 MHz.

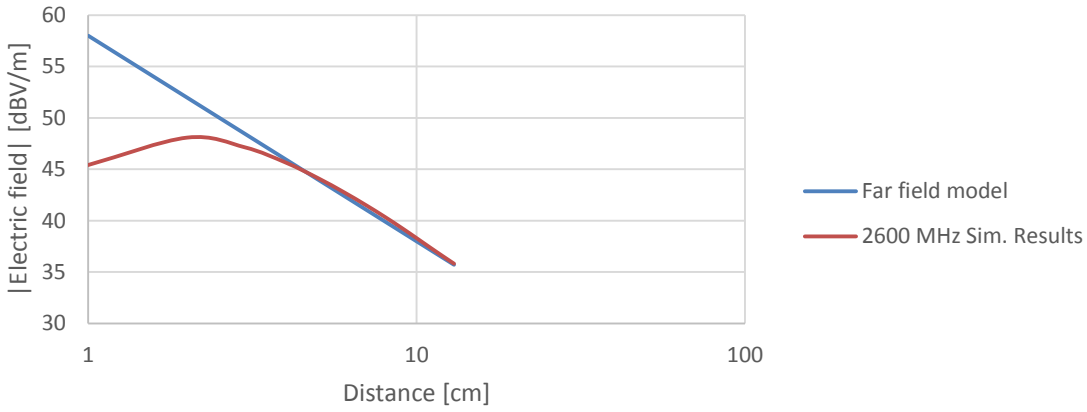

Figure B.5 – Comparison between simulation and far field model results for indoor 2600 MHz.

From Figure B.6 to Figure B.8, the comparison between the global indoor model coefficients and the ones obtained from equations is presented.

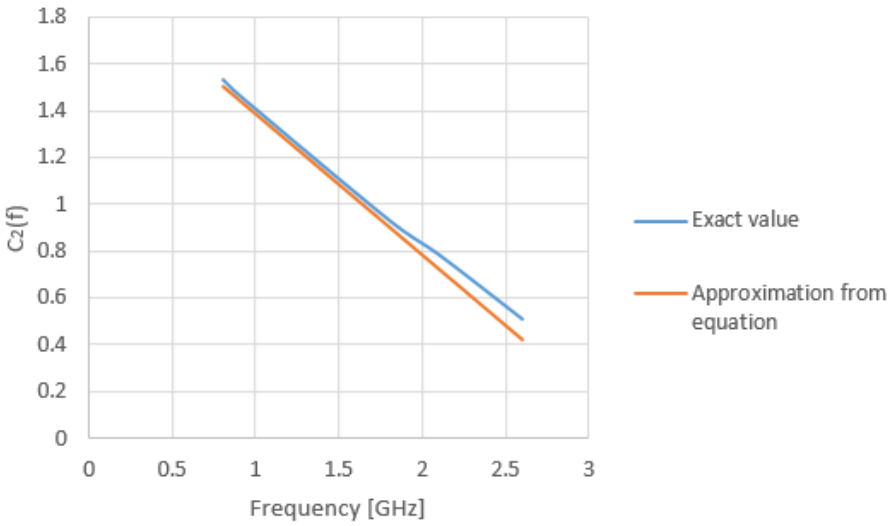

Figure B.6 – Comparison between $C_2(f)$ coefficient and the approximation obtained from equations for global indoor model.

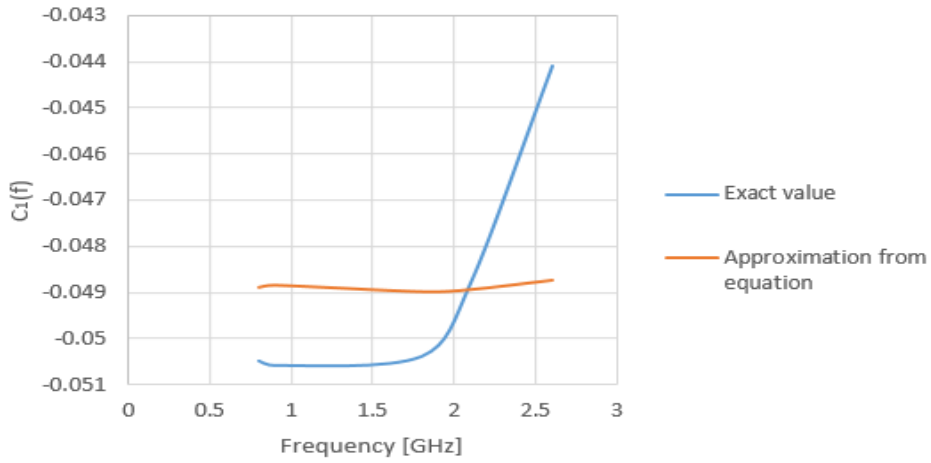

Figure B.7 - Comparison between $C_1(f)$ coefficient and the approximation obtained from equations for global indoor model.

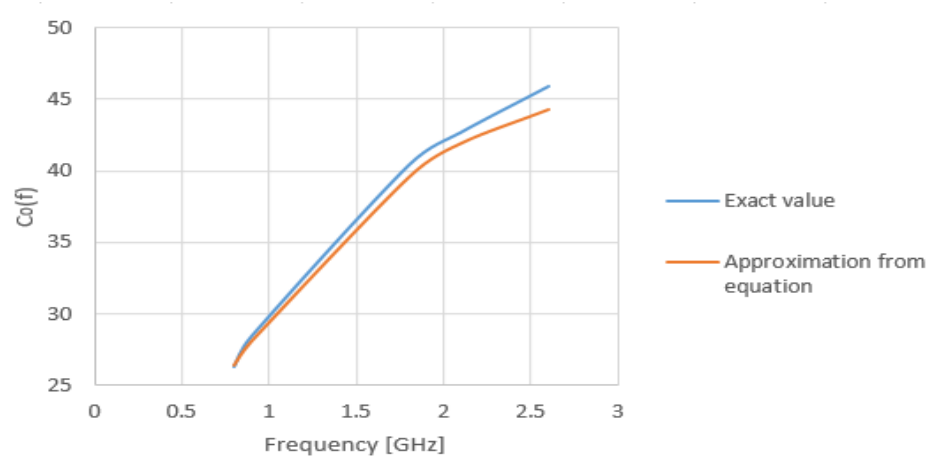

Figure B.8 - Comparison between $C_0(f)$ coefficient and the approximation obtained from equations for global indoor model.

From Figure B.9 to Figure B.13, the comparison between simulation results and the ones obtained from the global indoor model for all the frequencies considered in the scenario is presented.

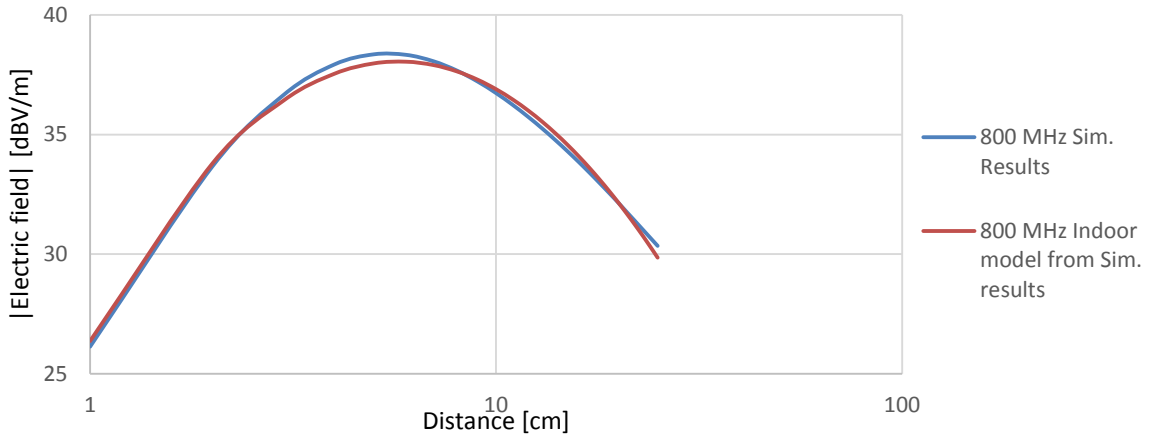

Figure B.9 – Comparison between simulation results and indoor model from simulations results for 800 MHz.

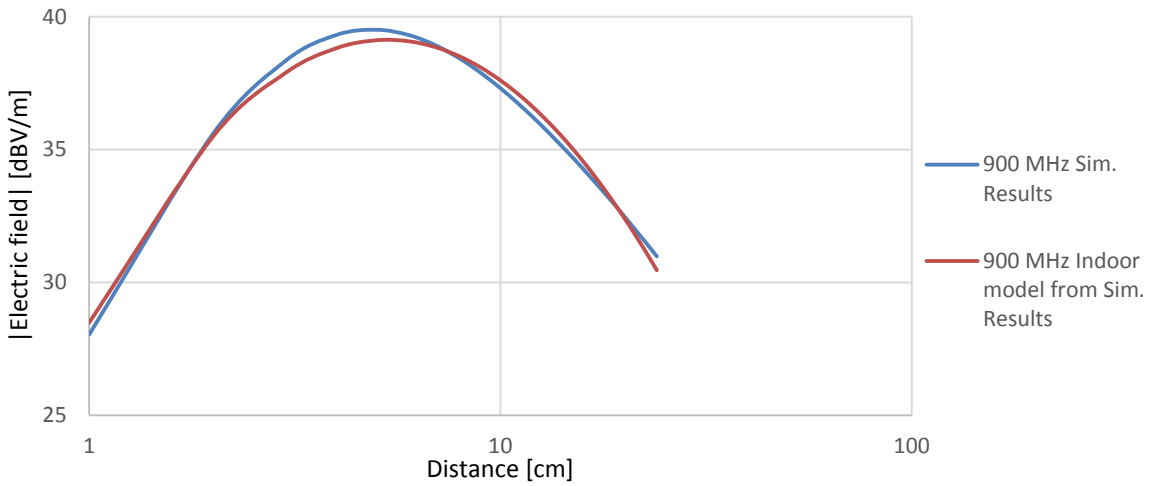

Figure B.10 - Comparison between simulation results and indoor model from simulations results for 900 MHz.

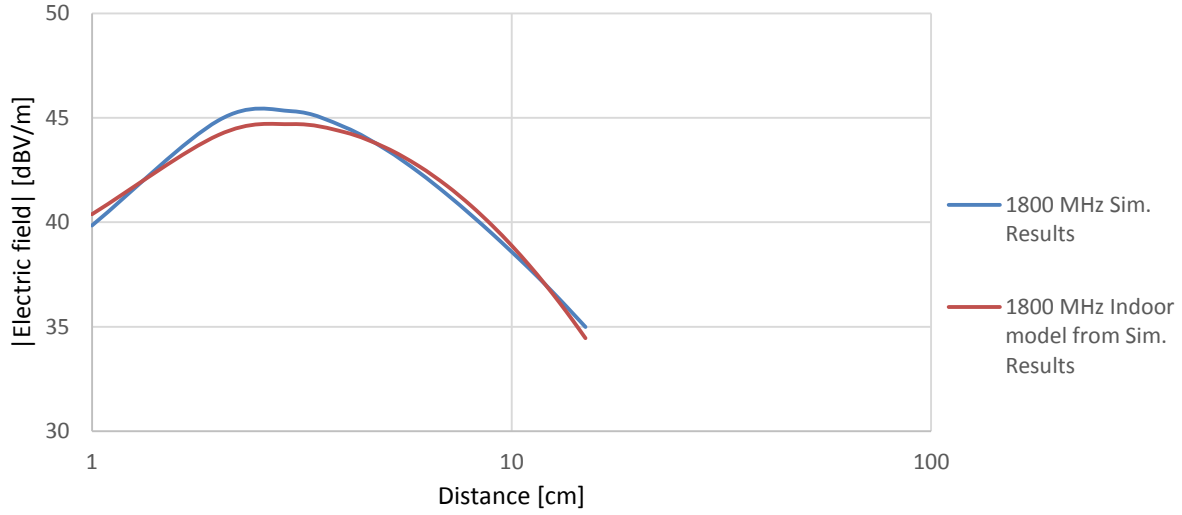

Figure B.11 – Comparison between simulation results and indoor model from simulations results for 1800 MHz.

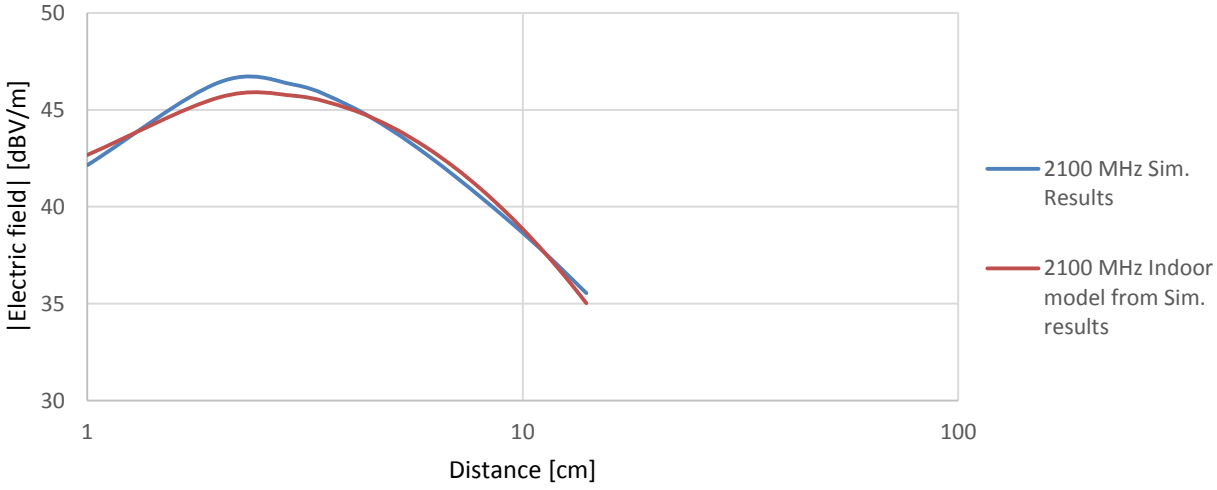

Figure B.12 - Comparison between simulation results and indoor model from simulations results for 2100 MHz.

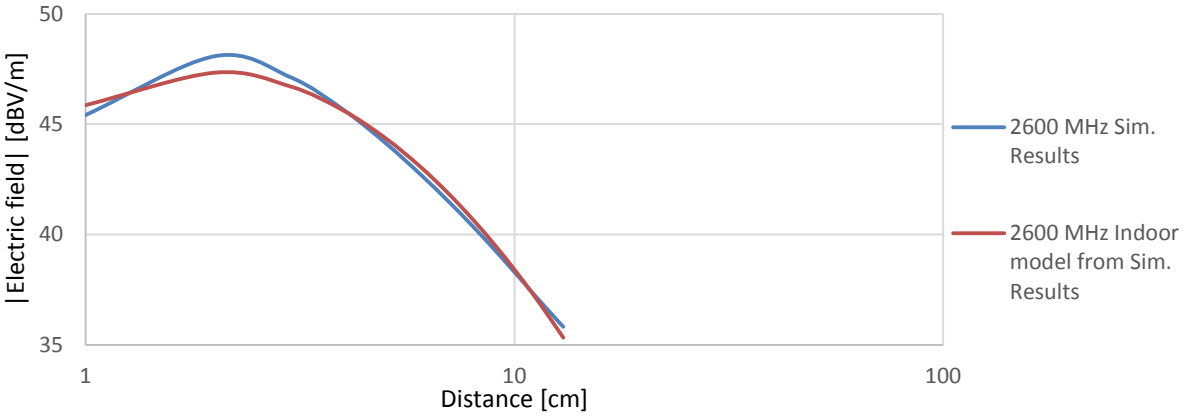

Figure B.13 - Comparison between simulation results and indoor model from simulations results for 2600 MHz.

The comparison between simulation results and the ones obtained from the far field model for the outdoor scenario for the considered frequencies is presented in the figures below.

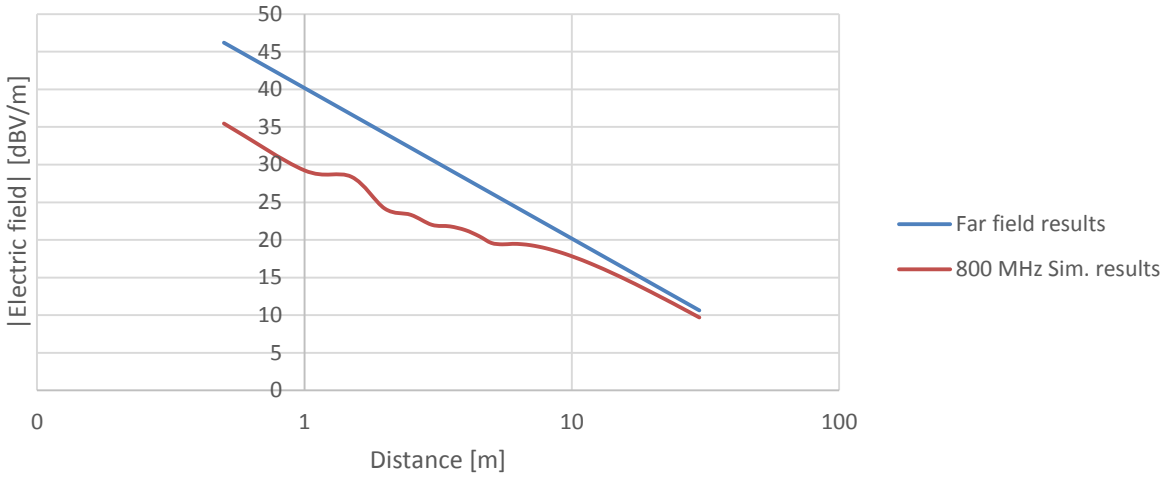

Figure B.14 - Comparison between simulation and far field model results for outdoor 800 MHz.

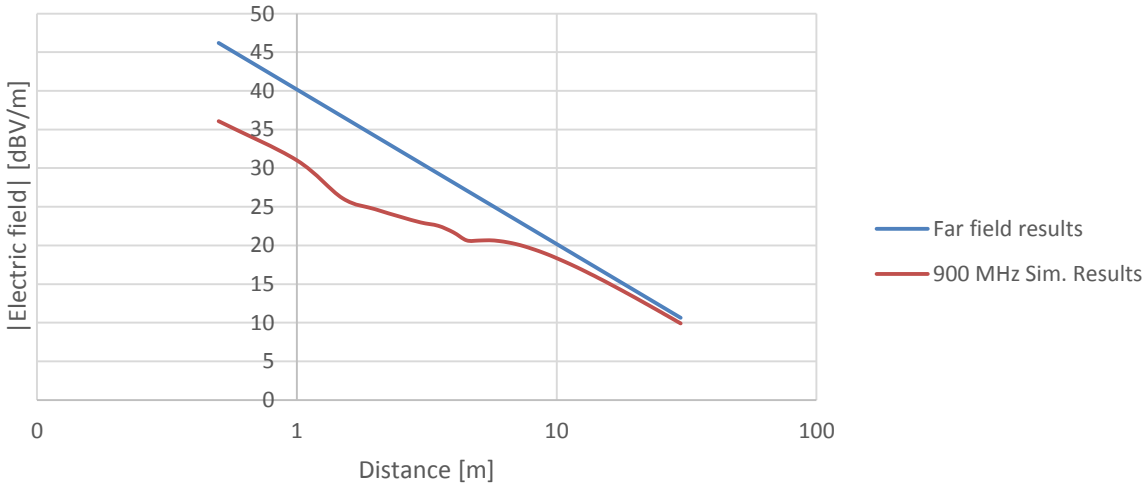

Figure B.15 - Comparison between simulation and far field model results for outdoor 900 MHz.

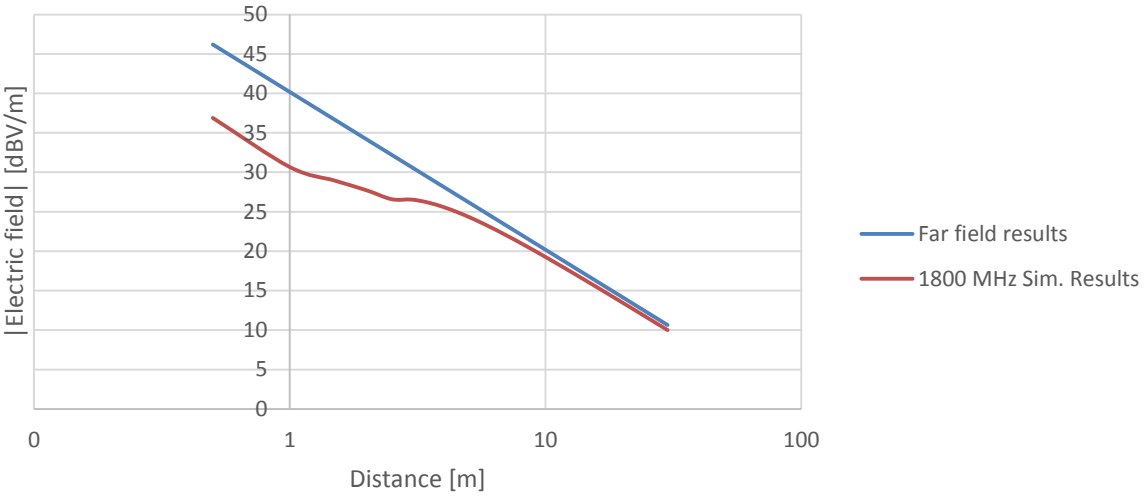

Figure B.16 - Comparison between simulation and far field model results for outdoor 1800 MHz.

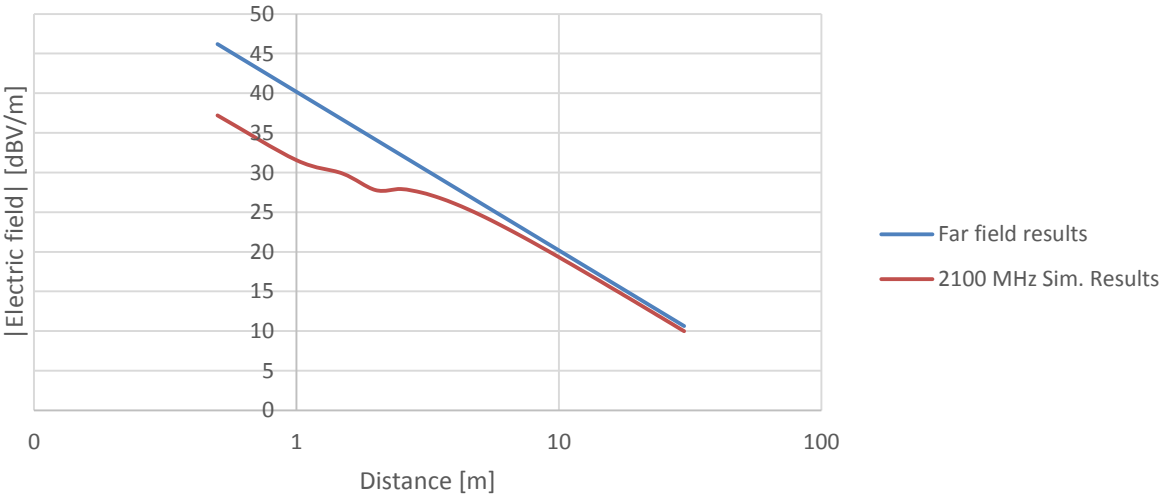

Figure B.17 - Comparison between simulation and far field model results for outdoor 2100 MHz.

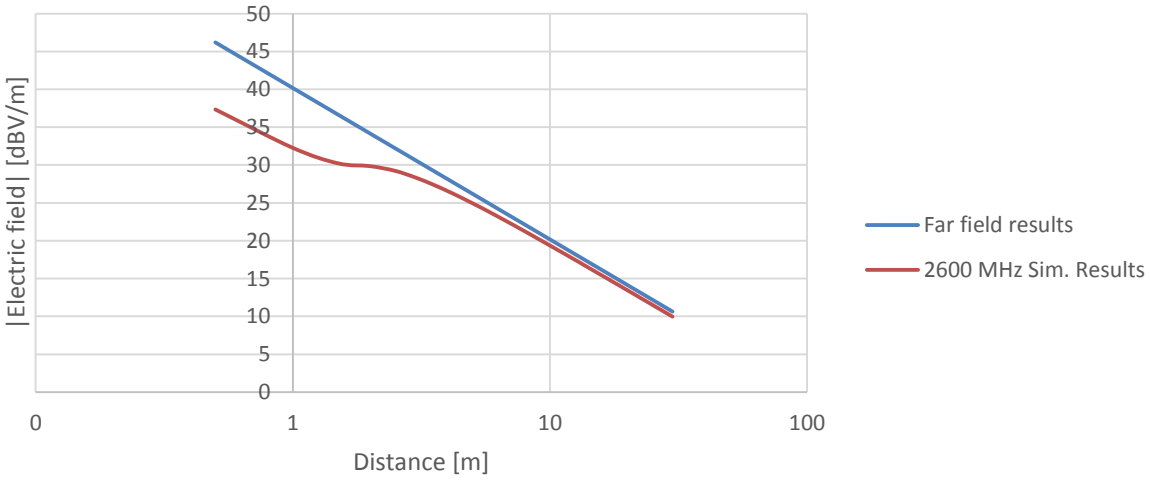

Figure B.18 - Comparison between simulation and far field model results for outdoor 2600 MHz.

In Figure B.19 and Figure B.20, a comparison between the outdoor model from simulations coefficients and the ones obtained from equations is presented.

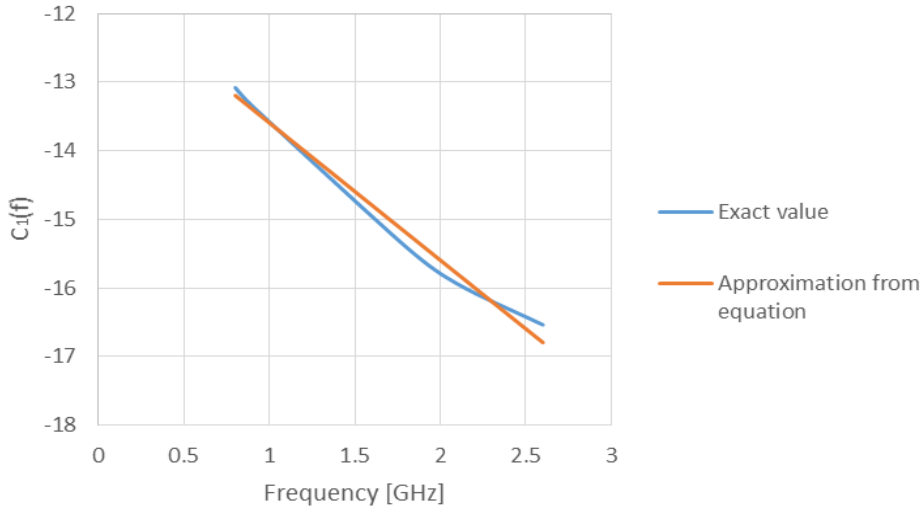

Figure B.19 - Comparison between $C_1(f)$ coefficient and the approximation obtained from equations for global outdoor model.

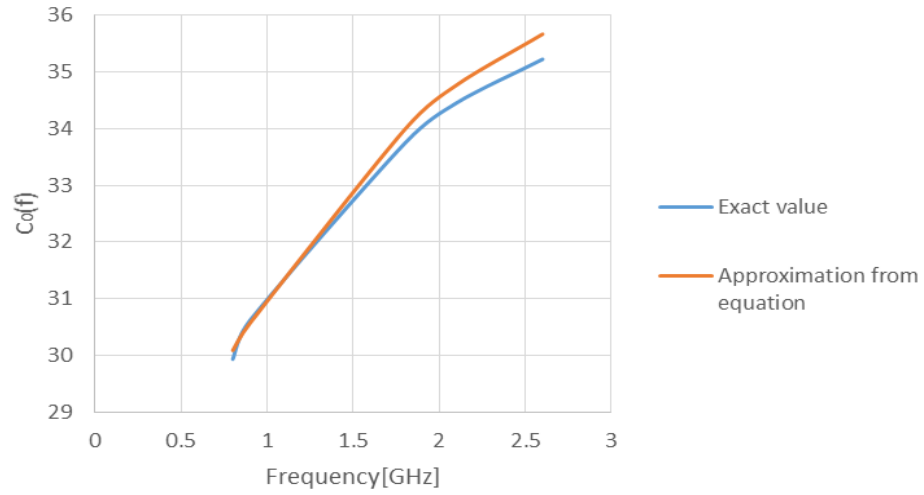

Figure B.20 - Comparison between $C_0(f)$ coefficient and the approximation obtained from equations for global outdoor model.

From Figure B.21 to Figure B.25, the comparison between simulation results and the ones obtained from the global outdoor model for all the frequencies considered in the scenario is presented.

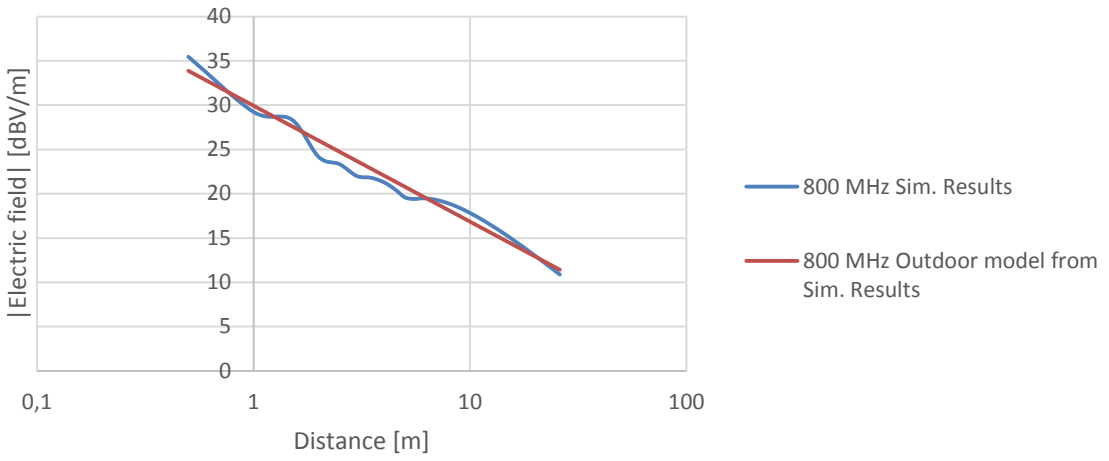

Figure B.21 - Comparison between simulation results and outdoor model from simulations results for 800 MHz.

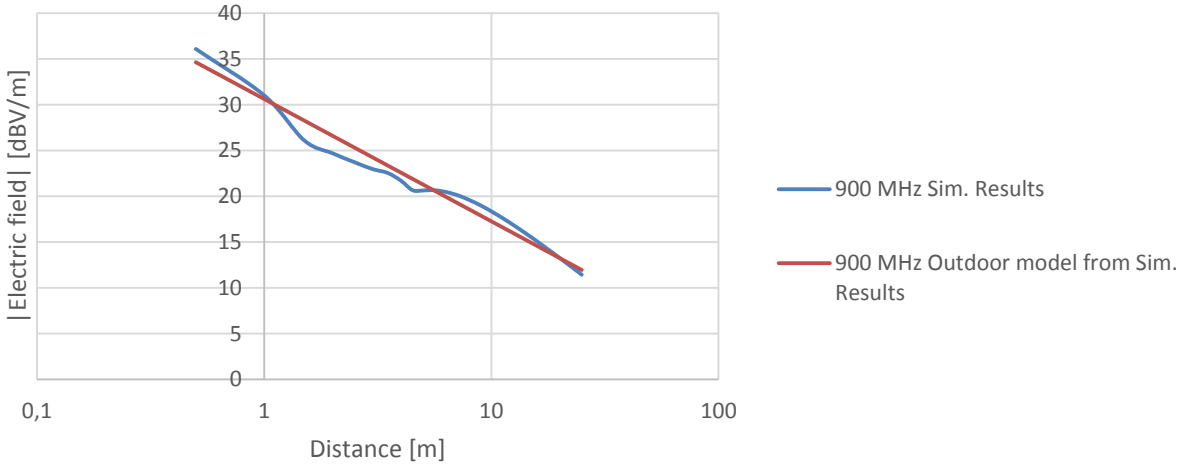

Figure B.22 - Comparison between simulation results and outdoor model from simulations results for 900 MHz.

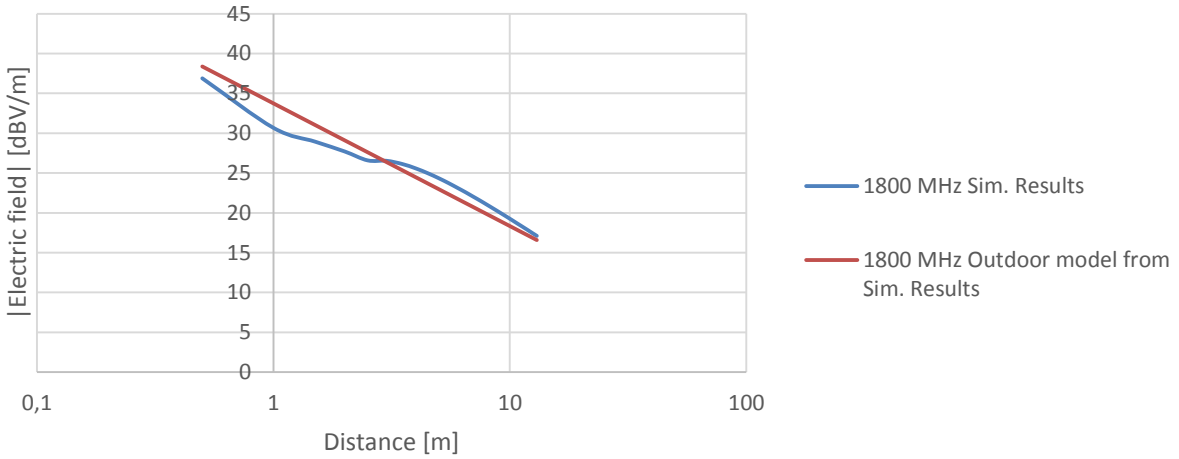

Figure B.23 - Comparison between simulation results and outdoor model from simulations results for 1800 MHz.

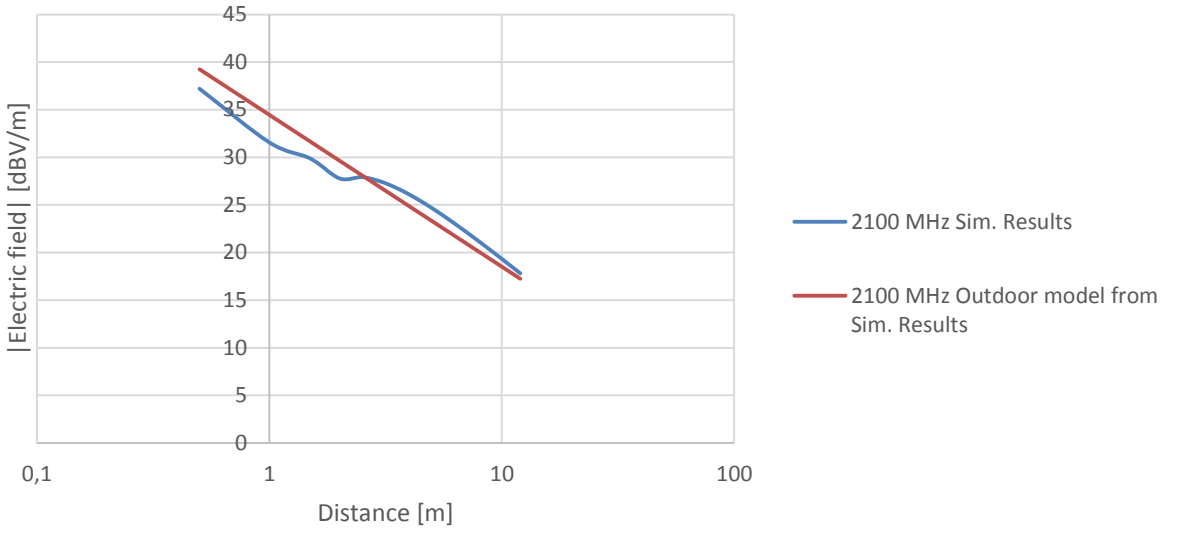

Figure B.24 - Comparison between simulation results and outdoor model from simulations results for 2100 MHz.

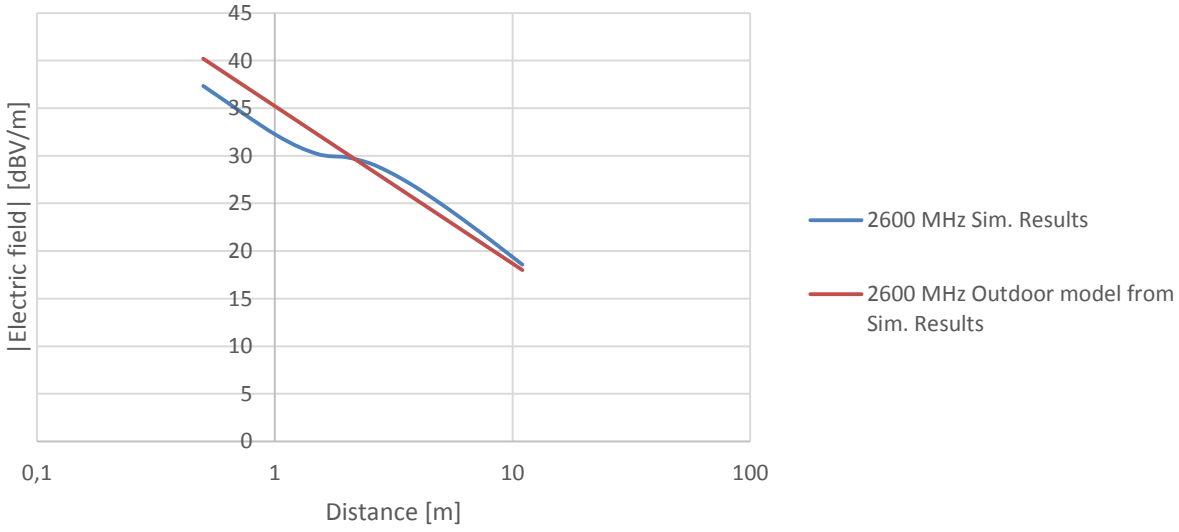

Figure B.25 - Comparison between simulation results and outdoor model from simulations results for 2600 MHz.

B.2 Comparison of Models

The following graphs present the result comparison between the global indoor model results and the theoretical model described in Section 3.1.3, regarding the indoor scenario.

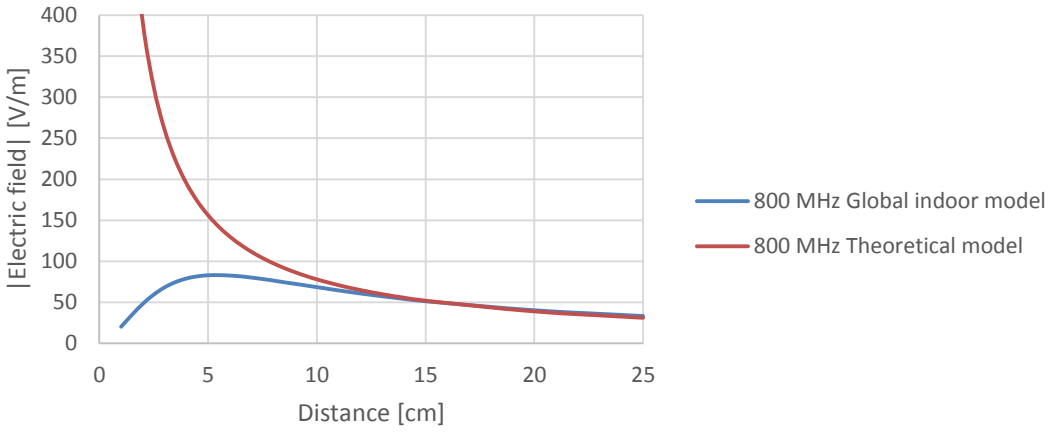

Figure B.26 – Comparison between global indoor model and theoretical results for indoor 800 MHz.

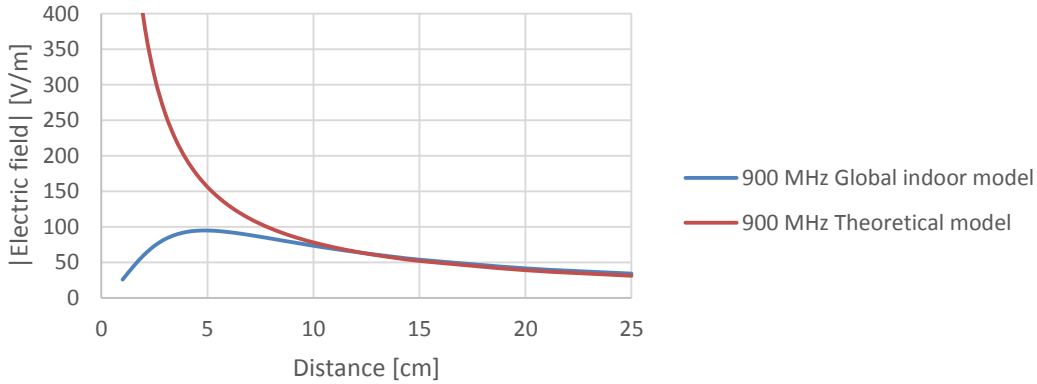

Figure B.27 - Comparison between global indoor model and theoretical results for indoor 900 MHz.

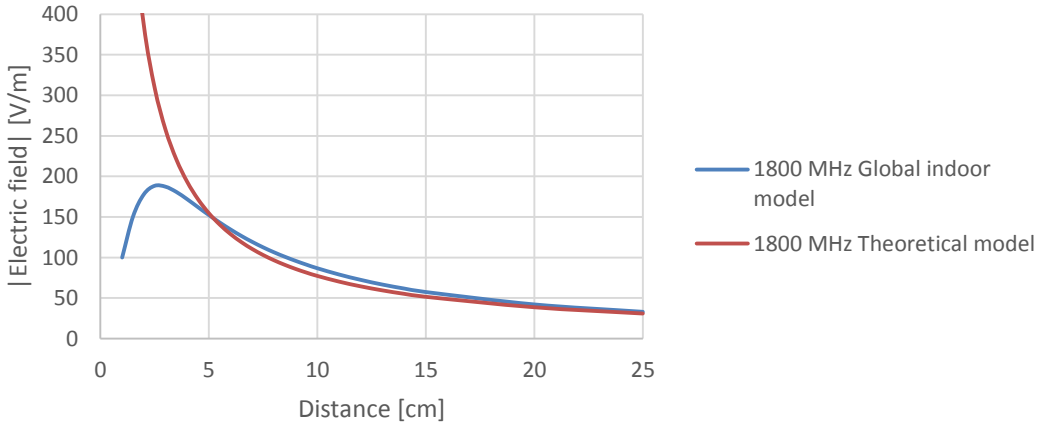

Figure B.28 - Comparison between global indoor model and theoretical results for indoor 1800 MHz.

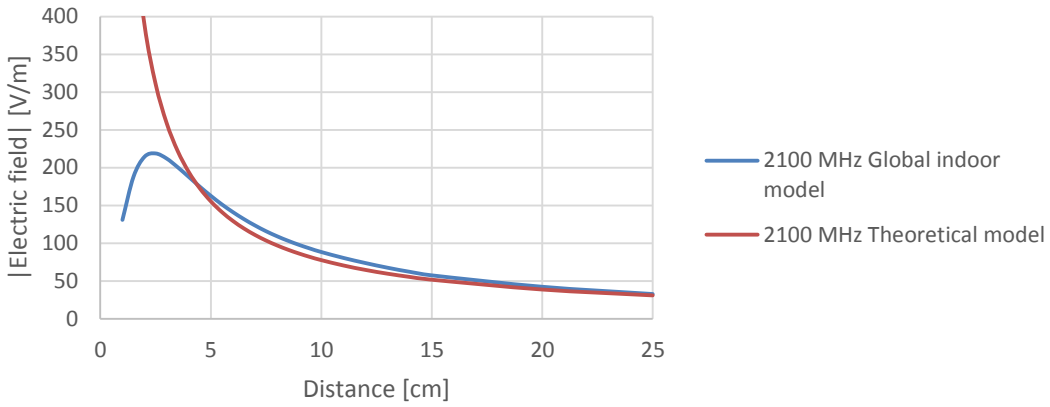

Figure B.29 - Comparison between global indoor model and theoretical results for indoor 2100 MHz.

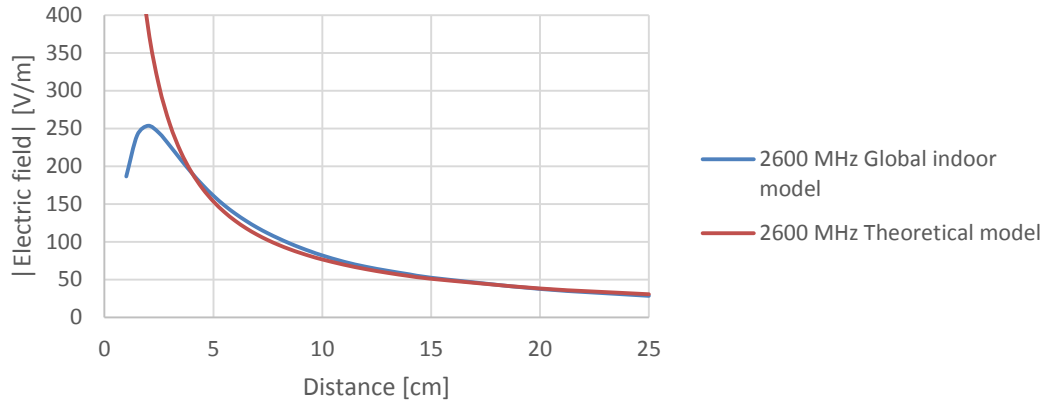

Figure B.30 - Comparison between global indoor model and theoretical results for indoor 2600 MHz.

For the outdoor scenario, the comparison between the global outdoor model and the results obtained from the electric field global model described in Section 3.1.4 as well as with measurement results for the visited BS is presented in the following figures. First, for BS1, the comparison results for the 900 MHz and 2100 MHz frequency bands are shown.

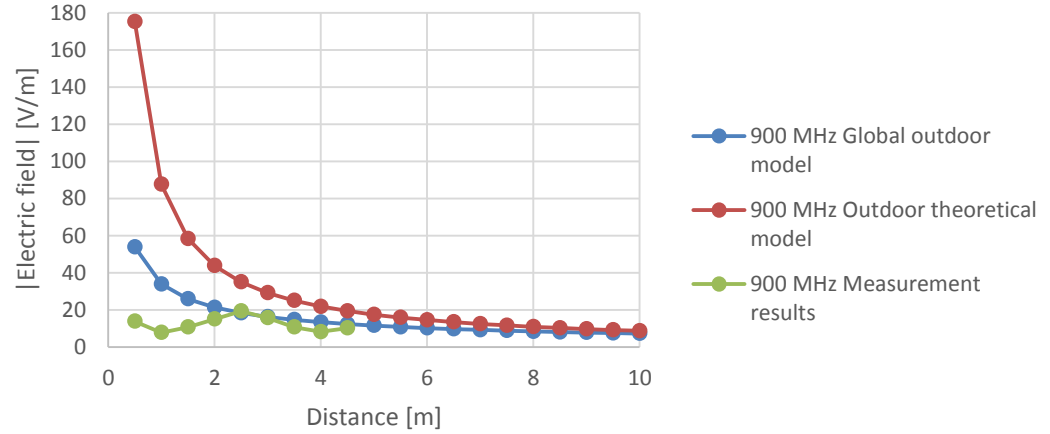

Figure B.31 - Comparison between results obtained from global outdoor model, theoretical model and measurement results for 900 MHz in BS1.

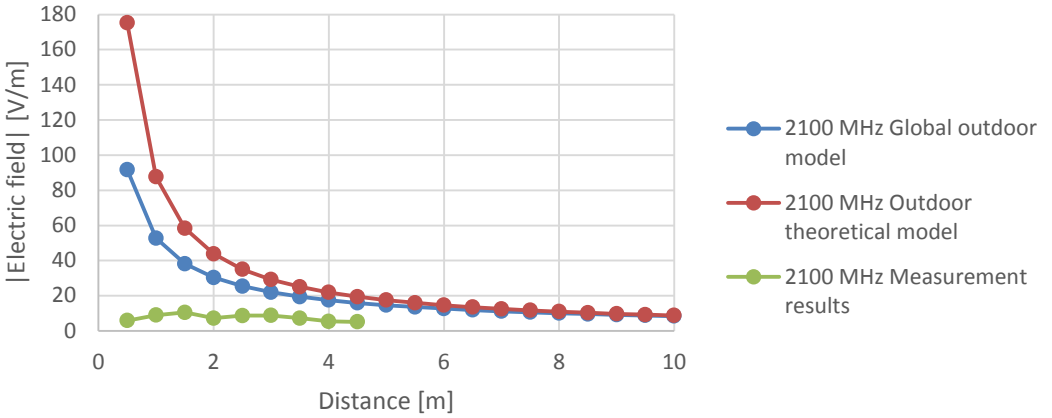

Figure B.32 - Comparison between results obtained from global outdoor model, theoretical model and measurement results for 2100 MHz in BS1.

For BS2, the comparison results for 800 MHz, 900 MHz and 2100 MHz are presented in the following figures.

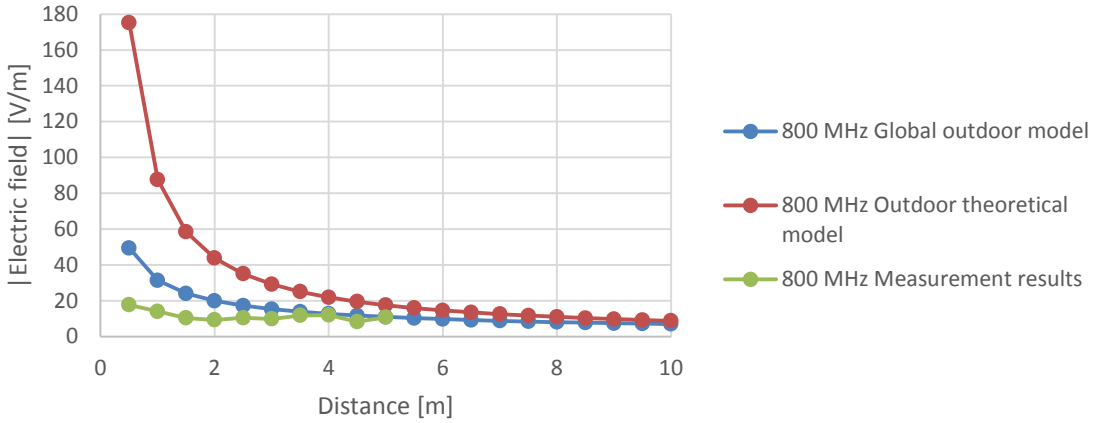

Figure B.33 - Comparison between results obtained from global outdoor model, theoretical model and measurement results for 800 MHz in BS2.

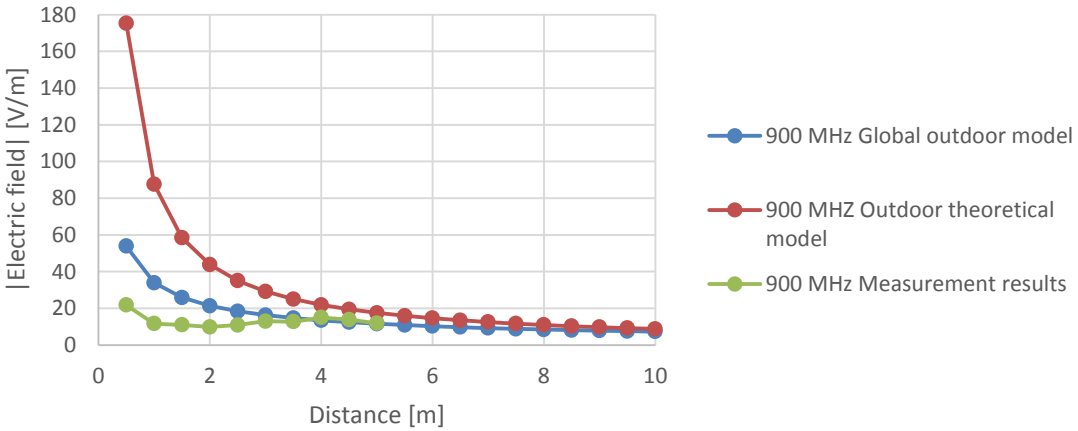

Figure B.34 - Comparison between results obtained from global outdoor model, theoretical model and measurement results for 900 MHz in BS2.

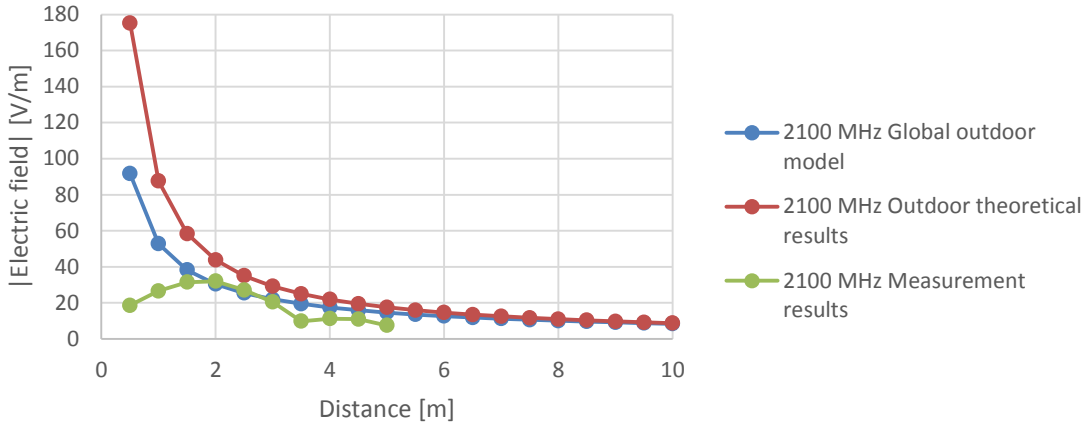

Figure B.35 - Comparison between results obtained from global outdoor model, theoretical model and measurement results for 2100 MHz in BS2.

The same approach is presented in the next figures for BS3, considering the 900 MHz and 2100 MHz frequency bands.

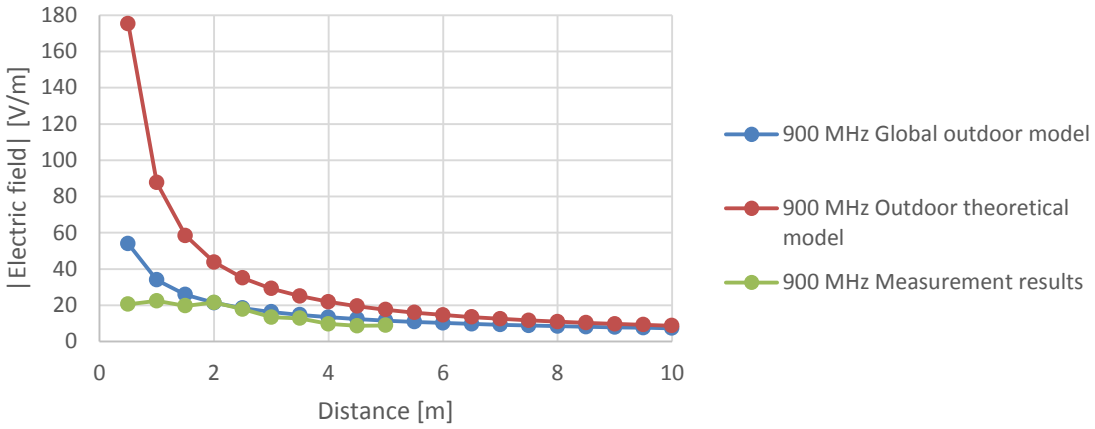

Figure B.36 - Comparison between results obtained from global outdoor model, theoretical model and measurement results for 900 MHz in BS3.

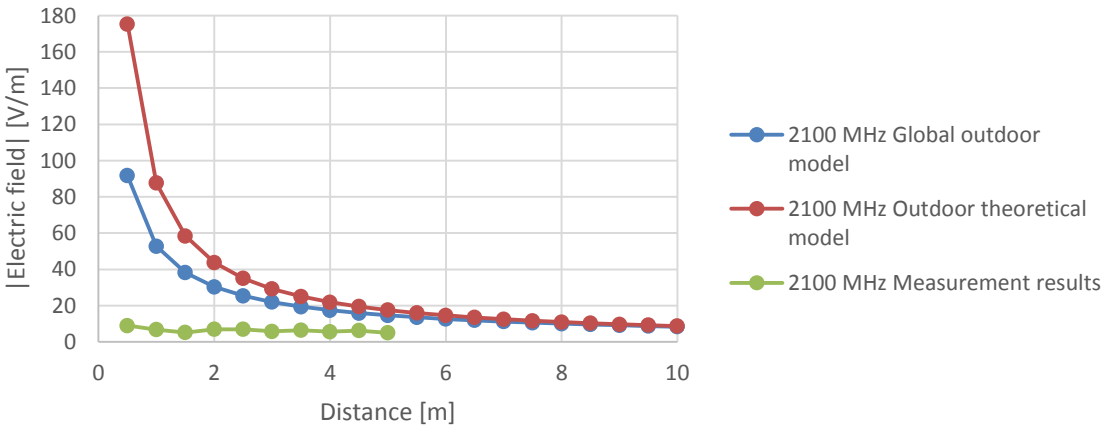

Figure B.37 - Comparison between results obtained from global outdoor model, theoretical model and measurement results for 2100 MHz in BS3.

Finally, for BS4, the comparison results for 900 MHz and 2100 MHz are presented in the following figures.

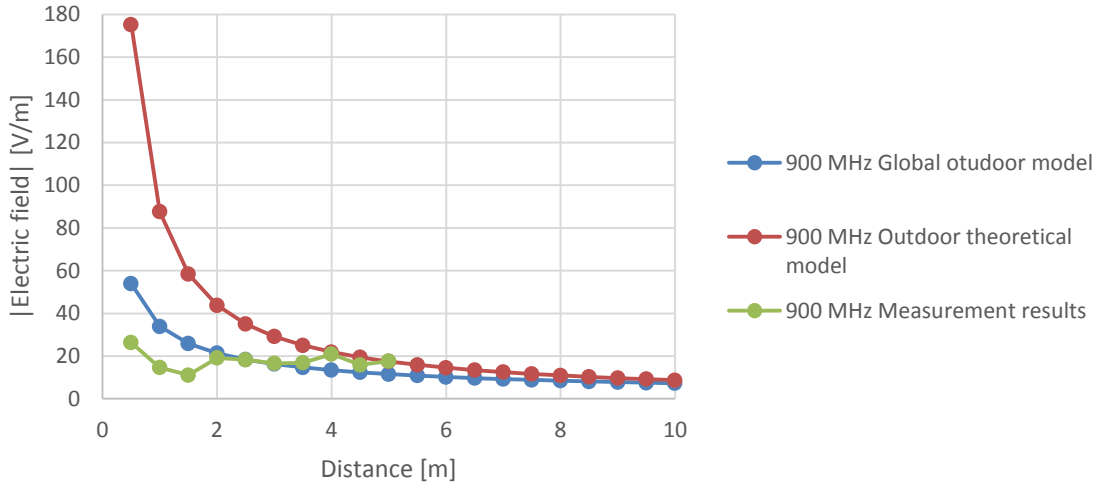

Figure B.38 - Comparison between results obtained from global outdoor model, theoretical model and measurement results for 900 MHz in BS4.

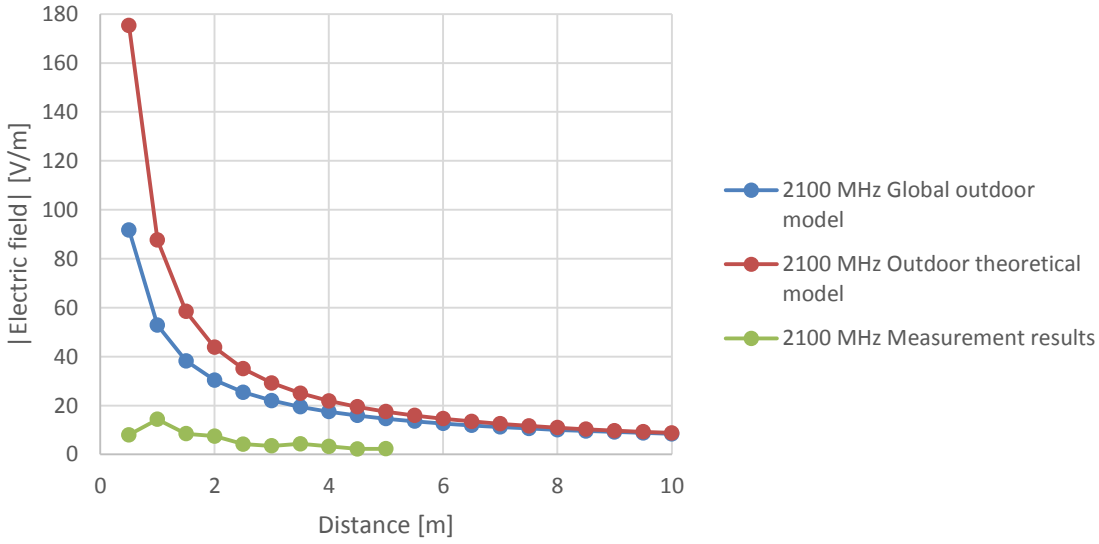

Figure B.39 - Comparison between results obtained from global outdoor model, theoretical model and measurement results for 2100 MHz in BS4.

B.3 Estimation of Exclusion Zones

Regarding the indoor scenario, the borders of the exclusion zone for the different frequencies considered are going to be presented. In Table B.1, the borders were computed considering an input power of 3 W, in Table B.2 4 W and in Table B.3 5 W.

Table B.1 – Exclusion zone borders computed with an input power of 3 W.

f [MHz]	800	900	1800	2100	2600
D_{front} [cm]	38	36	24	23	22
D_{side} [cm]	10	10	8	8	8
D_{top} [cm]	< 1	< 1	< 1	4	4

Table B.2 - Exclusion zone borders computed with an input power of 4 W.

f [MHz]	800	900	1800	2100	2600
D_{front} [cm]	42	41	27	26	24
D_{side} [cm]	12	12	10	10	9
D_{top} [cm]	< 1	< 1	5	5	5

Table B.3 - Exclusion zone borders computed with an input power of 5 W.

f [MHz]	800	900	1800	2100	2600
D_{front} [cm]	48	46	30	28	27
D_{side} [cm]	14	14	10	10	10
D_{top} [cm]	< 1	< 1	6	6	6

Annex C

Measurements

In this annex, the measurement scenarios as well as the obtained results are presented.

C.1 Measurement Scenarios

In this annex, the measurement scenarios are presented. For each visited BS, a sketch of the site as well as a picture of the BS is shown.

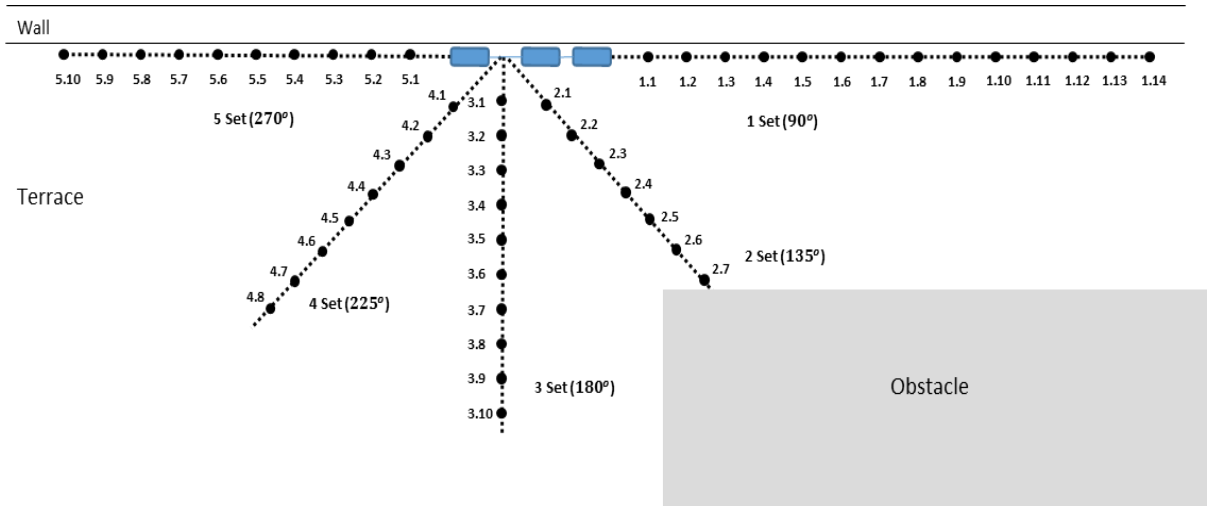

Figure C.1 - Sketch of the BS2 measurement site.

Figure C.2 - Point of view from the terrace access of the BS2.

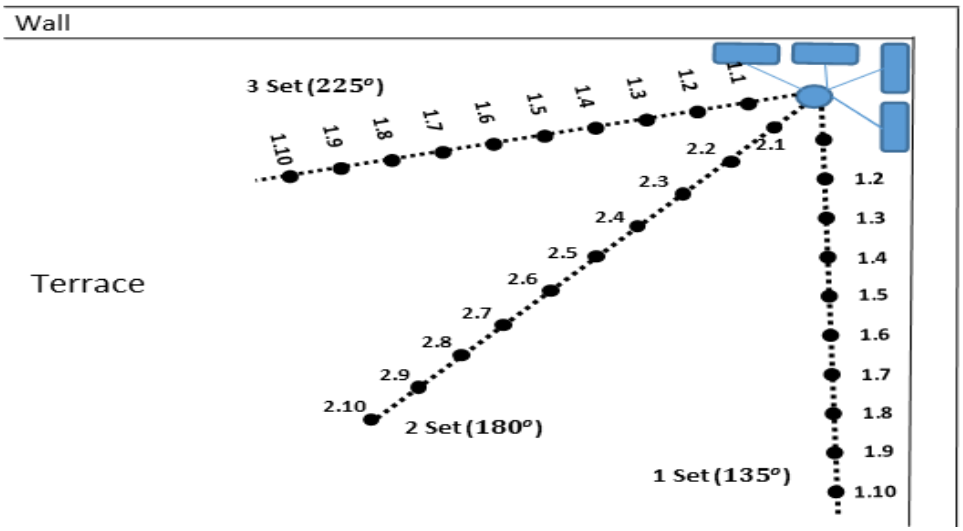

Figure C.3 - Sketch of the BS3 measurement site.

Figure C.4 - Point of view from the terrace access of the BS3.

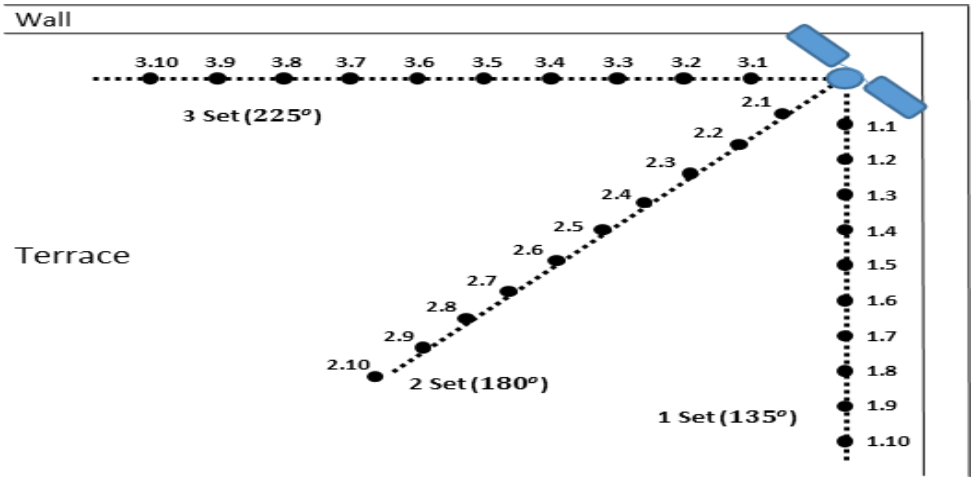

Figure C.5 - Sketch of the BS4 measurement site.

Figure C.6 - Point of view from the terrace access of the BS4.

C.2 Measurement Results

In this annex, the measurement results for the analysed BS are presented. For BS1, the measured values for 800 MHz, 900 MHz and 2100 MHz frequency bands are presented in the following figures.

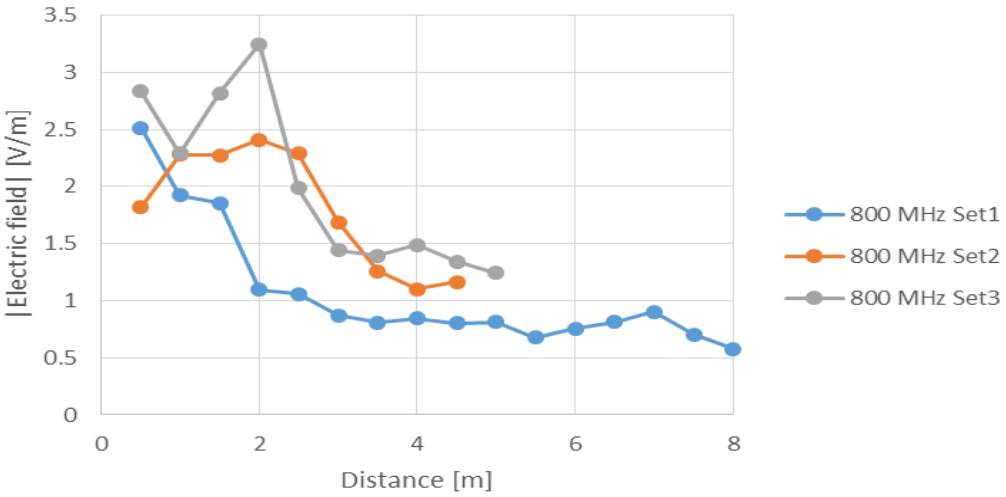

Figure C.7 - Measured values of the electric field for 800 MHz on BS1.

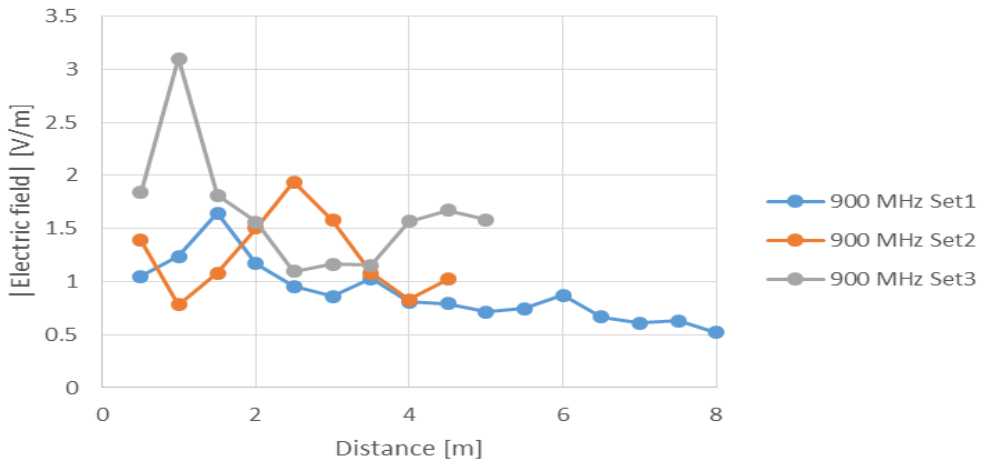

Figure C.8 - Measured values of the electric field for 900 MHz on BS1.

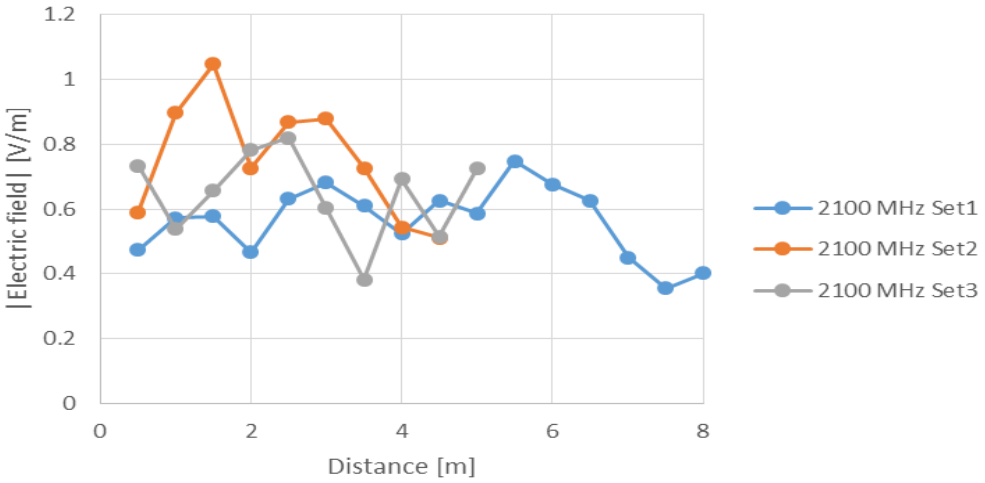

Figure C.9 - Measured values of the electric field for 2100 MHz on BS1.

For BS2, the following figures present the measurement data for the 800 MHz, 900 MHz and 2100 MHz frequency bands.

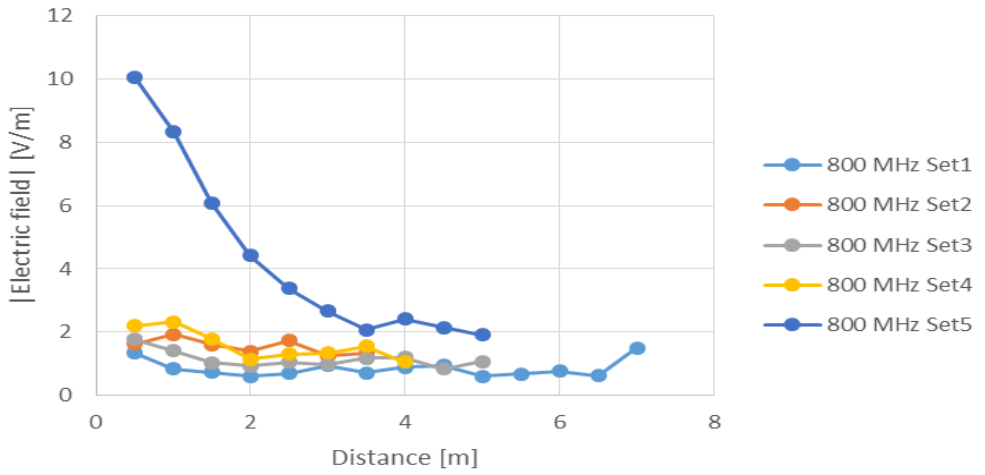

Figure C.10 - Measured values of the electric field for 800 MHz on BS2.

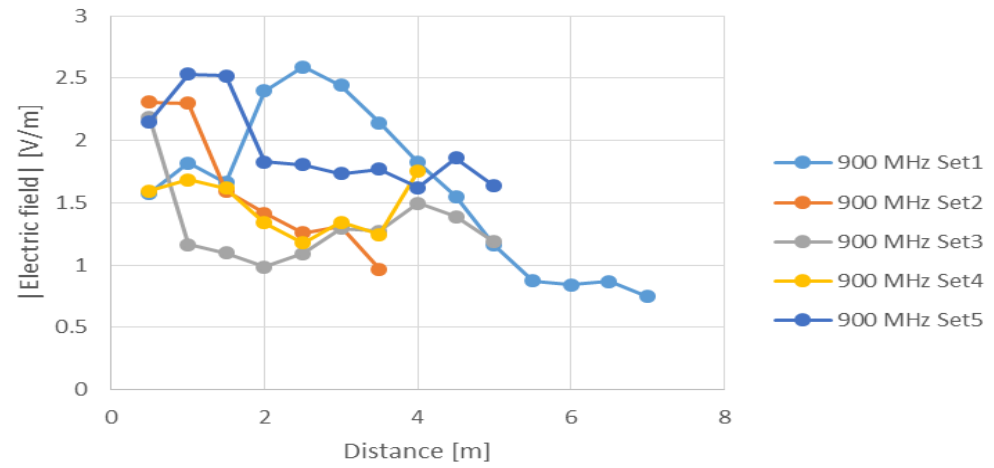

Figure C.11 - Measured values of the electric field for 900 MHz on BS2.

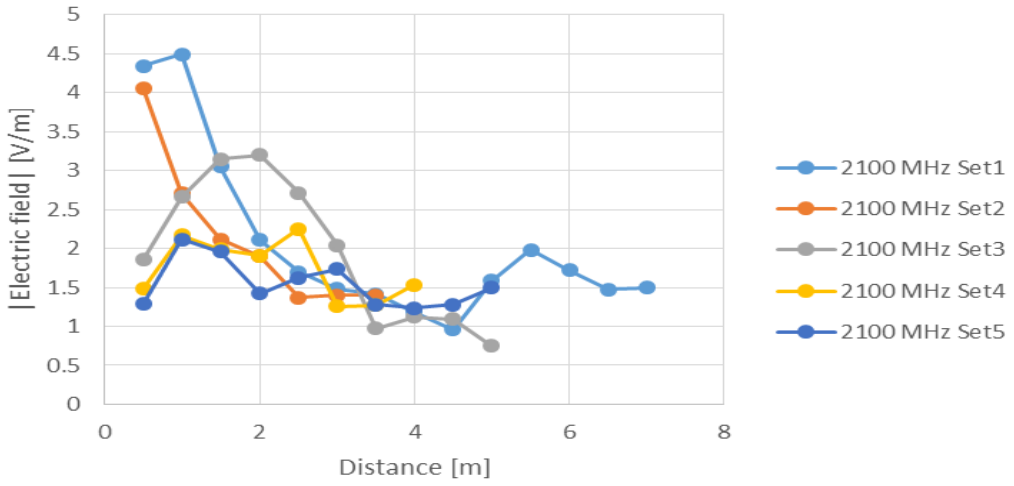

Figure C.12 - Measured values of the electric field for 2100 MHz on BS2.

For BS3, the measurement results for the 900 MHz and 2100 MHz frequency bands are presented in the following figures.

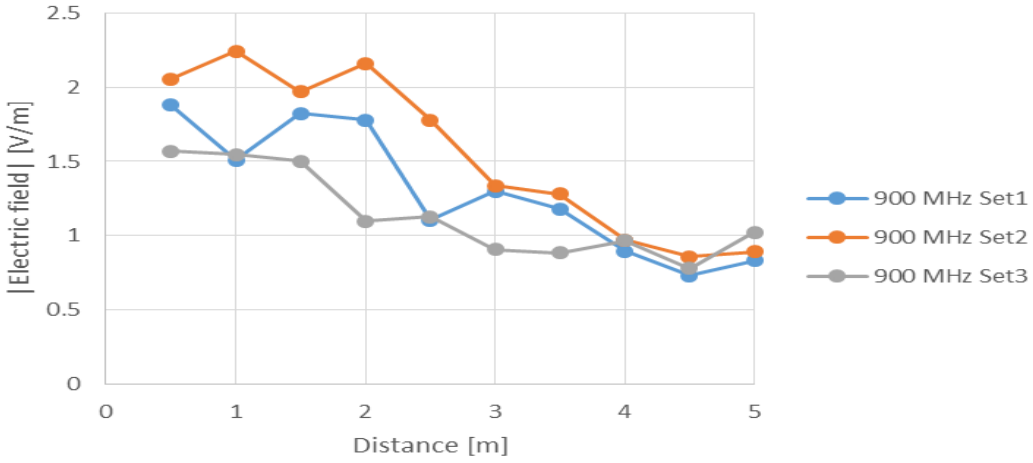

Figure C.13 - Measured values of the electric field for 900 MHz on BS3.

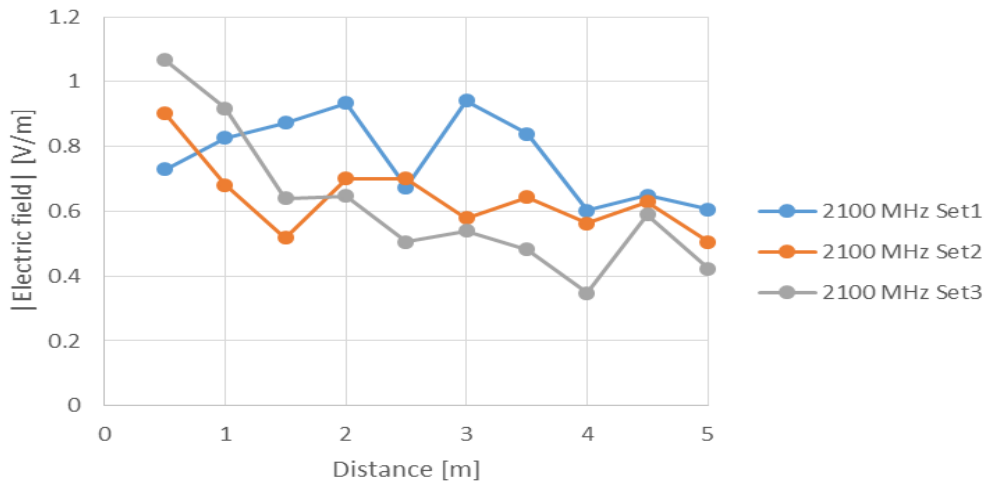

Figure C.14 - Measured values of the electric field for 2100 MHz on BS3.

Finally, the measurement results for BS4, concerning the 900 MHz and 2100 MHz frequency bands, are presented in the next set of figures.

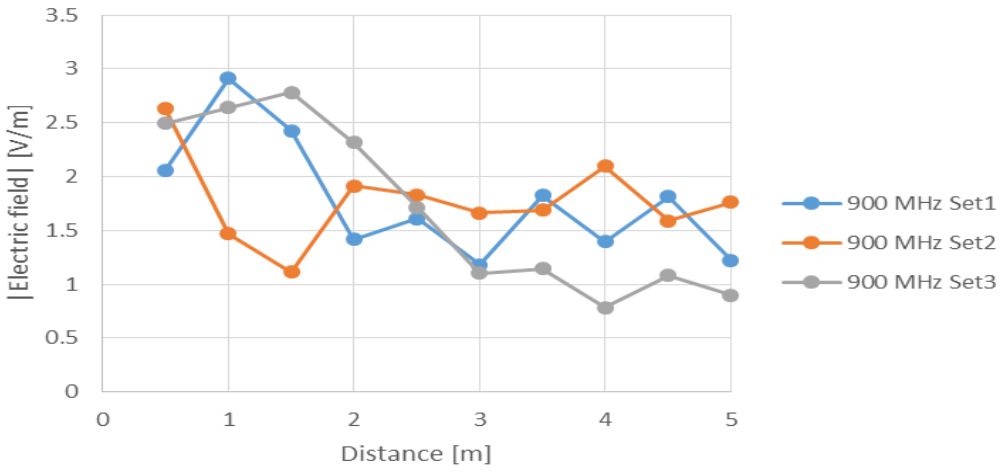

Figure C.15 - Measured values of the electric field for 900 MHz on BS4.

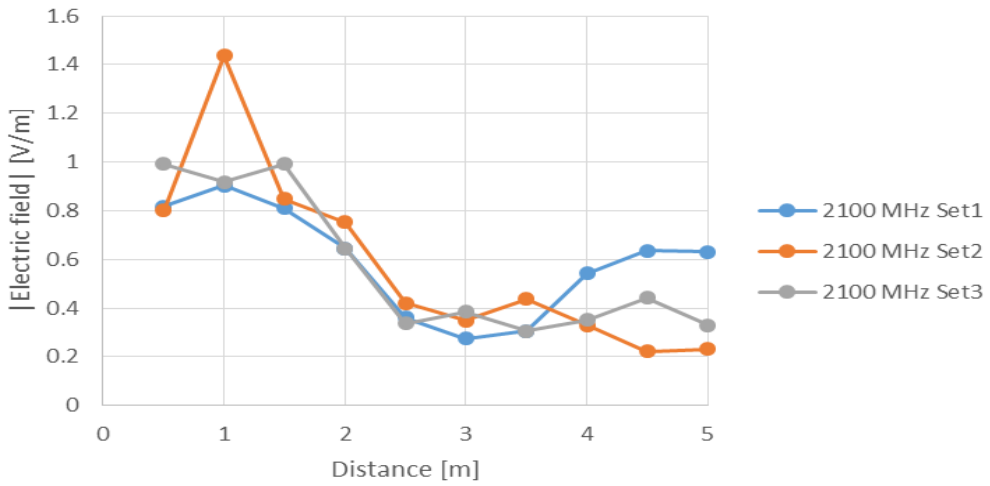

Figure C.16 - Measured values of the electric field for 2100 MHz on BS4.

References

[ABDK02] Altman,Z., Begasse,B., Dale,C., Karwowski,A., Wiart,J., Wong,M.-F. and Gattoufi,L., "Efficient Models for Base Station Antennas for Human Exposure Assessment", *IEEE Transactions on Electromagnetic Compatibility*, Vol. 44, No. 4, Nov. 2002, pp. 588-592.

[ABOM09] Ahmed,M.B, Bouhorma,M., Ouaai,F.E, Mamouni,A., "A new miniaturized patch antenna for wireless systems: GSM, UMTS, HIPERLAN", in *Proc. of WMCNC'2009 - IEEE International Conference on Wireless and Mobile Computing, Networking and Communications*, Marrakech, Morocco, Oct. 2009.

[AHIS13] Abdullah,K., Hashim,W., Ismail,A. and Sidek,N., "Predicting Radio Frequency Radiation from Mobile Communication Base Stations", *International Journal of Computer and Communication Engineering*, Vol. 2, No. 4, July 2013.

[ANAC07] ANACOM, "86/2007 Regulation: Procedures for monitoring and measurement of electromagnetic field strength levels originated by radiocommunication stations" (in Portuguese), *Diário da República, Series 2, No. 98*, May 2007, pp. 13650-13659.

[Antu12] Antunes,M.G., *Estimation of Exclusion Zones in LTE Base Station Antennas co-located with GSM/UMTS*, M.Sc. Thesis, Instituto Superior Técnico, Technical University of Lisbon, Lisbon, Portugal, 2012.

[ARPN02] Australian Radiation Protection and Nuclear Safety Agency, ARPNSA, *Radio Frequency EME Exposure Levels – Prediction Methodologies*, Sep. 2002.

[AyFa13] Ayinmode,B., Farai,I., *Measurement and Method in Radiofrequency Radiation Exposure Assessments*, University of Ibadan, Oyo State, Nigeria, Vol. 14, No. 2, Nov, 2013.

[Bala05] Balanis,C.A., *Antenna Theory - Analysis and Design*, John Wiley, New Jersey, United States of America, 2005.

[BCCP03] Bernardi,P., Cavagnaro,M., Cicchetti,R., Pisa,S., Piuzzi,E. and Testa,O., "A UTD/FDTD Model to Evaluate Human Exposure to Base-Station Antennas in Realistic Urban Environments", in *Proc. of 2003 IEEE MTT-S International Microwave Symposium*, Philadelphia, PA, USA, June 2003.

[BCDF02] Barbiroli,M., Carciofi,C., Degli-Esposti,V. and Faciasecca,G., "Evaluation of Exposure Levels Generated by Cellular Systems: Methodology and Results", *IEEE Transactions on Vehicular Technology*, Vol. 51, No. 6, Nov. 2002, pp.1322-1329.

[BCFF99] Barbiroli,M., Carciofi,C., Falciasecca,G. and Frullone,M., "Analysis of field strength levels near base station antennas", in *Proc. of VTC'99 - IEEE International Conference on*

Vehicular Technology, Houston, Texas, USA, May 1999.

[BFHM02] Bergqvist,U., Friedrich,G., Hamnerius,Y., Martens,L., Neubauer,G., Thuroczy,G., Vogel,E. and Wiart,J., *Mobile telecommunication base stations – exposure to electromagnetic field,* Short Term Mission Report, COST 244bis, Europe, 2002 (http://www.elettra2000.it/phocadownload/archivi/docymenti/cost244bis.pdf).

[BiGi99] Bizzi,M. and Gianola,P., "Electromagnetic fields radiated by GSM antennas, Electronic Letters", *Electronic Letters*, Vol. 35, No. 11, May 1999, pp. 855-857.

[CENE02a] CENELEC, *Basic standard for the calculation and measurement of electromagnetic field strength and SAR related to human exposure from radio base stations and fixed terminal stations for wireless telecommunication systems (110 MHz – 40 GHz)*, Ref. No. EN 50383:2002 E, Central Secretariat, Brussels, Belgium, July 2002 (http://www.cenelec.eu/dyn/www/f?p=104:110:3998399622877817::::FSP_PROJECT,FSP_LANG_ID:21117,25).

[CENE02b] CENELEC, *Product standard to demonstrate the compliance of radio base stations and fixed terminal stations for wireless telecommunication systems with the basic restrictions or the reference levels related to human exposure to radio frequency electromagnetic fields (110 MHz - 40 GHz) - Occupational*, Ref. No. EN 50384:2002 E, Central Secretariat, Brussels, Belgium, July 2002 (http://www.cenelec.eu/dyn/www/f?p=104:110:548671608646467::::FSP_PROJECT,FSP_LANG_ID:14407,25).

[CENE02c] CENELEC, *Product standard to demonstrate the compliance of radio base stations and fixed terminal stations for wireless telecommunication systems with the basic restrictions or the reference levels related to human exposure to radio frequency electromagnetic fields (110 MHz - 40 GHz) - General public*, Ref. No. EN 50385:2002 E, Central Secretariat, Brussels, Belgium, July 2002 (http://www.cenelec.eu/dyn/www/f?p=104:110:1475001556730739::::FSP_PROJECT:14880).

[CGLM99] Carli,E., Gianola,P., Lombardi,G., Mama,L. and Vescovo,R., "Antenna models for field level evaluation in proximity of GSM Base stations", in *Proc. of EPMCC'99 – 3rd European Personal and Mobile Communications Conference*, Paris, France, Mar. 1999.

[Cisc14] Cisco, *Cisco Visual Networking Index: Global Mobile Data Traffic Forecast Update, 2013–2018,* White Paper, San Jose, CA, USA, Feb 2014 (http://www.cisco.com/c/en/us/solutions/collateral/service-provider/visual-networking-index-vni/white_paper_c11-520862.html).

[CKLa11] Cela, S., Kamo, B., Lala, A., "*A Method of GSM Antenna Modeling for the Evaluation of the Exposed Field in the Vicinity",* IEEE International Conference on Network-Based Information Systems, 2011.

[CLJJX13] Cunzhen, P., Lei, W., Jie, Y., Jie, W., Xianli, L. and Yongjin, C., "A Prediction Model for Electromagnetic Radiation of Multi- system Base Station", in *Proc. of ICCSEE 2013 - 2nd International Conference on Computer Science and Electronics Engineering*, Chongqing,

China, Jan 2013.

[CoEU04] Council of the European Union, “Corrigendum to Directive 2004/40/EC of the European Parliament and of the Council of 29 April 2004 on the minimum health and safety requirements regarding the exposure of workers to the risks arising from physical agents (electromagnetic fields) (18th individual Directive within the meaning of Article 16(1) of Directive 89/391/EEC)”, *Official Journal of the European Communities L 184/1*, Brussels, Belgium, May 2004.

[CoEU99] Council of the European Union, “Council Recommendation of 12 July 1999 on the limitation of exposure of the general public to electromagnetic fields (0 Hz to 300 GHz)”, *Official Journal of the European Communities L 199/59*, Brussels, Belgium, July 1999.

[COST00] COST 244 bis, *Biomedical Effects of Electromagnetic Fields*, Final report, COST 244 bis, Nov. 2000.

[CSTe14] CST – Computer Simulation Technology, CST, 2014 (http://www.CST.com).

[ECCC07] Electronic Communications Committee (ECC) European Conference of Postal and Telecommunications Administrations (CEPT), *Measuring Non-Ionising Electromagnetic Radiation (9 kHz – 300 GHz),* ECC Recommendation (02)04, Edition 060207, Helsinki, Finland, 2007.

[EHFRA10] European Health Risk Assessment Network on Electromagnetic Fields Exposure (EHFRAN), *Report on the level of exposure (frequency, patterns and modulation) in the European Union*, August 2010.

[ETSI100] ETSI, *Digital cellular telecommunications system (Phase 2+); Radio transmission and Reception*, ETSI GSM 05.05, European Telecommunications Standards Institute, Sophia-Antipolis, France, Nov. 2000 (http://www.etsi.org).

[ETSI106] ETSI, *User Equipment (BS) radio transmission and reception (FDD)*, Report 3GPP TS 25.101, Ver. 3.19.0 (Release 1999), Dec 2006 (http://www.etsi.org).

[ETSI11a] ETSI, *Base Station (BS) radio transmission and reception (FDD)*, Report 3GPP TS 25.104, Ver. 8.13.0 (Release 8), June 2011 (http://www.etsi.org).

[ETSI11b] ETSI, *User Equipment (BS) radio transmission and reception (FDD)*, Report 3GPP TS 25.101, Ver. 10.3.0 (Release 10), Oct 2011 (http://www.etsi.org).

[GCKK09] Grosselin,M.C., Christ,A., Kuhn,S., Kuster,N., “*Dependence of the Occupational Exposure to Mobile Phone Base Stations on the Properties of the Antenna and the Human Body”,* IEEE Transactions on Electromagnetic Compatibility, Vol.51, No. 2, May 2009.

[Gree90] Green, E., “Radio link design for microcellular systems,” *Brit. Telecom Technol. J.*, Vol. 8, No. 1, Jan. 1990, pp. 85–96.

[HIKM08] Hansson, B., Ilvonen, S., Karkkainen, K., Meyer, F.J.C, Strydom, M.L., Tornevik, C. and

Zollman, P., "*On the Estimation of SAR and Compliance Distance Related to RF Exposure from Mobile Communication Base Station Antennas",* IEEE Transactions on Electromagnetic Compatibility, Vol.50, No. 4, Nov. 2008.

[HiTa11] Higashiyama, J., Tarusawa, Y., "*RF Exposure Compliance Assessment for Radio Base Station with Built-in Antenna",* IEEE Transactions on Electromagnetic Compatibility, Proc. of the 10th Int. Symposium on Electromagnetic Compatibility, York, UK, Sep. 2011.

[HoTo04] Holma,H., Toskala,A., *WCDMA FOR UMTS – Radio Access for Third Generation Mobile Communications*, John Wiley, Chichester, United Kingdom, 2004.

[HoTo09] Holma,H., Toskala,A., *LTE for UMTS: OFDMA and SC-FDMA Based Radio Access*, John Wiley, Chichester, United Kingdom, 2009.

[ICNI98] ICNIRP, "Guidelines for Limiting Exposure to Time-Varying Electric, Magnetic, and Electromagnetic Fields (up to 300 GHz)", *Health Physics Society*, Vol. 74, No. 4, pp. 494-522, 1998 (http://www.icnirp.de).

[KaTH12] KATHREIN- Werke KG, Basic Antenna Principles for Mobile Communications, 2012 (http://www.kathrein.de/en/mcs/techn-infos/download/basicantenna.pdf).

[KNNP14] Koprivica,M., Neskovic, A., Neskovic, N. and Paunovic, G., "statistical analysis of electromagnetic radiation measurements in the vicinity of GSM/UMTS base stations antenna masts", Oxford Journals, 2014 (http://rpd.oxfordjournals.org/content/early/2013/09/19/rpd.nct230.abstract).

[LeSu09] Lee,Y.C., Sun,J.S., "A New Printed Antenna for Multiband Wireless Applications", Antennas and Wireless Propagation Letters, IEEE, Vol. 8, May 2009, pp. 402-405.

[LEXN13] http://www.lexnet.fr/press-room.html, Dec.2013.

[MFRL02] Martínez-González,A.M., Fernández-Pascual,A., Reyes,E., Loock,W.V., Gabriel,C. and Sánchez-Hernández,D., "Practical procedure for verification of compliance of digital mobile radio base stations to limitations of exposure of the general public to electromagnetic fields", *IEE Proceedings Microwaves*, Antennas and Propagation, Vol. 149, No. 4, Aug. 2002, pp. 218-228.

[MNMV02] Martínez-Burdalo,M., Nonídez,L., Martín,A. and Villar,R., "On the calculation of safety distances for human exposure to electromagnetic fields from base-station antennas", *Microwave and Optical Technology Letters*, Vol. 43, No. 5, Sep. 2002, pp. 364-367.

[Moli11] Molisch, A.F., *Wireless Communications*, John Wiley, Chichester, United Kingdom, 2011.

[More12] Moreira,A.M., Microstrip Antennas (in Portuguese), Notes of Antennas, Instituto Superior Técnico, Lisbon, Portugal, 2012.

[Nard07] Narda Safety Test Solutions, "SRM-3000 Selective Radiation Meter - Operating Manual", Narda Safety Test Solutions, Pfullingen, Germany, 2007.

[OFRC05] Oliveira,C., Fernandes,C., Reis,C., Carpinteiro,G., Ferreira,L., Correia,L.M. and Sebastião,D., *Definition of Exclusion Zones around Typical Installations of Base Station Antennas*, monIT Project, Report Int_Tec_0102_15_BSExclZones, Ver. 15, Instituto de Telecomunicações, Lisbon, Portugal, Fev. 2005.

[OICa02] Oliveira,C.S., Carpinteiro,G., *Electromagnetic radiation exposure of GSM and UMTS Base Station Antennas* (in Portuguese), Final Graduation Project, Instituto Superior Técnico, Technical University of Lisbon, Lisbon, Portugal, 2002.

[Oliv06] Oliveira,C.S., *Estimation of Exclusion Zones for Base Station Antennas in Wireless Communication Systems*, Master M.Sc. Thesis, Instituto Superior Técnico, Technical University of Lisbon, Lisbon, Portugal, 2006.

[Oliv13] Oliveira,C.S., *Characterisation of On-Body Communications*, PhD. Thesis, Instituto Superior Técnico, Technical University of Lisbon, Lisbon, Portugal, 2013.

[PaPH12] Paul,D.L., Paterson,M.G., and Hilton,G.,S., "A Low-Profile Textile Antenna for Reception of Digital Television and Wireless Communications", Radio and Wireless Symposium (RWS), IEEE, Santa Clara, CA, Apr. 2012.

[Pars92] Parsons,J.D., *The Mobile Radio Propagation Channel*, Pentech, London, 1992.

[Sche43] Schelkunoff,S.A., *Electromagnetic Waves*, D. van Nostrand, New York, New York, USA, 1943.

[StTh81] Stutzman, W. L., Thiele, G. A., "*Antenna Theory and Design*", John Wiley & Sons, 1981.

[Tuan10] Tuan,T.M., "Design Dual Band Microstrip Antenna For Next Generation Mobile Communication", The 2010 International Conference on Advanced Technologies for Communications, Ho Chi Minh City, Vietnam, Oct. 2010.